

UNIVERSIDADE FEDERAL DO PARÁ  
INSTITUTO DE TECNOLOGIA  
PROGRAMA DE PÓS-GRADUAÇÃO EM ENGENHARIA ELÉTRICA

# Modelling and Mitigation of Alien Crosstalk for DSL Systems

Diego de Azevedo Gomes

TD: 14/2017

UFPA / ITEC / PPGEE  
Belem-Para-Brazil  
2017



UNIVERSIDADE FEDERAL DO PARÁ  
INSTITUTO DE TECNOLOGIA  
PROGRAMA DE PÓS-GRADUAÇÃO EM ENGENHARIA ELÉTRICA

Diego de Azevedo Gomes

# Modelling and Mitigation of Alien Crosstalk for DSL Systems

TD: 14/2017

Thesis submitted to the Examining Board of the Programa de Pós-Graduação em Engenharia Elétrica from Universidade Federal do Pará for obtaining a PhD degree in Electrical Engineering, with emphasis on Telecommunications.

UFPA / ITEC / PPGEE  
Belem-Para-Brazil  
2017

**UNIVERSIDADE FEDERAL DO PARÁ**  
**INSTITUTO DE TECNOLOGIA**  
**PROGRAMA DE PÓS-GRADUAÇÃO EM ENGENHARIA ELÉTRICA**

**Modelling and Mitigation of Alien Crosstalk for DSL Systems**

**AUTHOR: DIEGO DE AZEVEDO GOMES**

PHD THESYS SUBMITTED FOR ASSESSMENT OF THE EXAMINING BOARD APPROVED BY THE COLLEGIATE OF THE PROGRAMA DE PÓS-GRADUAÇÃO EM ENGENHARIA ELÉTRICA OF THE UNIVERSIDADE FEDERAL DO PARÁ TO BE JUDGED TO GET THE DEGREE OF DOCTOR OF ELECTRICAL ENGINEERING IN TELECOMMUNICATIONS.

**JUDGED IN 2017-12-11**

**EXAMINATION BOARD:**

.....  
**Prof. Dr. Evaldo Gonçalves Pelaes (Advisor - UFPA)**

.....  
**Prof. Dr. Aldebaro Barreto da Rocha Klautau Júnior (Co-advisor - UFPA)**

.....  
**Prof. Dr. Adoniran Judson Braga (Member - UNB)**

.....  
**Prof. Dr. João Crisóstomo Weyl Albuquerque Costa (Member - UFPA)**

.....  
**Dr. Vinicius Duarte Lima (Member - UFPA)**

.....  
**Dr. Francisco Carlos Frey Bentes Müller (Member - UFPA)**

**VISA:**

.....  
**Prof. Dr. Evaldo Gonçalves Pelaes**

**COORDINATOR OF THE PPGEE/ITEC/UFPA**

# Abstract

G.fast is the most recent ITU-T standard for DSL transmission, which targets copper topologies with short distances and adopts a bandwidth of 106 MHz extensible to 212 MHz. In several situations, G.fast systems will be composed by or coexist with uncoordinated (or alien) lines, which are sources of strong crosstalk, because these lines are not part of the vectored group. This document presents a formulation to explain the performance of the alien crosstalk mitigation methods according to the number of alien lines in a certain environment, the mechanism that defines the interference correlation of it and an alien crosstalk mitigation method for downstream DSL transmission impaired by multiple interferers called AMMIS. Simulation results show that alien crosstalk mitigation methods found in the literature can indeed improve the performance of G.fast systems, but only under specific conditions. We have contrasted these situations and we provide guidelines about the feasibility of the crosstalk mitigation techniques in scenarios with distinct number of alien lines. Additionally, the AMMIS shows promising results in relation to the bit rate when compared with literature methods in scenarios with a large number of interferers, with the additional advantage of allows power savings. As support for the simulations, we also present a set of alien crosstalk measurements.

**KEYWORDS:** G.fast, Alien Crosstalk Mitigation, Linear Prediction, Measurements.

# Resumo

G.fast é o padrão mais recente do ITU-T para transmissões DSL, o qual é destinado para topologias do cobre de curtas distâncias e adota uma largura de banda de 106 MHz, que pode ser estendida até 212 MHz. Em muitas situações os sistemas G.fast serão compostos ou coexistirão com linhas não-coordenadas (o linhas *alien*), as quais são fonte de forte *crosstalk*, pois estas linhas não fazem parte do grupo vetorizado. Este documento apresenta uma formulação que explica o desempenho de métodos de mitigação de *alien crosstalk* de acordo com o número de linhas *alien* no ambiente, o mecanismo que define a correlação desta interferência e um método de mitigação de *alien crosstalk* para transmissões DSL na direção de *downstream* afetadas por múltiplos interferentes, chamado AMMIS. Os resultados das simulações mostram que os métodos de mitigação de *alien crosstalk* encontrados na literatura podem de fato melhorar o desempenho de sistemas G.fast, mas apenas em condições específicas. Nós contrastamos estas situações e apresentamos diretrizes acerca da viabilidade destas técnicas de mitigação em cenários com números distintos de linhas *alien*. Adicionalmente, o AMMIS apresenta resultados promissores em relação a taxa de dados quando comparado com os métodos encontrados na literatura em cenários com grande quantidade de interferentes, com a vantagem adicional de ainda possibilitar economia de energia. Como suporte para as simulações, também apresentamos um conjunto de medições de *alien crosstalk*.

**Palavras-Chave:** G.fast, Mitigação de *Alien Crosstalk*, Predição Linear, Medições.

# Contents

<b>List of Figures</b>	<b>iii</b>
<b>List of Tables</b>	<b>vi</b>
<b>Glossary</b>	<b>vii</b>
<b>Symbol List</b>	<b>x</b>
<b>1 Introduction</b>	<b>1</b>
1.1 DSL Technology . . . . .	1
1.2 Discrete Multi-Tone (DMT) Modulation . . . . .	4
1.3 Interference in DSL Systems . . . . .	7
1.4 A Literature Review of Noise and Interference Mitigation in Copper-Based Transmission . . . . .	8
1.5 Objectives . . . . .	12
<b>2 Alien Crosstalk Mitigation: Literature Review</b>	<b>14</b>
2.1 Alien Crosstalk System Model . . . . .	14
2.2 Methods to Mitigate Alien Crosstalk . . . . .	15
2.2.1 First Ginis' Method: Two-sided coordination . . . . .	15
2.2.2 Second Ginis' Method: Receiver coordination with decision-feedback structure . . . . .	17
2.2.3 Third Ginis' Method: Receiver Coordination with Noise Prediction Structure (RxPred) . . . . .	19
2.2.4 Decision Feedback Cancellor (DFC) . . . . .	20
<b>3 Interference Modeling and Performance Evaluation of the AXT Prediction</b>	<b>23</b>

3.1	Evaluation of the Correlation matrix . . . . .	24
3.2	Evaluation of the Correlation Coefficient . . . . .	26
3.2.1	Impact of the Number of AL in the Correlation Coefficient . . . . .	26
3.2.2	Impact of the Number of ALs in the Prediction Error . . . . .	28
3.2.3	Effects of the White Noise on the Correlation . . . . .	29
3.3	Evaluation of the Effect of the AXT Channel Phase on the Correlation . . . . .	32
3.4	Determination of the Minimum Number of Prediction Lines Required for an Effective AXT Prediction . . . . .	34
<b>4</b>	<b>Mitigation of Alien Crosstalk for Downstream DSL Transmissions Impaired by Multiple Interferers</b>	<b>38</b>
4.1	System Model for AMMIS . . . . .	38
4.2	AXT Mitigation for Multiple Interference Sources (AMMIS) . . . . .	40
4.2.1	The Effect of Vectoring on AMMIS . . . . .	43
<b>5</b>	<b>Results</b>	<b>45</b>
5.1	Measurements . . . . .	45
5.1.1	Network Analyzer - NA . . . . .	45
5.1.2	Calibration . . . . .	46
5.1.3	Cable Measurements . . . . .	46
5.2	Simulation Results . . . . .	52
5.2.1	Results for the Correlation Analysis . . . . .	52
5.2.2	Evaluation of the Effect of the AXT Channel Phase in the Correlation	55
5.2.3	Results for Evaluation of the Ratio AL/VL in the Performance of the AXT Mitigation Methods . . . . .	58
5.3	Evaluation of the AMMIS . . . . .	66
<b>6</b>	<b>Conclusions</b>	<b>70</b>
6.1	List of Publications . . . . .	73
<b>A</b>	<b>Error Power Analysis of Linear Prediction Based on Cholesky Decomposition</b>	<b>74</b>



# List of Figures

- 1.1 A sketch of deployment volumes of DSL generation through the time [16]. . . . . 2
- 1.2 Network structure of the first and second DSL generations. . . . . 3
- 1.3 Network structure used for the third DSL generation [3]. . . . . 4
- 1.4 Channel spectrum splitted into  $K$  tones. . . . . 4
- 1.5 Simplified scheme of DMT modulation operation. . . . . 6
- 1.6 Interferences in a DSL environment. . . . . 8
- 1.7 Alien crosstalk between twisted pairs of different companies. . . . . 9
  
- 2.1 Complete system with VLs and AXT. . . . . 14
- 2.2 Graphical representation of the third Ginis' method. . . . . 20
- 2.3 Graphical representation of the DFC method. . . . . 22
  
- 3.1 Example of channel phase difference in the coupling between alien lines and vectored lines. It should be noted that there is the condition for a high correlation (on the right-hand side of the diagram),  $\phi_{b,1} - \phi_{c,1} = \phi_{b,2} - \phi_{c,2}$ . . . . . 33
  
- 4.1 System model for a DSL transmission in TC with one RC and multiple interference sources. . . . . 39
- 4.2 The schematic representation of the AMMIS method. . . . . 43
  
- 5.1 Network Analyzer Agilent E5071C. . . . . 46
- 5.2 The cross section scheme of a CAT5 and a CAT6 cable. . . . . 47
- 5.3 Measurement scheme for the coupling between different CAT5 and CAT6 cables. . . . . 47
- 5.4 Measurement setup. In-domain crosstalk is regarded as the crosstalk between twisted-pairs of the same CAT5 cable, while out-of-domain crosstalk is the coupling between pairs of distinct cables. The direct channel is also illustrated. . . . . 48

5.5	All the measurements in the scenario with 2 CAT5 cables. The blue lines represent the direct channels and the green lines are the coupling, both in-domain and out-of-domain. . . . .	49
5.6	All measurements in the scenario with the CAT5-B cable and the CAT6 cable. The blue lines represent the direct channels and the green ones are the coupling, both in-domain and out-of-domain. . . . .	49
5.7	Out-of-domain coupling in the scenario with 2 CAT5 cables. . . . .	50
5.8	Out-of-domain coupling in the scenario with the CAT6 cable and the CAT5 B cable. . . . .	50
5.9	Case where the gains of out-of-domain coupling (red lines) are less than those of in-domain coupling (green lines) in the scenario with 2 CAT5 cables. . . . .	51
5.10	Case where the gains of out-of-domain coupling (red lines) are greater than in-domain coupling (green lines) in the scenario with 2 CAT5 cables. . . . .	52
5.11	Comparison of the correlation matrix element produced by the Monte Carlo simulation and Theoretical derivation (both the real and imaginary part). Scenario with 4 AL and 4 VL. Element (3, 1) of the correlation matrix. . . . .	54
5.12	Comparison of correlation coefficient produced by the Monte Carlo simulation and Theoretical derivation in a situation with thermal noise. Scenario with 1 AL and 4 VL. Element (3, 1) of the correlation matrix. . . . .	55
5.13	Absolute correlation coefficient between the users $a$ and $b$ , and $a$ and $c$ . . . . .	57
5.14	Histogram of the similarity between the phase difference caused by the first AL over users $a$ and $b$ , and the phase difference caused by the second AL over users $a$ and $b$ . . . . .	58
5.15	Histogram of the similarity between the phase difference caused by the first AL over users $a$ and $c$ , and the phase difference caused by the second AL over users $a$ and $c$ . . . . .	58

5.16	Aggregate rates before and after interference mitigation according to the number of ALs using the RxPred algorithm. The (a) refers to the CAT5/CAT5 scenarios, and (b) refers to the scenario CAT6/CAT5. The upper bound represents the aggregate rates achieved in the absence of alien transmissions and the percentage label indicates the <i>recovered rate</i> . The percentage in the top of each group bars indicates the amount of recovered rate in each scenario.	61
5.17	Aggregate rates before and after interference mitigation according to the number of ALs using the DFC algorithm. The (a) refers to the CAT5/CAT5 scenarios, and (b) refers to the scenario CAT6/CAT5. The upper bound represents the aggregate rates achieved in the absence of alien transmissions and the percentage label indicates the <i>recovered rate</i> . The percentage in the top of each group bars indicates the amount of recovered rate in each scenario.	62
5.18	Prediction gain experienced by the VL 2 in scenario CAT5/CAT5, using RxPred. <i>AL</i> denotes number of ALs. . . . .	63
5.19	Prediction gain experienced by the VL 3 in scenario CAT5/CAT5, using RxPred. <i>AL</i> denotes number of ALs. . . . .	64
5.20	Prediction gain experienced by the VL 4 in scenario CAT5/CAT5, using RxPred. <i>AL</i> denotes number of ALs. . . . .	64
5.21	The PSD of the interference in each VL, in the scenario CAT6/CAT5, with 1 Al, using RxPred. . . . .	65
5.22	Results of the experiment with two longitudinally adjacent quad cables. The lines represent the prediction gain of the second line of a vectored group with two lines, in scenarios with 1 and 2 ALs. . . . .	66
5.23	Transmission rates achieved by each mitigation method with a different number of ALs in SCEN1 - 212 MHz. . . . .	69
5.24	Transmission rates achieved by each mitigation method with a different number of ALs in SCEN2 - 100 MHz. . . . .	69

# List of Tables

- 1.1 List of DSL technologies [2, 3, 9, 6, 5]. The *ATP* stands for *Aggregate Transmit Power*. . . . . 2
- 1.2 Taxonomy of interference mitigation methods and experiments. “Coord.” indicates if the coordination is at the receiver (Rx), at both sides (2s), or if there is no coordination at any end of the cable (no). DFE is if the method requires feedback decisions or not. HW indicates whether or not CPE hardware modification is required. “Sensing pair” is whether it uses a spare pair(s) for sensing. Disturb., Technol. and Simulat. mean, respectively, the number of disturbers, DSL technology and kind of simulation used in the experiments for validating the method and comparing it with the baselines. Simulat. can either be “Monte-Carlo” (MC) or “capacity” (Capac.). . . . . 12
- 5.1 Parameters used in the Monte Carlo simulation in the Sec. 5.2.1. . . . . 53
- 5.2 Absolute correlation coefficient according to the phase difference and magnitude of the AXT channels, in a scenario with 2 VL and 2 AL. . . . . 56
- 5.3 The absolute correlation coefficient according to phase difference and magnitude of the AXT channels, in a scenario with 2 VL and 3 AL. . . . . 57
- 5.4 Simulation Parameters. . . . . 59
- 5.5 Simulation parameters for evaluation of the AMMIS performance. . . . . 67
- 5.6 Computational cost of the RxPred, DFC and AMMIS by tone. . . . . 68

# Glossary

**ADSL** Assymetric DSL

**AL** Alien Line

**AMMIS** AXT Mitigation for Multiple Interference Sources

**AWGN** Additive White Gaussian Noise

**AXT** Alien Crosstalk

**BER** Bit Error Rate

**CAT5** Category 5 cable

**CAT6** Category 6 cable

**CO** Central Office

**DMT** Discrete Multitone

**DAC** Digital to Analog Converter

**DFE** Decision Feedback Equalizer

**DFT** Discrete Fourier Transform

**DP** Distribution Point

**DSL** Digital Subscriber Line

**DSLAM** Digital Subscriber Line Access Multiplexer

**DUT** Device Under Test

**FDM** Frequency Domain Modulation

**FEQ** Frequency Equalizer

**FEXT** Far-end Crosstalk

**FFT** Fast Fourier Transform

**FTTc** fiber to the cabinet

**FTTdp** fiber to the distribution point

**Gbps** Gigabit per seconds

**GDFE** Generalized Decision Feedback Equalizer

**G.fast** Fast Access to Subscriber Terminals

**HDSL** High-bit-rateDSL

**IFFT** Inverse Fast Fourier Transform

**ISDN** Integrated-Services Digital Network

**ITU** International Telecommunication Union

**LDL** LDL Decomposition

**MIMO** Multiple-Input-Multiple-Output

**NA** Network Analyzer

**PLC** Power Line Communication

**PSD** Power Spectral Density

**QR** QR Decomposition

**RC** Reference Channel

**RFI** Radio Frequency Interference

**RT** Remote Terminal

**SHDSL** Symmetrical High-Speed DSL

**SIC** Successive Interference Cancellation

**SINR** Signal to Interference plus Noise Ratio

**SISO** Single-Input-Single-Output

**SVD** Singular Value Decomposition

**TC** Transmission Channel

**VDSL** Very High Speed DSL

**VL** Vectored Line

# Symbol List

$H(f)$ : channel frequency response at frequency  $f$ .

$K$ : Number of tones used in a Discrete Multitone Transmission (DMT).

$\Delta f$ : DMT tone width.

$b_k$ : number of bits assigned to the  $k$ -th tone.

$B$ : sum of the bits assigned across all the tones.

$r$ : transmission rate.

$T$ : DMT symbol period.

$\mathcal{E}(k)$ : spectral mask applied to the transmitted symbols of the coordinated group.

$\sigma^2$ : white noise power per tone.

$\Gamma$ : SINR gap.

$l_{mod}$ : intentional SINR loss to achieve the target bit error rate.

$\gamma_m$ : SINR margin.

$\gamma_c$ : SINR gain due to the use of channel coding.

$L$ : the number of vectored lines.

$M$ : the number of alien lines.

$\mathbf{y}_k$ : column vector  $L \times 1$  with the received symbols of the  $L$  vectored lines at the  $k$ -th tone.

$\mathbf{y}$ : column vector  $L \times 1$  with the received symbols of the  $L$  vectored lines at an arbitrary tone.



$\mathbf{x}_k$ : column vector  $L \times 1$  with the transmitted symbols of the  $L$  vectored lines at the  $k$ -th tone.

$\mathbf{x}$ : column vector  $L \times 1$  with the transmitted symbols of the  $L$  vectored lines at an arbitrary tone.

$\mathbf{z}_k$ : column vector  $L \times 1$  which represents the whole interference (alien crosstalk plus white noise) observed at the  $L$  vectored lines.

$\mathbf{\Lambda}_k$ : diagonal  $L \times L$  matrix with the direct channel of the  $L$  vectored lines at the tone  $k$ .

$\mathbf{q}$  or  $\mathbf{q}_k$ : column vector  $L \times 1$  which represents the AXT observed at the  $L$  vectored lines.

$\mathbf{n}$ : column vector  $L \times 1$  which represents the white noise observed at the  $L$  vectored lines.

$\mathcal{E}_s$ : the power by tone of the alien lines.

$\mathbf{q}_l$ : the AXT across all tones of the vectored line  $l$ .

$\mathbf{s}_m$ : the  $2K$  time domain domain samples transmitted by the alien line  $m$ .

$\mathbf{A}_{l,m}$ : the convolution matrix to the channel from the alien line  $m$  to the vectored line  $l$ .

$\mathbf{T}_{l,m}$ : the FFT matrix from the alien line  $m$  to the vectored line  $l$ .

$\eta_{l,m}$ : the length of the nonzero part of the impulse response of the channel from the  $m$ -th AXT source to the  $l$ -th vectored line

$\mathbf{T}_{l,m}(k, :)$ : the  $k$ -th line of the  $\mathbf{T}_{l,m}$  matrix.

$\mathbf{p}_l$ : a  $L \times 1$  vector which has only a nonzero element equals to one in the  $l$ -th position.

$\mathbf{A}_m$ : a  $L \times 2K$  matrix which is given by  $\sum_{l=1}^L \mathbf{p}_l \mathbf{T}_{l,m}(k) \mathbf{A}_{l,m}$ .

$\mathbf{C}_q$ : correlation matrix of  $\mathbf{q}$ .

$C_q(b, c)$ : the element at the  $b$ -th line and  $c$ -th column of the correlation matrix of  $\mathbf{C}_q$ .

$\mathbf{C}_m$ : canonical correlation matrix of the channels from the  $m$ -th AL to the vectored system.

$C_m(b, c)$ : the element at the  $b$ -th line and  $c$ -th column of the correlation matrix of  $\mathbf{C}_m$ .

$\rho_{b,c}$ : the correlation coefficient between the AXT observed in the VLs  $b$  and  $c$ .

$P_m$ ,  $m = 1, \dots, M$ : the value of the diagonal of  $\mathbf{C}_m$ .

$\phi[\cdot]$  = phase of a complex number.

$\nu_\zeta$ : the column vector relative to the  $2K$  time-domain samples of the  $\zeta$ -th AWGN source.

$\Psi_{l,\zeta}$ : the correspondent convolution matrix to the coupling of the AWGN source  $\nu_\zeta$ .

$\Psi_\zeta$ : the coupling matrix due to the  $\zeta$ -th AWGN source, given by  $\sum_{l=1}^L \mathbf{p}_l \mathbf{T}_{l,\zeta}(k, :) \Psi_{l,\zeta}$ .

$x_{TC}$ : transmitted signal at TC.

$x_{RC}$ : transmitted signal at RC.

$y_{TC}$ : received signal at TC.

$y_{RC}$ : received signal at RC.

$z_{TC}$ : total interference at TC.

$z_{RC}$ : total interference at RC.

$\hat{\mathbf{H}}$ : equivalent channel after pre and post-processing at AMMIS.

$\mathbf{v}$ : resulting interference after processing at receiver in the AMMIS, with the elements  $[v_{tc} \ v_{rc}]^T$ .

$\hat{\mathbf{y}}$ : received symbols after whitening in the AMMIS.

$\tilde{\mathbf{y}}$ : received symbols after whitening and correlation induction in the AMMIS, with the elements  $[y_{tc} \ y_{rc}]^T$ .

$\mathbf{C}_u$ : desired correlation matrix of the interference in the AMMIS.

$\mathbf{G}_u$ : lower triangular matrix of the Cholesky decomposition of the  $\mathbf{C}_u$ .

$\mathbf{b}$ : vector with the elements of the  $\mathbf{v}$  in the changed positions,  $[v_{rc} \ v_{tc}]^T$ .

$\mathbf{C}_b$ : correlation matrix of the  $\mathbf{b}$  matrix.

$\mathbf{G}_b$ : lower triangular matrix of the LDL decomposition of the  $\mathbf{C}_b$ .

$\hat{v}_{tc}$ : prediction of  $v_{tc}$ .

$\mathcal{E}_{TC}$ : the transmission power of the  $x_{TC}$  by tone.

$\tau$ : the channel gain observed by the  $x_{TC}$ .

$e_{TC}$ : the error in the prediction of the  $v_{TC}$ .

# Chapter 1

## Introduction

### 1.1 DSL Technology

Metallic wires have been used to convey information since the 19<sup>th</sup> Century. These type of communication systems were first deployed by Samuel Morse, who showed that communication could be effected by means of electromagnetism, and by Alexander Graham Bell who invented the telephone [1, 3]. Since then, these experiments have inspired many inventors and engineers to improve the systems that rely on metallic wires to convey information in the form of electromagnetic waves. Among the many forms of wired communication today, one of the most widespread is the *Digital Subscriber Line*(DSL) [4, 1].

DSL technology has been available on the market since the 1980s [5]. Access to this kind of technology has become popular owing to the low cost of the equipment and cables (when compared with those of other technologies), and the fact that the legacy infrastructure of the telephone network can be reused. Since the 1980s, there have been several versions of DSL, as listed in Table 1.1.

Table 1.1: List of DSL technologies [2, 3, 9, 6, 5]. The *ATP* stands for *Aggregate Transmit Power*.

Version	Approved	Range (km)	Aggreg. Rate (Mbps)	Bandwidth (MHz)	Duplexing	Modulation	ATP (dBm)
ISDN	1988	5.5	2.048	0.16	-	2B1Q	-
HDSL	1994	3.5	2.048	0.196		2B1Q/CAP	13.5
SHDSL	1999		4.72	0.34	FDD	TC-PAM	14.5
ADSL	1999	5	9.5	1.1	FDD	DMT	19.9
ADSL2+	2003	5	25.5	2.2	FDD	DMT	19.9
VDSL	2004	1	70	17	FDD	DMT	14.5
VDSL2	2005	1	100	30	FDD	DMT	14.5
G.fast	2014	0.25	1000	106 (or 212)	TDD	DMT	4.0
XG.fast	-	0.25	10000	500	TDD	DMT	-

Table 1.1 shows the advance made in DSL technology, and the transmission features of each version. This Table also makes clear that the rate of transmission increases with the evolution of DSL, from 2.048 Mbps in ISDN to 1 Gbps in G.fast. A significant factor that adds to the information supplied in Table 1.1, is the volume in the deployment of DSL technologies through time - as showed in Fig. 1.1, which divides the application of DSL technologies into different generations.

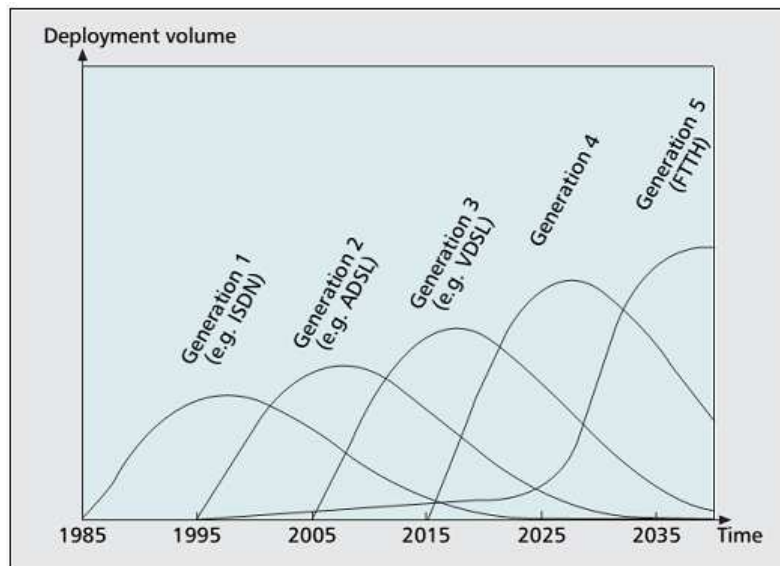


Figure 1.1: A sketch of deployment volumes of DSL generation through the time [16].

The first generation (ISDN- Integrated-services digital network, HDSL - High-bit-rate DSL, and SHDSL - Symmetrical high-speed DSL) depended on the voice bandwidth, and line code for transmission. However, in the case of the second generation (ADSL - Asymmetric DSL), the DSL began to use frequencies other than voice band. Other developments in the

second generation included the asymmetric use of the band to download and upload, with the larger part to download and the smaller to upload, and the use of *Discrete Multitone* (DMT) modulation. The third generation, represented by VDSL/VDSL2 (Very High Speed DSL), took the DSL to the scale of a hundred Mbps and backed the use of symmetric bands for downloading and uploading, although this technology requires the use of interleaved frequency bands. The fourth generation is the G.fast, which delivers up to 1 Gbps, using 106 MHz of bandwidth in the first deployment, and 212 MHz in the second [13, 11, 12]. On the basis of the estimates of [16], the next generation will offer rates of the order of 10 Gbps. This 5th generation (the last line of Table 1.1) has not been not standardized yet, although it has been investigated, and the preliminary results show that data rates of the order of tens of Gbps can be achieved [14, 15].

With regard to the structure of the network, in the first and second generations, it consisted of the *Central Office* (CO) of the provider, which contained the *Digital Subscriber Line Access Multiplexer* (DSLAM), the telephone cables (each with many twisted pairs inside), and the user's building (Fig. 1.2) [6]. With the introduction of the third generation, another structural paradigm was adopted to ensure the high-rates were conveyed. This means that instead of directly connecting the premisses of the user to the CO, the data could now be transmitted through optical fiber, to a distribution point (FTTdp - fiber to the distribution point) or to a cabinet (FTTc - fiber to the cabinet), and from this point a twisted pair connects the multi-user installations to the network. Thus, short copper loops can be employed, that allow the use of larger bandwidth and high transmission rates [3, 16], as depicted in Fig. 1.3, which highlights the loop length in some DSL technologies.

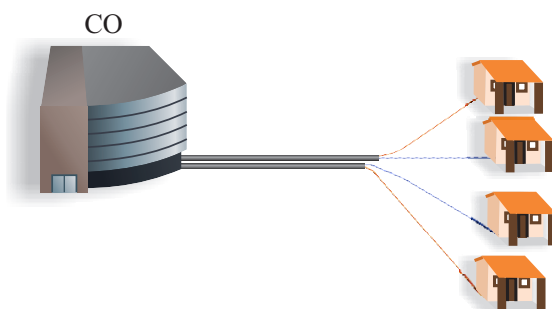


Figure 1.2: Network structure of the first and second DSL generations.

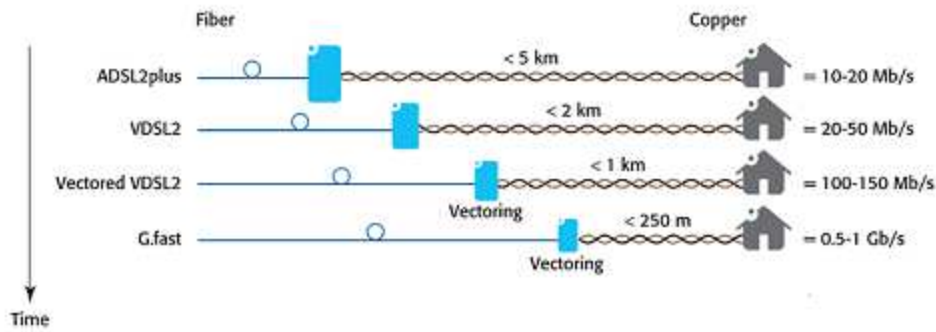


Figure 1.3: Network structure used for the third DSL generation [3].

As well as being long time in action, it is expected that the DSL systems will be used in the next decade, because of its widespread coverage through the world, and the investment of the great telecommunication companies in the new DSL standard (G.fast) as an access technology to serve high data rates [13, 11].

## 1.2 Discrete Multi-Tone (DMT) Modulation

DMT is a multicarrier modulation, i.e., it divides the available transmission band into subbands (also called tones), where independent signals are transmitted. This kind of modulation differs from the standard FDM (Frequency Division Multiplexing) insofar as all the tones are used to transmit a single bitstream. Fig. 1.4 shows an example in which the frequency response of the transmission channel,  $H(f)$ , was split into  $K$  tones. Each tone has the  $\Delta f$  width in the frequency domain, which is called *tone bandwidth* (in DSL all the tones have the same bandwidth, so that their time representation will have the same period). It can also be seen in this diagram that each tone is centered on a frequency ( $f$ ), which is called the nominal frequency of the tone. The signals sent in these tones are transmitted in parallel, so that the unified time representation of the tones form a DMT symbol  $s$  [7, 17].

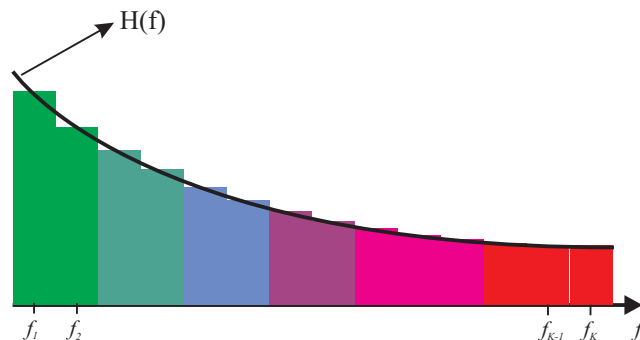


Figure 1.4: Channel spectrum splitted into  $K$  tones.

A number  $b_k$  of bits can be transmitted in each tone, and this is defined by the quality of each tone. Thus, the total number of bits transmitted, ( $B$ ), in a DMT symbol is

$$B = \sum_{k=1}^K b_k. \quad (1.1)$$

Therefore, the transmission rate achieved by the system is  $r = B/T$  [17], where  $T$  is the DMT symbol period.

The operation of the DMT transmission is shown in a simplified form in Fig. 1.5. The process begins with a bistream arriving as input of Block **1** where the serial-to-parallel conversion takes place. In this block, the bits are also grouped in accordance with the capacity of each tone and the mapping from bits to QAM symbols is performed [10]. These QAM symbols are then passed to Block **2**. In Block **2**, each QAM symbol will be treated as a frequency-domain coefficient, to which an *Inverse Fast Fourier Transform* (IFFT) [10] is applied. However, before the execution of the IFFT, it is necessary to order the QAM symbols to ensure they have Hermitian symmetry, so that real numbers can be obtained at the output of the IFFT. This procedure doubles the number of QAM symbols, and then we have  $2K$  values in the IFFT output. It should be noted here that IFFT then becomes the channels orthogonal and thus avoids inter carrier interference. After Block **3** receives the samples of the IFFT, it performs the parallel-to-serial conversion, and adds the cyclic extension. These samples are then sent to the *Digital to Analog Converter* (DAC) [18], in order to get a time domain signal. Apart from the steps listed above, the process also carries out some filtering operations.

The inverse processing is carried out on the receiver side and includes the following: analog-to-digital conversion, removal of cyclic extension, serial to parallel conversion, application of FFT, removal of half of the coefficients (due to Hermitian symmetry), frequency equalization, decoding of the QAM symbols to bits, and parallel to serial conversion.



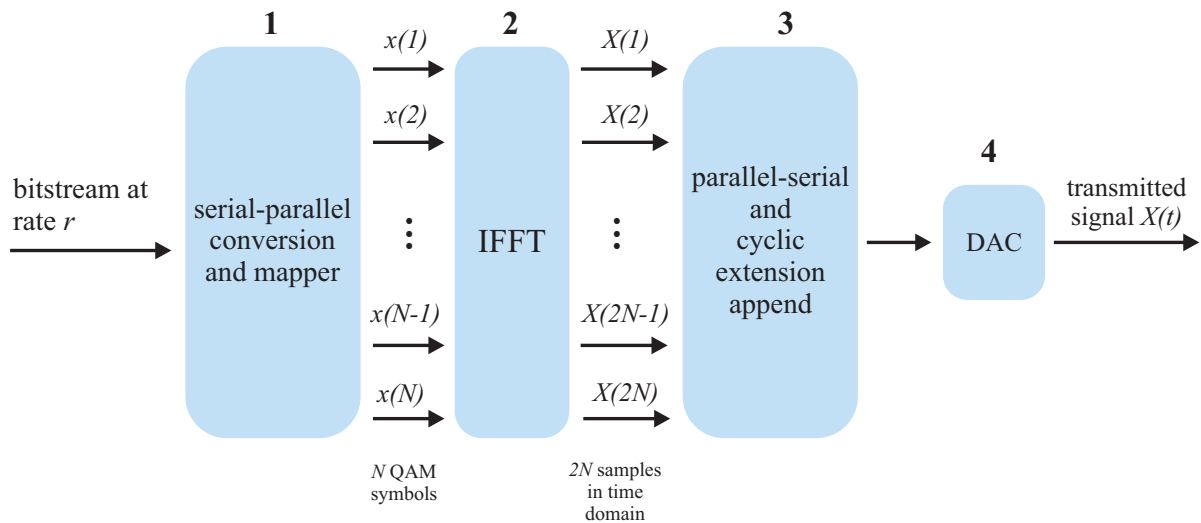


Figure 1.5: Simplified scheme of DMT modulation operation.

As stated earlier, the number of bits allocated for each tone depends on the channel quality of the tone. This quality is generally measured by the *Signal-to-Interference-plus-noise Ratio* (SINR) of the tone, as expressed in the equation below

$$\text{SINR} = \frac{\mathcal{E}(k)|H(k)|^2}{\sigma^2 + z(k)}, \quad (1.2)$$

where  $\mathcal{E}(k)$  is the spectral mask of the direct channel,  $H(k)$  is the channel frequency response at tone  $k$ ,  $\sigma^2$  is the power of the thermal noise at tone  $k$ , and  $z(k)$  is the sum of the interference signals, in tone  $k$  [20]. The bit allocation procedure assigns the number of bits according to the magnitude of the SINR of the tone. In general, the equation for bit allocation is given by

$$b_k = \log_2(1 + \text{SINR}). \quad (1.3)$$

Note that Eq. 1.3 has the range from 0 to  $\infty$ , but the number of bits assigned to one tone must correspond to the maximum and minimum number of bits by tone defined by the system. Although Eq. 1.2 is in accordance with the theoretical formulation, the SINR is generally scaled by a factor  $\Gamma$

$$\Gamma = l_{mod} + \gamma_m - \gamma_c, \quad (1.4)$$

where  $L_{mod}$  is an intentional loss that seeks to achieve a *bit error rate* (BER) defined by the system,  $\gamma_m$  is called *margin* (an extra amount that is included to avoid decline in performance as a result of unexpected interference levels), and  $\gamma_c$  is the gain made from the use of a channel code.

## 1.3 Interference in DSL Systems

The DSL systems are plagued by a wide range of interferences like background noise, impulsive noise, crosstalk, *radio frequency interference* (RFI), etc. Background noise, also termed thermal noise, is the signal which is observed in an idle twisted pair, when there is no transmission in the adjacent pairs of the cable bundle. This signal is modeled as a white gaussian sequence, and owing to the additive effect on the target received signals, it is called Additive White Gaussian Noise (AWGN). The *power spectral density* (PSD) of this noise is generally assumed to be flat with level  $-140$  dBm/Hz or  $-150$  dBm/Hz [10, 21, 22].

The study on impulsive noise dates from the 1960s, when errors induced into voiceband modems over dial-up links began to be investigated [8]. The impulsive noise is a nonstationary stochastic interference, characterized by short pulses with significant amounts of energy. This interference arises from a wide range of man-made equipment and also from environmental disturbances such as signaling circuits, transmission and switch gear, electrostatic discharges, lighting power surges, etc [19].

The RFI interference that occurs in DSL systems is caused by the properties of a twisted pair to acts like an antenna and both radiates to and receives energy from radio signals in the overlapping bands between the DSL and the radio systems [23, 8]. This matter is particularly serious because when the telephone network was first developed several decades ago, the RFI was not a problem since low frequencies were used in voice communications. At that time, the aerial placement of the twisted pairs was not regarded as a technical constraint. In the early versions of DSL, the main RFI source was the amateur radio (HAM) [23], particularly for VDSL, but the new versions of DSL can be subject to RFI from other wired communication systems, like *power line communication* (PLC) [24].

Crosstalk is generated by the electromagnetic coupling that occurs between twisted pairs. These are the main limiting factors in the data rates achievable in DSL systems, because they can attain all transmission bands, due to the intensity of the interferer signals, and due to the cable organization of the twisted pairs, which increases the number of interferers [8, 25, 26]. Fig 1.6 shows all the previous types of interferences in a single diagram.

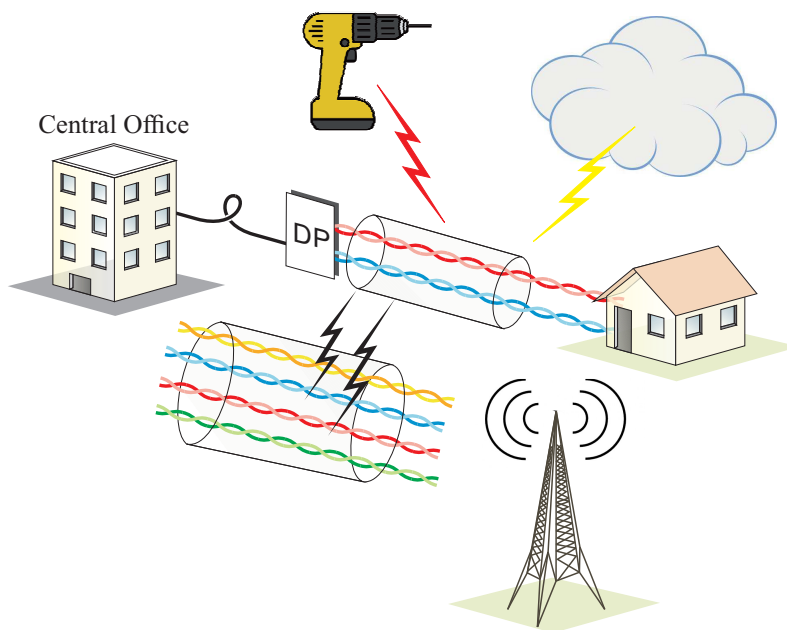


Figure 1.6: Interferences in a DSL environment.

## 1.4 A Literature Review of Noise and Interference Mitigation in Copper-Based Transmission

The G.fast standard [27] is based on the *Fiber to the Distribution Point* (FTDP) architecture, in which an optical fiber reaches a DP and, from the DP, copper cables establish connection to the user's premises. Owing to its relatively large bandwidth, the existing far end crosstalk (FEXT) from coordinated twisted pairs, requires the adoption of crosstalk mitigation techniques that are collectively called *vectoring* [28, 4, 22].

Vectored DSL G993.5 [29] led to a significant rate increase by means of *in-domain crosstalk* cancellation, i.e., the crosstalk between the coordinated twisted pairs. Other approach to cancel in-domain crosstalk is based in a non-linear precoding, which is suitable for the high frequencies in the G.fast band [89, 90]. However, the operation of the system can still be significantly constrained by the presence of *alien* or *out-of-domain crosstalk*, which arises from interference sources that lie outside the vectored DSL system but share the same cable binder [84, 30, 47, 24]<sup>1</sup>, as in Fig. 1.7.

<sup>1</sup>Some works consider radio frequency interference as part of alien crosstalk, as in [30].

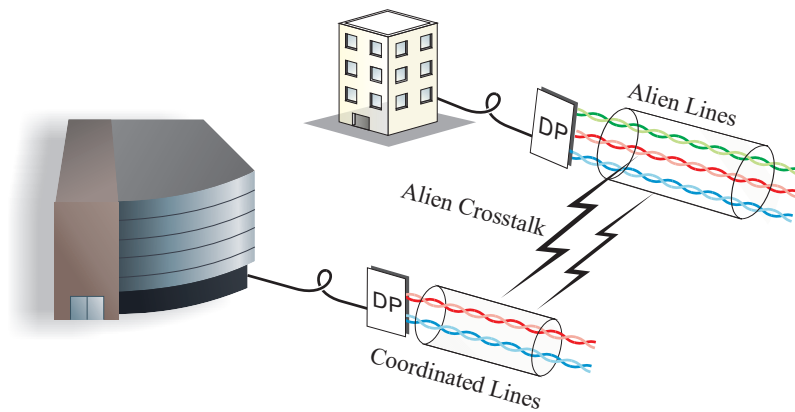


Figure 1.7: Alien crosstalk between twisted pairs of different companies.

Most of the mitigation techniques are based on joint signal processing at the receiver, or transmitter or both ends, and are generally described as MIMO (Multiple-Input-Multiple-Output) techniques with coordinated reception, transmission or “two-sided” coordination, respectively. While MIMO is a term used for all of them, “vectoring” will be restricted here to the strategy based on linear precoding and coordinated reception as standardized in ITU G993.5 [29] and adapted to G.fast with a 106 MHz profile [27]. In this context, interference between G.fast and other systems such as PLC are of current interest [24].

This work is concerned with interference mitigation for G.fast vectored lines (VL). But some of the algorithms can also be used for copper-based transmission systems other than G.fast, such as radio-over-copper architectures (see, e. g., [31]).

In a similar way to in-domain crosstalk cancellation, alien crosstalk (AXT) cancellation techniques take advantage of the co-location at one or two sides of the communication. Hence, practical scenarios include both access networks, which have lines that are co-located at the central office (CO), remote terminal (RT) or distribution point (DP), and copper-based backhauling, the lines of which that arrive at or leave both sides, are co-located and can use *bonding* [15] (the use of several pairs to transmit a single stream).

The following paragraphs provide a brief overview of the literature on interference mitigation for DSL (including G.fast). Instead of concentrating only on AXT mitigation, other types of interferences are covered, such as radio frequency (RFI) to give a more comprehensive view.

One important aspect of interference mitigation for DSL, is the use of common-mode signals. In [32, 33, 34, 35, 36, 37, 38] a common mode signal was used as reference in a linear adaptive filtering approach to mitigate AXT in differential mode. The approach adopted by these methods required modifications in the modem hardware/firmware to allow access to the common mode signal, which is a drawback in some cases. In [40], the method does not rely

on joint signal processing of signals from multiple pairs.

A set of operations must be found to get the AXT cancellation in a suitable way so that the diagonal structure of the vectored channel matrix is preserved and, at the same time, the effects of the AXT components on in-domain transmitted symbols are mitigated. There have been several works that address these requirements.

The seminal work in [41] proposed *decision-feedback* and *noise-predictive* approaches to achieve noise decorrelation by coordinating the transmitter with the receiver. It worked not on DMT (frequency-domain), but on time-domain and used generalized Yule-Walker equations to define the weights of the predictors. The noise-predictive *decision-feedback equalizer* (DFE) discussed early and used by many other algorithms, was examined in [42] and is discussed e. g. in [43]. However, it has presented just the formulation for SISO system. Nevertheless, [44] presented a general framework for multiple-input multiple-output (MIMO) receivers and introduced the generalized DFE (GDFFE).

Some mitigation methods proposed an AXT mitigation algorithm that requires co-location on both sides, as in [45, 39, 46]. These carry out a tone-based MIMO post and pre-processing to decorrelate the AXT parcel on symbols received by the VLs.

In [47], three methods for AXT mitigation are discussed, and it is shown that all three achieve the same capacity with regard to the sum rate. Hence, these three methods achieve the same theoretical performance, although with different computational costs and in different application scenarios. It should be noted that, even if the method achieves the same sum rate capacity, the individual rates achieved by the coordinated lines may not be balanced and this can be problematic [83]. [47] also conducted an experiment with a single alien line (AL) by running a T1 line code to illustrate that the correlation of crosstalk signals is stronger on a tone-basis and leads to methods that explore this “spatial” correlation. In summary, the three methods discussed in [47] are:

- *First method (2sWpSVD): Two-sided coordination.* This is based on [48] and uses a Cholesky decomposition for noise whitening and singular value decomposition (SVD) to restore the channel partitioning (diagonalization of the channel matrix of VLs).
- *Second method (RxGDFFE): Receiver coordination with decision-feedback structure.* This method applies the GDFFE of [44] to the AXT mitigation problem, which only requires coordination at the receiver side. As discussed e. g. in [9], the GDFFE is used for the purpose of noise decorrelation.
- *Third method (RxPred): Receiver Coordination with a Noise Prediction Structure.* This method is an original contribution according to [47], and consists of an extended version

---

of the noise-predictive approach of [41], applied to DMT transmission. It is similar to RxGDFE but, instead of decorrelating the noise with the GDFE feedforward section and then canceling the interference by subtracting the weighted estimates of the symbols as in RxGDFE, the receiver noise in RxPred is directly decorrelated by estimating and subtracting the error of the decoder. This follows the concept of a noise-predictive decision-feedback equalizer [43].

More recently, several studies have addressed the question of AXT mitigation [49, 30, 50, 51, 88]. For example, [51] employed a method to estimate the autocorrelation matrix on the basis of a cyclostationary signal analysis. In [88] a strategy to train an alien crosstalk canceler in the presence of intermittent interference, in which the common-mode is used to sense the interference. Table 1.2 lists some of the published works. The header “Coord.” indicates if the method needs one-sided coordination (Rx), two-sided coordination (2s), or no coordination (no). “Type” refers to the type of interference for which the method is intended. “DFE” denotes if the method provides feedback for the decision. “HW” indicates if the method needs modifications in its hardware, like in some cases where information is used in a common mode. “Sensing” pair is if it uses spare pair(s) for sensing. “Disturb”, “Technol.” and “Simulat.”, refer to the number of disturbers considered in simulation, the DSL technology and the simulation type used for validating the method and compare it with the baselines. “Simulat.” can be “Monte-Carlo” (MC) or “capacity” (Capac.).

Table 1.2: Taxonomy of interference mitigation methods and experiments. “Coord.” indicates if the coordination is at the receiver (Rx), at both sides (2s), or if there is no coordination at any end of the cable (no). DFE is if the method requires feedback decisions or not. HW indicates whether or not CPE hardware modification is required. “Sensing pair” is whether it uses a spare pair(s) for sensing. Disturb., Technol. and Simulat. mean, respectively, the number of disturbers, DSL technology and kind of simulation used in the experiments for validating the method and comparing it with the baselines. Simulat. can either be “Monte-Carlo” (MC) or “capacity” (Capac.).

Publication		Method					Experiment(s)		
Reference	Year	Coord.	Type	DFE	HW	Sensing	Disturb.	Technol.	Simulat.
[32]	2003	no	RFI	no	yes	yes	-	VDSL	MC
[37]	2005	no	Axtalk	no	yes	yes	-	ADSL	MC
[38]	2005	Rx	Axtalk/RFI	no	yes	yes	-	MultiCh	-
[52]	2005	no	IN	no	no	no	-	OFDM	MC
[47]	2006	2s	Axtalk	no			1	ADSL2+	Capac.
[47]	2006	Rx	Axtalk	yes			1	ADSL2+	Capac.
[47]	2006	Rx	Axtalk	yes			1	ADSL2+	Capac.
[35]	2007	no	Axtalk	no	yes	yes	5	VDSL2	MC
[53]	2010	no	NBI	no	no	yes	-	OFDM	MC
[54]	2012	Rx	RFI	no	yes	yes	-	xDSL	-
[50]	2013	Rx	Axtalk	yes	no	no	4	VDSL	MC
[51]	2014	Rx	Axtalk	yes	no	no	3	VDSL2	MC
[24]	2014	no	PLC	no	yes	yes	1	xDSL	MC

## 1.5 Objectives

This study seeks to evaluate the characteristics of the AXT that affect the spatial correlation of the interference observed in the vectored group and ultimately restrict the performance achieved by the prediction-based AXT mitigation method within the G.fast application scenario. Special attention is paid both to the behavior (with regard to the number of out-of-domain crosstalk sources in the system) and the individual transmission rate imbalance resulting from the mitigation scheme. The purpose of the work is to supplement the findings of our earlier feasibility study of AXT in G.fast [81], which addressed the problem

---

of AXT mitigation with regard to the way of the interference is generated. This was a study that was driven by the importance of AXT owing to the effect it has on G.fast systems. However, [81] did not set out the formal conditions required for a suitable performance of AXT prediction. In view of this, this study develops the formulations for this issue. Although the formulations outlined here can be applied to a performance analysis of prediction-based methods, in general, the third method employed in [47] is used here as a reference-point. It should be noted, however, that some of the results may also be applicable to other copper-based transmission systems apart from G.fast, such as radio-over-copper architectures [31].

Additionally, this work employs an effective AXT mitigation method for downstream transmissions that have been impaired by multiple interference sources, in which a minimum coordination at the receivers is created through the use of one reference channel per information transmitter. This method needs both precoding and post-coding, and includes a stage of signal conditioning at the receiver, that can enable the interference to be removed in a suitable way by only using one reference channel through an AXT prediction-based procedure in the next stage.

This study is organized as follows. In Chapter 2 we present the standard model for the AXT and some literature mitigation methods for AXT mitigation. While Chapter 2 is based on the literature, Chapter 3 is a contribution of this work to a better understanding of the AXT mitigation methods. In the Chapter 4 we present an alien crosstalk mitigation suitable for downstream transmissions impaired by multiple inference sources called AMMIS. The theoretical analysis is underpinned by the results that are shown in Chapter 5, where a performance evaluation is carried out of the AXT mitigation method in the literature and AMMIS, in different scenarios. Additionally, this chapter provides details of the measurements that we have obtained to evaluate the AXT mitigation method. Finally, Chapter 6 summarizes the conclusions of this work.



# Chapter 2

## Alien Crosstalk Mitigation: Literature Review

This chapter sets out the standard systems model of a DSL transmission impaired by AXT, as well some algorithms created in the literature to mitigate the effects of the AXT on DSL communications.

### 2.1 Alien Crosstalk System Model

Alien crosstalk can be interpreted as the crosstalk caused by sources outside the vectored group into the pairs that form it. Fig. 2.1 illustrates this scenario, where  $L$  vectored lines (VLs) are affected by the AXT (represented by arrows) caused by  $M$  alien lines.

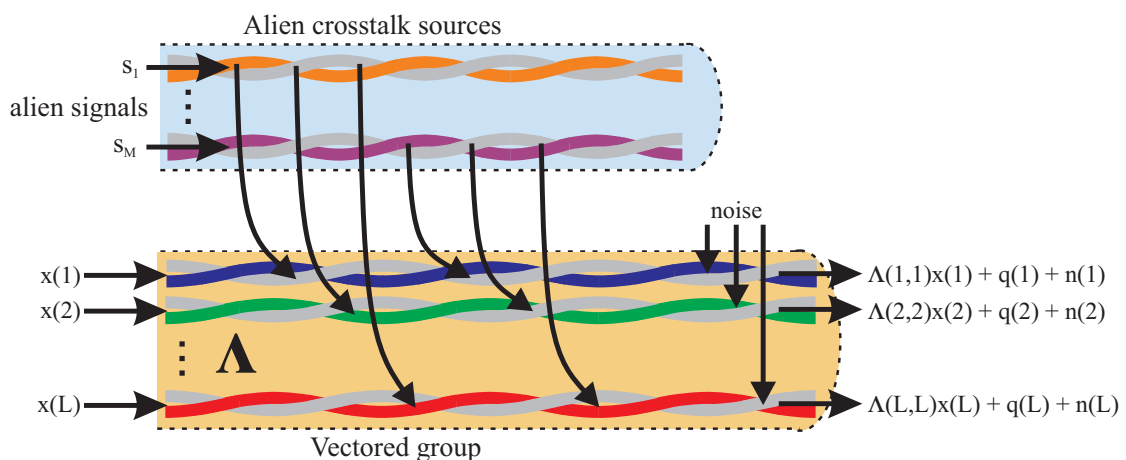


Figure 2.1: Complete system with VLs and AXT.

In this work, in-domain crosstalk is assumed to be perfectly cancelled by the standardized *vectoring* techniques described in [29]. Hence, it is assumed that AXT and background noise are the only factors that impair the vectored group. In this case, the frequency domain symbols  $\mathbf{y}_k = [y_k(1), \dots, y_k(L)]^T$  received by the  $L$  VLS at tone  $k$ , can be modeled by:

$$\mathbf{y}_k = \mathbf{\Lambda}_k \mathbf{x}_k + \mathbf{z}_k \quad k = 1, \dots, K, \quad (2.1)$$

where  $K$  is the length of the *Discrete Fourier Transform* (DFT),  $\mathbf{\Lambda}_k$  is a complex  $L \times L$  diagonal matrix comprising the direct vectored channel frequency response values at tone  $k$ ,  $\mathbf{x}_k = [x_k(1), \dots, x_k(L)]^T$  is the  $L \times 1$  vector containing the QAM encoded transmitted symbols at the  $k$ -th tone and  $\mathbf{z}_k$  is an  $L \times 1$  vector corresponding to both additive white Gaussian noise and AXT at the  $k$ -th tone. The following formulations will be tone based, then, to improve the readability we will omit the under script  $k$ . Then, (2.1) can be written in an expanded form as

$$\mathbf{y} = \mathbf{\Lambda} \mathbf{x} + \mathbf{q} + \mathbf{n}, \quad (2.2)$$

where  $\mathbf{q} = [q(1), \dots, q(L)]^T$  and  $\mathbf{n} = [n(1), \dots, n(L)]^T$  are the vectors corresponding to AXT and background noise, respectively. The  $l$ -th element  $z(l)$  of the total noise vector  $\mathbf{z}$  in (2.1) is formed of two parcels: the white background noise  $n(l)$  and the AXT  $q(l)$  experienced by line  $l$  in a specific tone.

## 2.2 Methods to Mitigate Alien Crosstalk

The study carried out by [47] employed three methods for AXT mitigation. The first method relies on decorrelation technique, the second adopts decision feedback equalization to remove the effects of AXT and the third involves noise linear prediction. Additionally, the method presented in [51] used whitening and QR decomposition in a structure like *successive interference cancellation*. In this section, these 4 methods are presented. We chosen these methods to examine because together they present the majority of the strategies used in the literature related to alien crosstalk mitigation.

### 2.2.1 First Ginis' Method: Two-sided coordination

The first method in, [47], requires additional processing at both the transmitter and the receiver (two-sided coordination) to achieve noise decorrelation and maintain the diagonalized channel for the vectored group. As a result of the processing, the received symbols at a given

tone become:

$$\tilde{\mathbf{y}} = \mathbf{\Sigma}\tilde{\mathbf{x}} + \tilde{\mathbf{z}}, \quad (2.3)$$

where  $\mathbf{\Sigma}$  is a diagonal matrix and  $\tilde{\mathbf{z}}$  is the  $L \times 1$  vector with the total noise after the decorrelation. In the sequel, the stages followed to achieve this result are shown.

Let  $\mathbf{C}_z$  represent the correlation matrix for the total noise  $\mathbf{z}$  (sum of AXT and background noise) at a given tone, which is calculated as

$$\mathbf{C}_z = E[\mathbf{z}\mathbf{z}'], \quad (2.4)$$

where  $\mathbf{E}[\cdot]$  denotes the expected value and the superscript  $'$  denotes the conjugate transpose (Hermitian) operation. The Cholesky decomposition (also called *LDL decomposition*) [55] of  $\mathbf{C}_z$ , give us

$$\mathbf{C}_z = \mathbf{G}\mathbf{D}\mathbf{G}', \quad (2.5)$$

where  $\mathbf{G}$  is lower-triangular and monic (i.e., has ones along the main diagonal) and  $\mathbf{D}$  is a diagonal matrix with real values. The reason why this decomposition exists, is that a correlation matrix is by definition symmetric and positive definite [76].

Hence, if the received symbols are multiplied by  $(\mathbf{G}\mathbf{D}^{1/2})^{-1}$ , the resulting total noise,  $\mathbf{D}^{-1/2}\mathbf{G}^{-1}\mathbf{z}$ , will have a correlation matrix given by

$$\begin{aligned} \mathbf{C}_{\tilde{\mathbf{z}}} &= E\left[(\mathbf{D}^{-1/2}\mathbf{G}^{-1}\mathbf{z})(\mathbf{D}^{-1/2}\mathbf{G}^{-1}\mathbf{z})'\right] \\ &= \mathbf{D}^{-1/2}\mathbf{G}^{-1}E[\mathbf{z}\mathbf{z}'](\mathbf{G}^{-1})'(\mathbf{D}^{-1/2})' \\ &= \mathbf{D}^{-1/2}\mathbf{G}^{-1}\{\mathbf{C}_z\}(\mathbf{G}^{-1})'(\mathbf{D}^{-1/2})' \\ &= \mathbf{D}^{-1/2}\mathbf{G}^{-1}\{\mathbf{G}\mathbf{D}^{1/2}(\mathbf{D}^{1/2})'\mathbf{G}'\}(\mathbf{G}^{-1})'(\mathbf{D}^{-1/2})' \\ &= \mathbf{I}, \end{aligned} \quad (2.6)$$

where (2.5) was used and  $\mathbf{I}$  is an identity. Thus, the total noise becomes uncorrelated.

Without a loss of generality, if the correlation matrix can be expressed as a product between two non-singular matrices:

$$\mathbf{C}_z = \mathbf{C}_z^{1/2}(\mathbf{C}_z^{1/2})', \quad (2.7)$$

then, in order to achieve noise decorrelation, it suffices to multiply the vector with the subsymbols received by the VLS at tone  $k$  by  $\mathbf{C}_z^{-1/2}$ .

Once the residual noise part in the received symbols  $\tilde{\mathbf{z}}_k$  is no longer correlated, it can be treated as white noise. Hence, at this point, the remaining requirement is to ensure that the vectored channel matrix for each tone  $k$  is still diagonal. To achieve this, it should be

noted that after the decorrelation the effective channel  $\tilde{\Lambda}$  (at a given tone with regard to the original diagonal channel  $\Lambda$  in 2.1) becomes:

$$\tilde{\Lambda} = \mathbf{C}_z^{-1/2} \Lambda. \quad (2.8)$$

Then, through its SVD decomposition [66], it can be expressed as:

$$\tilde{\Lambda} = \mathbf{U} \Sigma \mathbf{V}', \quad (2.9)$$

where  $\mathbf{U}$  and  $\mathbf{V}'$  are unitary matrices, and  $\Sigma$  is a diagonal matrix with positive elements in descending order. Hence, the received subsymbols at the given tone can be expressed as:

$$\mathbf{y} = \mathbf{U} \Sigma \mathbf{V}' \mathbf{x} + \tilde{\mathbf{z}}. \quad (2.10)$$

From an inspection of Eq. 2.10, it becomes clear that if  $\mathbf{V}\mathbf{x}$  is transmitted in place of  $\mathbf{x}$  and  $\mathbf{U}'\mathbf{C}_z^{-1/2}$  it is used to decorrelate the noise in the received symbols in place of  $\mathbf{C}_z^{-1/2}$ , then the subsymbols received by the VLs at tone  $k$  become:

$$\begin{aligned} \tilde{\mathbf{y}} &= \mathbf{U}' \mathbf{U} \Sigma \mathbf{V}' \mathbf{V} \mathbf{x} + \mathbf{U}' \tilde{\mathbf{z}} \\ \tilde{\mathbf{y}} &= \Sigma \mathbf{x} + \mathbf{U}' \tilde{\mathbf{z}}, \end{aligned} \quad (2.11)$$

where the fact that  $\mathbf{U}$  and  $\mathbf{V}'$  are unitary matrices was used. Additionally, since  $\mathbf{U}$  is unitary, the  $\mathbf{U}'\tilde{\mathbf{z}}$  parcel remains uncorrelated and has the same power. Thus, Eq. 2.11 can be reduced to the original expression in 2.3.

It is important to note that, besides being a tool for maintaining the vectored channel diagonal (with no in-domain crosstalk), the SVD decomposition also keeps a relation which preserves the signal to noise ratio (SNR), as observed in [48].

### 2.2.2 Second Ginis' Method: Receiver coordination with decision-feedback structure

The previous method achieved mitigated interference by introducing processing at both the transmitter and the receiver. In contrast, the second method in [47] only requires additional processing at the receiver side, in what is defined as the *Generalized Decision Feedback Equalizer* (GDFE) [44]. Although GDFE is generally a technique used to mitigate self-FEXT [56], in this method this structure is used to achieve AXT mitigation.

In essence, the GDFE first decorrelates the noise in the received symbols (formed of AXT and background noise) and then iteratively removes the in-domain crosstalk introduced

in the vectored group through this decorrelation procedure. Hence, the first stage is to multiply the received symbols by  $\mathbf{G}^{-1}$ :

$$\begin{aligned}\bar{\mathbf{y}} &= \mathbf{G}^{-1}\mathbf{y} \\ &= \mathbf{G}^{-1}\mathbf{\Lambda}\mathbf{x} + \mathbf{G}^{-1}\mathbf{z} \\ &= \mathbf{G}^{-1}\mathbf{\Lambda}\mathbf{x} + \mathbf{e},\end{aligned}\tag{2.12}$$

where  $\mathbf{G}$  is the lower-triangular matrix in (2.5), and the formulation in (2.1) was used as a reference. At this point, the noise parcel  $\mathbf{e} = \mathbf{G}^{-1}\mathbf{z}$  has a correlation matrix that is given by:

$$\begin{aligned}\mathbf{C}_e &= E \left\{ (\mathbf{G}^{-1}\mathbf{z}) (\mathbf{G}^{-1}\mathbf{z})' \right\} \\ &= \mathbf{G}^{-1} E \{ \mathbf{z}\mathbf{z}' \} (\mathbf{G}^{-1})' \\ &= \mathbf{G}^{-1}\mathbf{G}\mathbf{D}\mathbf{G}' (\mathbf{G}^{-1})' \\ &= \mathbf{D},\end{aligned}\tag{2.13}$$

where Eq. 2.5 was used. Thus, since  $\mathbf{D}$  is diagonal with positive elements, the effective noise  $\mathbf{e}$  is uncorrelated.

Note that the decorrelation provided by the multiplication of the received symbol by  $\mathbf{G}^{-1}$  changed the effective channel matrix at a given tone into  $\mathbf{G}^{-1}\mathbf{\Lambda}$ , which is non-diagonal. Thus, this decorrelation introduced an in-domain crosstalk within the vectored group. Nonetheless, this crosstalk can be eliminated due to the fact that the new channel matrix  $\mathbf{G}^{-1}\mathbf{\Lambda}$  is lower triangular. To do this, a feedback can be introduced in which the received symbols are given by:

$$\tilde{\mathbf{y}} = \bar{\mathbf{y}} - (\mathbf{G}^{-1}\mathbf{\Lambda} - \mathbf{f}) \hat{\mathbf{x}},\tag{2.14}$$

where  $\mathbf{f}$  is the diagonal of  $\mathbf{G}^{-1}\mathbf{\Lambda}$ , and  $\hat{\mathbf{x}}$  is the decoded symbol (in the frequency domain), which is assumed to be always correct. Hence, the decoder output is fed back multiplied by  $(\mathbf{G}^{-1}\mathbf{\Lambda} - \mathbf{U})$  to the incoming symbol  $\bar{\mathbf{y}}$  (received symbol after noise decorrelation). Substituting the definition of  $\bar{\mathbf{y}}$  in 2.12 with 2.14, yields:

$$\begin{aligned}\tilde{\mathbf{y}} &= \mathbf{G}^{-1}\mathbf{\Lambda}\mathbf{x} + \mathbf{x} - (\mathbf{G}^{-1}\mathbf{\Lambda} - \mathbf{f}) \hat{\mathbf{x}} \\ &= \mathbf{f}\hat{\mathbf{x}} + \mathbf{e} \\ &= \mathbf{\Lambda}\hat{\mathbf{x}} + \mathbf{e},\end{aligned}\tag{2.15}$$

where the assumption was made that the detected symbol  $\hat{\mathbf{x}}$  is correct, and  $\mathbf{f}$  is the diagonal of  $\mathbf{G}^{-1}\mathbf{\Lambda}$ . The fact that  $\mathbf{G}$  is monic resulted in  $\mathbf{f} = \mathbf{\Lambda}$ .

### 2.2.3 Third Ginis' Method: Receiver Coordination with Noise Prediction Structure (RxPred)

The third method outlined in [47] (also called *RxPred* through the present work) adopts the strategy of estimating the interference in each pair and then subtracting these estimates in their respective lines. Before examining the method, let us analyse the LDL decomposition of the correlation matrix

$$\mathbf{C}_z = \mathbf{G}\mathbf{C}_e\mathbf{G}', \quad (2.16)$$

where  $\mathbf{G}$  is a lower-triangular matrix with ones in the diagonal, and  $\mathbf{C}_e$  is a diagonal matrix with positive elements. Here, it is worth to show an application of *LDL* decomposition, which is the estimation of a sequence based on another one. Taking the variables of our problem  $\mathbf{z}$  and  $\mathbf{e}$ , we are faced with the following situation which is to estimate  $\mathbf{z}$  through  $\mathbf{e}$  (which is also called innovations, since it behaves like noise and then provides new information). This task can be carried out if we have the correlation matrix of  $\mathbf{z}$ , and we can then get  $\mathbf{G}$  matrix by *LDL*. Thus  $\mathbf{z}$  can be estimated through

$$\hat{\mathbf{z}} = \mathbf{G}\mathbf{e}, \quad (2.17)$$

where  $\hat{\mathbf{z}}$  is the estimate of the total noise,  $\mathbf{G}$  is the lower triangular of the Cholesky decomposition of  $\mathbf{C}_z$  in (2.16), and  $\mathbf{e}$  is an error vector, which can be obtained by making an error decision in the *decoder* of each VL. Then, the operation to mitigate AXT becomes

$$\begin{aligned} \tilde{\mathbf{y}} &= \mathbf{y} + (\mathbf{I} - \mathbf{G})\mathbf{e} \\ &= \mathbf{\Lambda}\mathbf{x} + \mathbf{z} + (\mathbf{I} - \mathbf{G})\mathbf{e} \\ &= \mathbf{\Lambda}\mathbf{x} + \mathbf{z} + \mathbf{e} - \mathbf{G}\mathbf{e} \\ &= \mathbf{\Lambda}\mathbf{x} + \mathbf{z} + \mathbf{e} - \hat{\mathbf{z}} \\ &= \mathbf{\Lambda}\mathbf{x} + \mathbf{e}, \end{aligned} \quad (2.18)$$

where  $\tilde{\mathbf{y}}$  represents the received symbols after mitigation. The equation above shows the formulation model of the third method, but it can be understood better through the graph in Fig. 2.2. Some key areas of the graph are highlighted by red circles. In region **I** there is a strategy which is used to extract  $\mathbf{e}$ , which is to subtract the received signal from the decoded symbol multiplied by the frequency response of channel  $\Lambda_1$  (which is equivalent to the received

signal in situation without interference). As can be noted in the chart, the signal received by user 1 has not received any processing to remove interference. The reason for this is that user 1, in this case, is the *reference pair*, i.e., this pair acts just like a *sensor* for interference. This feature of *sensor* is achieved setting a proper *bitloading* to the transmission in this line, without interference mitigation to user 1, so that  $e(1)$  will be a good estimative of interference in that pair, because symbols of pair 1 will be correctly decoded on most occasions. It should be noted, that in this case the transmission rate of the pair 1 will not be improved.

Region **II** shows how  $e(1)$  is used together with  $G(2,1)$  to estimate interference in pair 2 ( $\hat{z}(2)$ ), and how that estimative is subtracted from the received signal at line 2. Region **III** shows how  $e(1)$ ,  $e(2)$ ,  $G(3,1)$  and  $G(3,2)$  are used to calculate  $\hat{z}(3)$ .

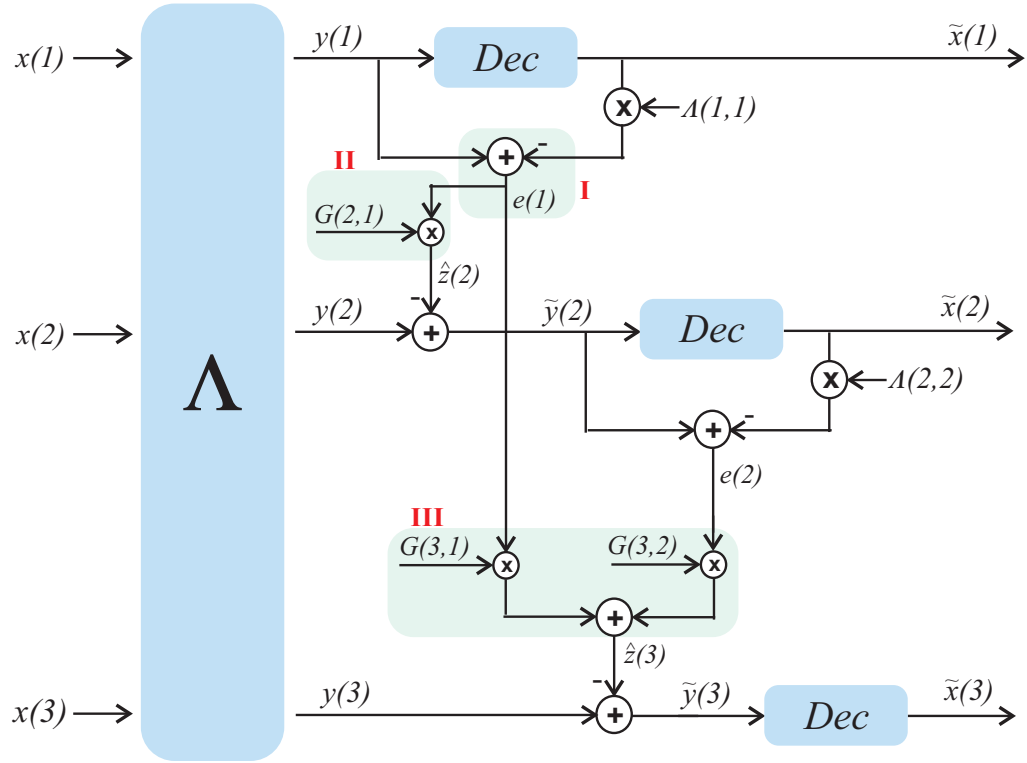


Figure 2.2: Graphical representation of the third Gini's method.

### 2.2.4 Decision Feedback Cancellor (DFC)

The algorithm that will be called DFC (Decision Feedback Canceller), was examined in [51]. This method is intended for upstream transmission, in which the lines are coordinated at the receiver. The algorithm begins with the computation of the whitening filter [57] for coloured noise  $\mathbf{z}$ , which is the decorrelation matrix  $\mathbf{C}_z^{-1/2}$ .

It should be noted that here is considered that  $\mathbf{C}_z$  was already calculated in training

phase. In showtime (the stage after training, in which already there is a connection between the DSLAM and the user's premisses), the filter  $\mathbf{C}_z^{-1/2}$  is applied to the received symbols, yielding

$$\begin{aligned}\tilde{\mathbf{y}} &= \mathbf{C}_z^{-1/2}\mathbf{H}\mathbf{x} + \mathbf{C}_z^{-1/2}\mathbf{z} \\ &= \tilde{\mathbf{H}}\mathbf{x} + \tilde{\mathbf{z}},\end{aligned}\tag{2.19}$$

where  $\tilde{\mathbf{y}}$ ,  $\tilde{\mathbf{H}}$  and  $\tilde{\mathbf{z}}$  are the received symbols vector, channel matrix and noise vector after whitening, respectively. Note that in this method the channel is not a diagonal matrix (as in RxPred), because it performs in the upstream direction and then vectoring cannot be applied in the transmission due to the geographical separation of the transmitters. At this point we have  $E[\tilde{\mathbf{z}}\tilde{\mathbf{z}}'] = \varepsilon\mathbf{I}$ , where  $\varepsilon$  is the power of residual noise, and it indicates that the noise was whitened. However, the parcel  $\mathbf{C}_z^{-1/2}\mathbf{H}\mathbf{x}$  is not diagonal, which implies that some processing must be done to allow decoding. When the QR decomposition of the channel matrix is calculated after whitening,  $\tilde{\mathbf{H}}$ , we have

$$\tilde{\mathbf{H}} = \tilde{\mathbf{Q}}\tilde{\mathbf{R}},\tag{2.20}$$

where  $\tilde{\mathbf{Q}}$  is a unitary matrix and  $\tilde{\mathbf{R}}$  is an upper triangular matrix. Then, left multiplying  $\tilde{\mathbf{y}}$  by  $\tilde{\mathbf{Q}}'$ , we obtain

$$\bar{\mathbf{y}} = \tilde{\mathbf{R}}\mathbf{x} + \tilde{\mathbf{Q}}'\tilde{\mathbf{z}}.\tag{2.21}$$

Note that to multiply  $\tilde{\mathbf{z}}$  by  $\tilde{\mathbf{Q}}'$ , does not changes the power of the whitened noise, because  $\mathbf{Q}$  is unitary. In addition,  $\tilde{\mathbf{R}}\mathbf{x}$  has an upper triangular structure, which allows decoding by *successive interference cancellation* (SIC) [85]. The decision process can be executed through

$$\hat{x}(i) = \text{dec} \left[ \frac{1}{\tilde{R}(i, i)} \left( \bar{y}(i) - \sum_{j=i+1}^L \tilde{R}(i, j)\hat{x}(j) \right) \right],\tag{2.22}$$

where  $\text{dec}()$  denotes the decision operation. The Fig. 2.3 presents an scheme which resumes the whole process of the DFC.



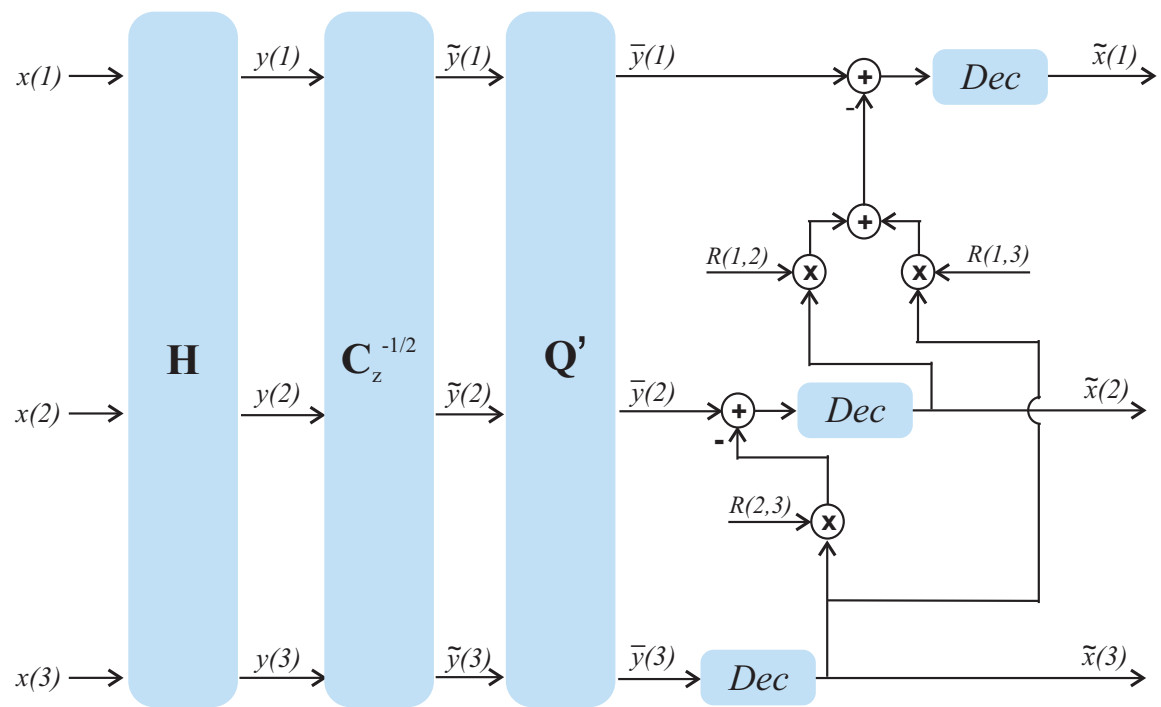


Figure 2.3: Graphical representation of the DFC method.

# Chapter 3

## Interference Modelling and Performance Evaluation of the AXT Prediction

There is a difficulty with regard to AXT mitigation which is that the “victim system” does not have information about the transmitted signals in the alien system or about the channels between the alien and the vectored lines. The only information they can obtain about the AXT comes from its statistics, which in most cases can be found in the interference correlation matrix. Thus, it is extremely important to characterize the factors that affect the interference correlation, as well the scenarios that are more favorable to interference cancellation.

In this section, an analysis will be conducted of the characteristic features of AXT interference. We will begin by representing the generation of AXT from the time domain in order to accommodate the situation in which the AXT systems are unsynchronized with the vectored system. Then, we will describe the correlation matrix of the AXT in the frequency domain in a decomposed way to determine the effect of each alien line (AL) on the total correlation matrix. Following this, we will examine the interaction between the ALs that define the correlation. Finally, an analysis of the performance of the prediction based AXT mitigation methods will be presented. This section will be structured on the basis of the methods outlined in [47] and [30], and will be called RxPred.

First let us lay down some guiding principles to simplify the analysis:

**Assumption 1** *DMT modulation is used both by the ALs and the vectored lines (VLs);*

**Assumption 2** *The vectored and the alien signals operate in the same symbol rate;*

**Assumption 3** *The vectored and the alien signals are unsynchronized;*

**Assumption 4** *All the ALs transmit with the same power  $\mathcal{E}_s$ ;*

**Assumption 5** *The transmitted signals (both in the ALs and the VLs) are statistically independent of each other;*

**Assumption 6** *The crosstalk generated at a given DMT tone by a particular AL couples with equal magnitude into all VLs.*

**Assumption 7** *The vectored and alien crosstalk channels are time-invariant.*

**Assumption 8** *The signals regard to background noise are independent and identically distributed, and are not correlated with the signals in the coordinated and in the alien groups.*

**Assumption 9** *All signals have zero mean.*

These assumptions were defined in order to the model represent some aspects of system that can be found in a practical deployment, like Assumption 1, Assumption 2 and Assumption 4. The Assumption 5, Assumption 8 and Assumption 9 are conditions which are standard assumed in the literature. By other hand, Assumption 7, Assumption 3 and Assumption 6 are conditions which are not strictly representative of real systems, but are used here in order to simplify the model.

### 3.1 Evaluation of the Correlation matrix

In this section an analytical evaluation is carried out of the effects of adding ALs to the correlation matrix. Let us represent the AXT observed by a single vectored line, in all the tones, as

$$\mathbf{q}_l = \sum_{m=1}^M \mathbf{T}_{l,m} \mathbf{A}_{l,m} \mathbf{s}_m, \quad (3.1)$$

where the column vector  $\mathbf{s}_m$  contains the  $2K$  time domain samples transmitted by the  $m$ -th AXT source, the matrix  $\mathbf{A}_{l,m}$  is  $(2K + \eta_{l,m}) \times (2K)$  represents the convolution matrix of the channel from the alien source  $m$  to the vectored line  $l$ ,  $\mathbf{T}_{l,m}$  is  $K \times (2K + \eta_{l,m})$  and corresponds

to the FFT (*Fast Fourier Transform*) matrix [62]. The parameters  $K$  and  $\eta_{l,m}$  represent the total number of tones and the length minus one of the nonzero part of the impulse response of the channel from the  $m$ -th AXT source to the  $l$ -th vectored line, respectively. The (3.1) in fact represents the effect of an alien transmission on a vectored line because it accounts for the propagation of the alien signal from its source, passing by a linear time-invariant coupling channel up to the vectored line through a convolution operation [77], represented in its matrix form [78], and denoted by the multiplication  $\mathbf{A}_{l,m}\mathbf{s}_m$ . Additionally, the multiplication by  $\mathbf{T}_{l,m}$  obtains the frequency-domain representation of this propagated signals [62].

The formulation in (3.1) supports the AXT generated from both FEXT and NEXT, since it does not specify any synchronization between the AL and the VL. The AXT observed in a specific tone of the VL  $l$ , is determined by only keeping the line of the FFT matrix which corresponds to that particular tone  $k$

$$q_l(k) = \sum_{m=1}^M \mathbf{T}_{l,m}(k, :) \mathbf{A}_{l,m} \mathbf{s}_m, \quad (3.2)$$

where  $\mathbf{T}_{l,m}(k, :)$  denotes the  $k$ -th line of the matrix  $\mathbf{T}_{l,m}$ . Note that we used a notation like the one used in MatLab for indexing the columns of a matrix, because we are using the subscripts to identify the type of matrix or vector, and the superscripts to denote operations like transpose and conjugation. Then, we will use values in parenthesis to denote indexing of elements, columns and rows of matrices across the text.

Thus, to represent the AXT observed by each VL in a specific tone, we take account of (3.2) across the VLs, which yield the  $\mathbf{q}_k$  vector ( $L \times 1$ ). This is described by

$$\begin{aligned} \mathbf{q}_k &= \sum_{l=1}^L \sum_{m=1}^M \mathbf{p}_l \mathbf{T}_{l,m}(k, :) \mathbf{A}_{l,m} \mathbf{s}_m \\ &= \left( \sum_{l=1}^L \mathbf{p}_l \mathbf{T}_{l,1}(k, :) \mathbf{A}_{l,1} \right) \mathbf{s}_1 + \dots + \left( \sum_{l=1}^L \mathbf{p}_l \mathbf{T}_{l,M}(k, :) \mathbf{A}_{l,M} \right) \mathbf{s}_M \\ &= \mathcal{A}_1 \mathbf{s}_1 + \dots + \mathcal{A}_M \mathbf{s}_M, \end{aligned} \quad (3.3)$$

where  $\mathbf{p}_l$  represents a  $L \times 1$  vector which only has a nonzero element equal to one in the  $l$ -th position. It is responsible for positioning the corresponding signals in the  $\mathbf{q}_k$  vector, and  $\mathcal{A}_m$  is a  $L \times 2K$  matrix which is given by  $\sum_{l=1}^L \mathbf{p}_l \mathbf{T}_{l,m}(k, :) \mathbf{A}_{l,m}$ . The term  $\mathbf{p}_l$  makes each term in the sum  $\sum_{l=1}^L \mathbf{p}_l \mathbf{T}_{l,m}(k, :) \mathbf{A}_{l,m}$  to be a matrix of zeros with exception for the  $l$ -th line, which will contain the line vector due to the multiplication  $\mathbf{T}_{l,m}(k, :) \mathbf{A}_{l,m}$ . Then, the sum  $\sum_{l=1}^L \mathbf{p}_l \mathbf{T}_{l,m}(k, :) \mathbf{A}_{l,m}$  in (3.3) yields a matrix with  $L$  lines. To simplify the notation, the underscript  $k$  will be omitted in the following equations. The decomposition in the second line of (3.3) with regard to the AXT sources, is possible because  $\mathbf{s}_m$  does not depend on  $l$  and there may be a chance to interchange the order of summation.

Now, we are able to derive the correlation matrix of the AXT at one tone for all the VLs as

$$\begin{aligned}
\mathbf{C}_q &= E[\mathbf{q}\mathbf{q}'] \\
&= E[(\mathcal{A}_1\mathbf{s}_1 + \dots + \mathcal{A}_M\mathbf{s}_M)(\mathcal{A}_1\mathbf{s}_1 + \dots + \mathcal{A}_M\mathbf{s}_M)'] \\
&= E[\mathcal{A}_1\mathbf{s}_1(\mathcal{A}_1\mathbf{s}_1)' + \dots + \mathcal{A}_1\mathbf{s}_1(\mathcal{A}_M\mathbf{s}_M)' + \dots + \mathcal{A}_M\mathbf{s}_M(\mathcal{A}_M\mathbf{s}_M)'] \\
&= E[\mathcal{A}_1\mathbf{s}_1\mathbf{s}_1'\mathcal{A}_1'] + \dots + E[\mathcal{A}_1\mathbf{s}_1\mathbf{s}_M'\mathcal{A}_M'] + \dots + E[\mathcal{A}_M\mathbf{s}_M\mathbf{s}_M'\mathcal{A}_M'] \\
&= \mathcal{A}_1 E[\mathbf{s}_1\mathbf{s}_1'] \mathcal{A}_1' + \dots + \mathcal{A}_1 E[\mathbf{s}_1\mathbf{s}_M'] \mathcal{A}_M' + \dots + \mathcal{A}_M E[\mathbf{s}_M\mathbf{s}_M'] \mathcal{A}_M', \tag{3.4}
\end{aligned}$$

where the superscript  $'$  stands for transpose and conjugation, and the separation in multiple expectations and the extraction of the  $\mathcal{A}_m$  terms were possible owing to the linearity properties of the statistical expectation [74, 73]. Additionally, the Assumption 5 and the Assumption 9 allows us to eliminate the crossed terms, which yields:

$$\mathbf{C}_q = \mathcal{E}_s \mathbf{C}_1 + \mathcal{E}_s \mathbf{C}_2 + \dots + \mathcal{E}_s \mathbf{C}_M, \tag{3.5}$$

where  $\mathbf{C}_m = \mathcal{A}_m \mathcal{A}_m^H$  is the  $L \times L$  canonical correlation matrix of the channels from the  $m$ -th AL to the vectored system, and the power of the alien lines is given by  $\mathcal{E}_s = E[s_m s_m']$  for the alien line  $m$ .

## 3.2 Evaluation of the Correlation Coefficient

Henceforth, we will evaluate the correlation coefficient of the AXT that is present at the received signals in the VLs. We will consider situation with distinct numbers of AL, in order to evaluate how the number of AL affects the correlation between the AXT observed in the VLs, and hence the efficiency of the AXT prediction. It should be underline that since we are dealing with multiple sensors that are spatially separated, the term correlation stands for spatial correlation [75].

### 3.2.1 Impact of the Number of AL in the Correlation Coefficient

If there is only 1 AL, i.e., a single parcel in (5.1), the absolute correlation coefficient between the AXT observed in the VLs  $b$  and  $c$  is defined as [76]:

$$|\rho_{b,c}| = \frac{|C_q(b,c)|}{\sqrt{C_q(b,b)}\sqrt{C_q(c,c)}}, \tag{3.6}$$

where  $C_q(b, c)$  is the element at line  $b$  and column  $c$  of the correlation matrix  $\mathbf{C}_q$ . Then, it follows that

$$\begin{aligned}
|\rho_{b,c}| &= \frac{|\mathcal{E}_s C_1(b, c)|}{\left| \sqrt{\mathcal{E}_s C_1(b, b)} \sqrt{\mathcal{E}_s C_1(c, c)} \right|} \\
&= \frac{\mathcal{E}_s |C_1(b, c)|}{\left| \sqrt{\mathcal{E}_s P_1} \sqrt{\mathcal{E}_s P_1} \right|} \\
&= \frac{\mathcal{E}_s |C_1(b, c)|}{\mathcal{E}_s |P_1|} \\
&= \frac{\mathcal{E}_s P_1}{\mathcal{E}_s |P_1|} \\
&= 1,
\end{aligned} \tag{3.7}$$

where  $P_1$  is a real number observed in all the elements of the diagonal of  $\mathbf{C}_1$ , and  $|C_1(b, c)| = P_1$  because it was assumed that one AL couples with the same magnitude for each VL. This is carried out on the basis of the Assumption 6, which causes all the diagonal elements of one  $\mathbf{C}_m$  to be equal, and all the complex number in  $\mathbf{C}_m$  to have the same magnitude. The value 1 in the last line of the (3.7) leads us to conclude that when the AXT is generated by only one source, we can get complete information about the AXT affecting the vectored line  $b$  from the AXT in vectored line  $c$ , and, for example, the AXT in  $b$  can be completely determined by the AXT in  $c$  by a simple linear relation [76]. The generalization of the correlation coefficient for  $M$  ALs yields

$$\begin{aligned}
|\rho_{b,c}| &= \frac{|C_q(b, c)|}{\left| \sqrt{C_q(b, b)} \sqrt{C_q(c, c)} \right|} \\
&= \frac{|\mathcal{E}_s C_1(b, c) + \dots + \mathcal{E}_s C_M(b, c)|}{\left| \sqrt{\mathcal{E}_s C_1(b, b) + \dots + \mathcal{E}_s C_M(b, b)} \sqrt{\mathcal{E}_s C_1(c, c) + \dots + \mathcal{E}_s C_M(c, c)} \right|} \\
&= \frac{\mathcal{E}_s |C_1(b, c) + \dots + C_M(b, c)|}{\left| \sqrt{\mathcal{E}_s P_1 + \dots + \mathcal{E}_s P_M} \sqrt{\mathcal{E}_s P_1 + \dots + \mathcal{E}_s P_M} \right|} \\
&= \frac{\mathcal{E}_s |C_1(b, c) + \dots + C_M(b, c)|}{\left| \sqrt{\mathcal{E}_s (P_1 + \dots + P_M)} \sqrt{\mathcal{E}_s (P_1 + \dots + P_M)} \right|} \\
&= \frac{\mathcal{E}_s |C_1(b, c) + \dots + C_M(b, c)|}{\left| \sqrt{\mathcal{E}_s^2 (P_1 + \dots + P_M)^2} \right|} \\
&= \frac{\mathcal{E}_s |C_1(b, c) + \dots + C_M(b, c)|}{|\mathcal{E}_s (P_1 + \dots + P_M)|} \\
&= \frac{|C_1(b, c) + \dots + C_M(b, c)|}{|P_1| + \dots + |P_M|},
\end{aligned} \tag{3.8}$$

where  $P_m$  is the value of the diagonal of  $\mathbf{C}_m$ . In this case,  $|\rho_{b,c}| = 1$  only when  $C_1(b, c), \dots, C_M(b, c)$  are in the same phase, otherwise  $|C_1(b, c) + C_2(b, c) + \dots + C_M(b, c)| <$

$|P_1| + |P_2| + \dots + |P_M|$ , which implies  $|\rho_{b,c}| < 1$ . The reason for this is that  $C_m(b,c)$  has the same modulus as  $P_m$  (supported by the Assumption 6), and in a situation with  $\phi[C_1(b,c)] = \dots = \phi[C_M(b,c)]$ , where  $\phi[\cdot]$  denotes the phase of a complex number, the equality  $|C_1(b,c) + C_2(b,c) + \dots + C_M(b,c)| = |P_1| + |P_2| + \dots + |P_M|$  holds.

(3.8) reveals how each alien line affects the correlation between the interference observed in two distinct VLs. Additionally, it shows that even in the presence of many ALs is difficult to achieve a high correlation in the crosstalk that affects two VLs, since there is a need for phase alignment in all the elements  $C_m(b,c)$ .

### 3.2.2 Impact of the Number of ALs in the Prediction Error

Since many AXT mitigation methods rely on linear prediction, we will now demonstrate how the formulation outlined above, affects the power of the prediction error [58]. For example, in a scenario with 1 AL and 2 VLs, the power of the prediction error in the second VL (the element (2, 2) of the diagonal matrix of the  $\mathbf{D}$  of the LDL decomposition [58]), according to [59, 67] and the App. A, is given by

$$D(2,2) = C_q(2,2) - C_q(2,1) \left( \frac{C_q(2,1)}{C_q(1,1)} \right)^*, \quad (3.9)$$

where the superscript  $*$  denotes conjugation. Applying (5.1) in (3.9), we get

$$\begin{aligned} D(2,2) &= \mathcal{E}_s P_1 - \frac{\mathcal{E}_s^2 C_1(2,1) C_1(2,1)^*}{\mathcal{E}_s P_1} \\ &= \frac{\mathcal{E}_s^2 P_1^2 - \mathcal{E}_s^2 P_1^2}{\mathcal{E}_s P_1} \\ &= 0, \end{aligned} \quad (3.10)$$

where on basis of the Assumption 6,  $|C_1(2,1)| = P_1$ , and then  $C_1(2,1)C_1(2,1)^* = P_1^2$ . This result means that in a scenario with only 1 AL, the prediction error is zero. Then, the entire AXT in the VLs can be predicted, with the exception of the reference line [47]. However, in a scenario with 2 ALs and 2 VLs, the power of the prediction error is given by (see App. A)

$$\begin{aligned} D(2,2) &= \mathcal{E}_s(P_1 + P_2) - \frac{[\mathcal{E}_s(C_1(2,1) + C_2(2,1))] [\mathcal{E}_s(C_1(2,1) + C_2(2,1))]^*}{\mathcal{E}_s(P_1 + P_2)} \\ &= \frac{\mathcal{E}_s^2(P_1 + P_2)^2 - [\mathcal{E}_s(C_1(2,1) + C_2(2,1))] [\mathcal{E}_s(C_1(2,1) + C_2(2,1))]^*}{\mathcal{E}_s(P_1 + P_2)}. \end{aligned} \quad (3.11)$$

As noted in (3.11), the condition for  $D(2,2)$  to be zero, is for the second term of the sum in the numerator to be equal to  $\mathcal{E}_s^2(P_1 + P_2)^2$ . This will occur when there is a maximum correlation of the AXT among the VLs. According to (3.8), the maximum correlation is achieved when

$\phi[C_1(2, 1)] = \phi[C_2(2, 1)]$ . In this situation, as  $C_1(2, 1)$  and  $C_2(2, 1)$  have the same phase  $\phi_l$ , the sum inside the brackets of the numerator in the second line of 3.11, can be expressed as

$$\begin{aligned} C_1(2, 1) + C_2(2, 1) &= P_1 e^{j\phi_l} + P_2 e^{j\phi_l} \\ &= (P_1 + P_2) e^{j\phi_l}. \end{aligned} \quad (3.12)$$

Then, the (3.11) can now be represented as

$$\begin{aligned} D(2, 2) &= \frac{\mathcal{E}_s^2(P_1 + P_2)^2 - [\mathcal{E}_s(P_1 + P_2)e^{j\phi_l}] [\mathcal{E}_s(P_1 + P_2)e^{j\phi_l}]^*}{\mathcal{E}_s(P_1 + P_2)} \\ &= \frac{\mathcal{E}_s^2(P_1 + P_2)^2 - [\mathcal{E}_s^2(P_1 + P_2)^2 e^{j(\phi_l - \phi_l)}]}{\mathcal{E}_s(P_1 + P_2)} \\ &= \frac{\mathcal{E}_s^2(P_1 + P_2)^2 - \mathcal{E}_s^2(P_1 + P_2)^2}{\mathcal{E}_s(P_1 + P_2)} \\ &= 0. \end{aligned} \quad (3.13)$$

On the other hand, the error will be maximum when  $\phi[C_1(2, 1)] - \phi[C_2(2, 1)] = \pi$ . In this case the sum inside the brackets of the numerator in the second line of the (3.11), can be written as  $P_1 e^{j\phi_l} + P_2 e^{j(\phi_l + \pi)}$ , and (3.11) becomes

$$\begin{aligned} D(2, 2) &= \frac{\mathcal{E}_s^2(P_1 + P_2)^2 - [\mathcal{E}_s(P_1 e^{j\phi_l} + P_2 e^{j(\phi_l + \pi)})] [\mathcal{E}_s(P_1 e^{j\phi_l} + P_2 e^{j(\phi_l + \pi)})]^*}{\mathcal{E}_s(P_1 + P_2)} \\ &= \frac{\mathcal{E}_s^2(P_1 + P_2)^2 - \mathcal{E}_s^2 [P_1^2 + P_2^2 + P_1 P_2 (e^{j\pi} + e^{-j\pi})]}{\mathcal{E}_s(P_1 + P_2)} \\ &= \frac{\mathcal{E}_s^2 P_1^2 + \mathcal{E}_s^2 P_2^2 + 2\mathcal{E}_s^2 P_1 P_2 - \mathcal{E}_s^2 (P_1^2 + P_2^2)}{\mathcal{E}_s(P_1 + P_2)} \\ &= \frac{2\mathcal{E}_s^2 P_1 P_2}{\mathcal{E}_s(P_1 + P_2)}. \end{aligned} \quad (3.14)$$

The (3.14) will yield the worst case when  $P_1 = P_2 = P_a$ , where  $P_1 = C_1(2, 1)$  and  $P_2 = C_2(2, 1)$ , because  $D(2, 2) = \mathcal{E}_s P_a = C_q(2, 2)$ , i.e., none of the AXT in the second VL will be predicted.

### 3.2.3 Effects of the White Noise on the Correlation

It will now be shown how the *Additive White Gaussian Noise* (AWGN) affects the correlation. In this context, the AWGN will be taken as the result of the combined effect of infinite sources of spurious signals, other than AXT sources. Then, when the AWGN is taken into account, the total interference (AXT plus noise) at the VL  $l$  becomes

$$\mathbf{z}_l = \sum_{m=1}^M \mathbf{T}_{l,m} \mathbf{A}_{l,m} \mathbf{s}_m + \sum_{\zeta=1}^{\infty} \mathbf{T}_{l,\zeta} \mathbf{\Psi}_{l,\zeta} \nu_{\zeta}, \quad (3.15)$$



where  $\nu_\zeta$  is the column vector relative to the  $2K$  time-domain samples of the  $\zeta$ -th AWGN source,  $\Psi_{l,\zeta}$  is the corresponding convolution matrix to the coupling of the AWGN, and  $\mathbf{T}_{l,\zeta}$  performs the mapping from time to frequency domain of the noise. Then, the total amount of interference observed in a specific tone across all the VLS is given by

$$\begin{aligned}
\mathbf{z}_k &= \sum_{l=1}^L \sum_{m=1}^M \mathbf{p}_l \mathbf{T}_{l,m}(k, :) \mathbf{A}_{l,m} \mathbf{s}_m + \sum_{l=1}^L \sum_{\zeta=1}^{\infty} \mathbf{p}_l \mathbf{T}_{l,\zeta}(k, :) \Psi_{l,\zeta} \nu_\zeta \\
&= \left( \sum_{l=1}^L \mathbf{p}_l \mathbf{T}_{l,1}(k, :) \mathbf{A}_{l,1} \right) \mathbf{s}_1 + \dots + \left( \sum_{l=1}^L \mathbf{p}_l \mathbf{T}_{l,M}(k, :) \mathbf{A}_{l,M} \right) \mathbf{s}_M + \left( \sum_{l=1}^L \mathbf{p}_l \mathbf{T}_{l,1}(k, :) \Psi_{l,1} \right) \nu_1 + \\
&\quad + \dots + \left( \sum_{l=1}^L \mathbf{p}_l \mathbf{T}_{l,\infty}(k, :) \Psi_{l,\infty} \right) \nu_\infty \\
&= \mathcal{A}_1 \mathbf{s}_1 + \dots + \mathcal{A}_M \mathbf{s}_M + \Psi_1 \nu_1 + \dots + \Psi_\infty \nu_\infty,
\end{aligned} \tag{3.16}$$

where  $\Psi_\zeta = \sum_{l=1}^L \mathbf{p}_l \mathbf{T}_{l,\zeta}(k, :) \Psi_{l,\zeta}$ . Thus, the correlation of the total interference can be expressed as

$$\begin{aligned}
\mathbf{C}_z &= E [(\mathcal{A}_1 \mathbf{s}_1 + \dots + \mathcal{A}_M \mathbf{s}_M + \Psi_1 \nu_1 + \dots + \Psi_\infty \nu_\infty)(\mathcal{A}_1 \mathbf{s}_1 + \dots + \mathcal{A}_M \mathbf{s}_M + \Psi_1 \nu_1 + \dots + \Psi_\infty \nu_\infty)'] \\
&= \mathcal{A}_1 E [\mathbf{s}_1 \mathbf{s}_1'] \mathcal{A}_1' + \dots + \mathcal{A}_1 E [\mathbf{s}_1 \mathbf{s}_M'] \mathcal{A}_M' + \dots + \mathcal{A}_M E [\mathbf{s}_M \mathbf{s}_M'] \mathcal{A}_M' + \mathcal{A}_1 E [\mathbf{s}_1 \nu_1'] \Psi_1' + \\
&\quad + \dots + \Psi_\infty E [\nu_\infty \nu_\infty'] \Psi_\infty' \\
&= \mathbf{C}_1 \mathcal{E}_s + \mathbf{C}_2 \mathcal{E}_s + \dots + \mathbf{C}_M \mathcal{E}_s + (\Psi_1 \Psi_1' E [\nu_1 \nu_1'] + \dots + \Psi_\infty \Psi_\infty' E [\nu_\infty \nu_\infty']) \\
&= \mathbf{C}_1 \mathcal{E}_s + \mathbf{C}_2 \mathcal{E}_s + \dots + \mathbf{C}_M \mathcal{E}_s + \mathbf{I}_L \sigma^2,
\end{aligned} \tag{3.17}$$

where  $\mathbf{I}_L \sigma^2 = \Psi_1 \Psi_1' E [\nu_1 \nu_1'] + \dots + \Psi_\infty \Psi_\infty' E [\nu_\infty \nu_\infty']$ ,  $\mathbf{I}_L$  is an identity matrix of dimension  $L$ , and  $\sigma^2$  is the power of the resulting AWGN at some tone. The contribution of the AWGN yielded the addition of a diagonal matrix in (3.17) due to the Assumption 8, which makes the all the crossed terms to be zero and the multiplications  $\Psi_\zeta \Psi_\zeta'$  yield diagonal matrices. In (3.17) the properties of the statistical expectation were used as in (3.4), in order to simplify

its representation. Then, the absolute spatial correlation coefficient is given by

$$\begin{aligned}
|\rho'_{b,c}| &= \frac{|C_z(b,c)|}{\left| \sqrt{C_z(b,b)} \sqrt{C_z(c,c)} \right|} \\
&= \frac{\left| \mathcal{E}_s \left[ \sum_{m=1}^M C_m(b,c) \right] \right|}{\left| \sqrt{\mathcal{E}_s C_1(b,b) + \dots + \mathcal{E}_s C_M(b,b) + \sigma^2} \sqrt{\mathcal{E}_s C_1(c,c) + \dots + \mathcal{E}_s C_M(c,c) + \sigma^2} \right|} \\
&= \frac{\mathcal{E}_s \left| \sum_{m=1}^M C_m(b,c) \right|}{\left| \sqrt{\mathcal{E}_s \left( \sum_{m=1}^M P_m \right) + \sigma^2} \sqrt{\mathcal{E}_s \left( \sum_{m=1}^M P_m \right) + \sigma^2} \right|} \\
&= \frac{\mathcal{E}_s \left| \sum_{m=1}^M C_m(b,c) \right|}{\left| \mathcal{E}_s \left( \sum_{m=1}^M P_m \right) + \sigma^2 \right|} \\
&= \frac{\mathcal{E}_s \left| \sum_{m=1}^M C_m(b,c) \right|}{\left| \mathcal{E}_s \left( \sum_{m=1}^M P_m \right) \left( 1 + \frac{\sigma^2}{\mathcal{E}_s \left( \sum_{m=1}^M P_m \right)} \right) \right|} \\
&= \frac{\mathcal{E}_s \left| \sum_{m=1}^M C_m(b,c) \right|}{\mathcal{E}_s \left| \sum_{m=1}^M P_m \right| \left| 1 + \frac{\sigma^2}{\mathcal{E}_s \left( \sum_{m=1}^M P_m \right)} \right|} \\
&= \frac{\left| \sum_{m=1}^M C_m(b,c) \right|}{\left| \sum_{m=1}^M P_m \right|} \left( \frac{1}{\left| 1 + \frac{\sigma^2}{\mathcal{E}_s \left( \sum_{m=1}^M P_m \right)} \right|} \right) \\
&= \frac{|\rho_{b,c}|}{\left| 1 + \frac{\sigma^2}{\mathcal{E}_s \left( \sum_{m=1}^M P_m \right)} \right|}, \tag{3.18}
\end{aligned}$$

in which

$$|\rho_{b,c}| = \frac{\left| \sum_{l=1}^M C_l(b,c) \right|}{\left| \sum_{l=1}^M P_l \right|}, \tag{3.19}$$

is the absolute correlation coefficient of a scenario with no AWGN, as in (3.8). Then, we can conclude from (3.18) that thermal noise reduces the correlation coefficient according to the ratio between its power and the power of the AXT,  $\mathcal{E}_s \left( \sum_{l=1}^M P_l \right)$ . In cases where the power of the AXT is much larger than the power of the AWGN, the second term of the sum in the denominator of the last line of (3.18) tends towards zero, and  $|\rho'_{b,c}| \approx |\rho_{b,c}|$ . However, when  $\sigma^2 \gg \mathcal{E}_s \left( \sum_{l=1}^M P_l \right)$ , the denominator of the last line of (3.18) becomes much larger than the numerator, and  $|\rho'_{b,c}| \approx 0$ .

The numerical reason for the reduction of the correlation coefficient is that the correlation matrix of the thermal noise is only non-zero within the diagonal, due to the

Assumption 8, which means that only the denominator is increased, as observed in the second line of (3.18), in which the term  $\sigma^2$  appears only in the denominator.

### 3.3 Evaluation of the Effect of the AXT Channel Phase on the Correlation

In this section, we will evaluate how the phase of each AXT channel affects the interference correlation between the VLs. A study was carried in this area in [60], in which a statistical model was designed for the correlation of the crosstalk, based on the number of ALs. However, in the present study, we seek to extend this analysis by evaluating the contribution made by each AL.

The AXT channel phase has a direct effect on the correlation coefficient, as seen in the previous section. In (3.8) it was demonstrated that the correlation coefficient of the interference between 2 VL,  $b$  and  $c$ , is high if the elements  $C_1(b, c), C_2(b, c), \dots, C_M(b, c)$ , of the matrices  $\mathbf{C}_1, \mathbf{C}_2, \dots, \mathbf{C}_M$ , respectively, are in phase. Each element of the correlation matrix related to the alien line  $m$  is calculated as  $C_m(b, c) = \mathcal{A}_m(b, :)\mathcal{A}_m(c, :)'$ , where  $\mathcal{A}_m(l, :)$  denotes the  $l$ -th line of the  $\mathcal{A}_m$  matrix. Each line of the  $\mathcal{A}_m$  matrix can be expressed as

$$\mathcal{A}_m(l, :) = \mathbf{T}_{l,m}(k, :)\mathbf{A}_{l,m}, \quad (3.20)$$

where underscript  $k$  has been omitted from 3.2. Note that in (3.20) we are taking only one line of the  $\mathbf{T}_{l,m}$  matrix, which means that the channel is being evaluated in a specific frequency, or the tone  $k$ . Since  $\mathbf{A}_{l,m}$  is a cyclic convolution matrix, with  $2K$  columns, in which its columns are delayed versions of its first column [78, 62], we can write

$$\begin{aligned} \mathcal{A}_m(l, :) &= [\mathbf{T}_{l,m}(k, :)\mathbf{A}_{l,m}(:, 1), \quad \mathbf{T}_{l,m}(k, :)\mathbf{A}_{l,m}(:, 2), \quad \dots, \quad \mathbf{T}_{l,m}(k, :)\mathbf{A}_{l,m}(:, 2K)] \\ &= [g_m e^{j[\phi_{l,m}]}, \quad g_m e^{j[\phi_{l,m} - 2\pi k/2K]}, \quad \dots, \quad g_m e^{j[\phi_{l,m} - 2\pi k(2K-1)/2K]}], \end{aligned} \quad (3.21)$$

where  $\mathbf{A}_{l,m}(:, f)$  is the  $f$ -th column of the  $\mathbf{A}_{l,m}$  matrix,  $g_m e^{j[\phi_{l,m}]}$  is the frequency response of the channel from the  $m$ -th AL to the  $l$ -th VL (in a specific tone),  $\phi_{l,m}$  is the phase of this complex number, and its magnitude is  $g_m$ . Note that due Assumption 6, the magnitude of the channel coupling between the  $m$ -th AL and any VL is  $g_m$ . The second term of the sums in the exponents represents the effect of the delay in the frequency domain (*shift property* of

the FFT [61]). Then, the inner product  $\mathcal{A}_m(b, :)\mathcal{A}_m(c, :)'$  yields

$$\begin{aligned}\mathcal{A}_m(b, :)\mathcal{A}_m(c, :)' &= g_m^2 e^{j[\phi_{b,m}-\phi_{c,m}]} + \sum_{i=1}^{2K-1} g_m^2 e^{j[\phi_{b,m}-\phi_{c,m}-2\pi ki/2K+2\pi ki/2K]} \\ &= 2K g_m^2 e^{j[\phi_{b,m}-\phi_{c,m}]}.\end{aligned}\quad (3.22)$$

Thus, the phase of each  $C_m(b, c)$  element can be expressed as

$$\begin{aligned}\phi [C_1(b, c)] &= \phi_{b,1} - \phi_{c,1} \\ \phi [C_2(b, c)] &= \phi_{b,2} - \phi_{c,2} \\ &\vdots \\ \phi [C_M(b, c)] &= \phi_{b,M} - \phi_{c,M}.\end{aligned}\quad (3.23)$$

Then, it can be seen from (3.23), that the correlation of the interference between 2 VLs is high if all the differences in (3.23) are equal, i.e., when all the ALs have channels with the same phase difference between these VLs,  $b$  and  $c$ . However, this does not imply that the channel phase from all the ALs to the VLs must be the same. For example, in a scenario with 2 ALs and 2 VLs, if the first AL has channel phases  $\pi/3$  and  $\pi/6$  in the VLs  $b$  and  $c$ , respectively, and the second AL has the channel phases  $2\pi/3$  and  $\pi/2$ , the correlation coefficient between these 2 VLs will be high, because the difference between the phase channels of each AL is the same, i.e.,  $\pi/6$ . An illustrated example is shown in Fig. 3.1, in which only the phases of the channels are highlighted to draw attention to the relation between these parameters. This fact suggests that the interference caused by multiple ALs can be strongly correlated, in accordance with the phase of the channel between the ALs and the VLs.

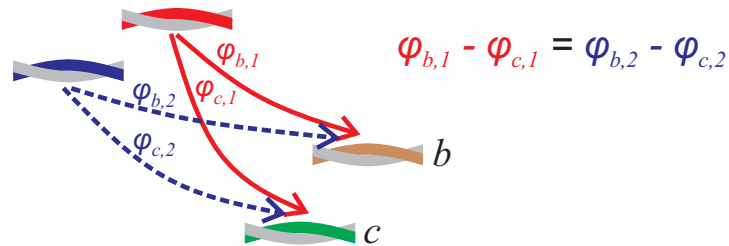


Figure 3.1: Example of channel phase difference in the coupling between alien lines and vectored lines. It should be noted that there is the condition for a high correlation (on the right-hand side of the diagram),  $\phi_{b,1} - \phi_{c,1} = \phi_{b,2} - \phi_{c,2}$ .

### 3.4 Determination of the Minimum Number of Prediction Lines Required for an Effective AXT Prediction

In the literature on linear regression and linear prediction, the effect of the correlation on the performance of a prediction is well defined and regarded as the most significant determining factor [58, 63, 64, 65]. However, to the best of our knowledge there is no formulation that states the way in which the signals are generated as a limiting factor on the performance of the prediction. Thus, in addressing this aspect of the prediction, in this section an attempt is made to tackle the AXT problem as a means of understanding how variations in performance are linked to the relation between the number of ALs and VLs. In this respect, a procedure is followed in a DFE manner, in which the first processed lines provide information for the last ones (as in RxPred), and after this, we define the minimum number of previous VLs necessary to make a complete prediction of the AXT in the current line, in a scenario with no AWGN.

Let us begin with the analysis of the scenario with 1 AL and 3 VL. In this case, the AXT observed in each VL can be given by the linear transformation [87]

$$\mathbf{q} = \begin{bmatrix} \mathcal{A}_1(1, :) \\ \mathcal{A}_1(2, :) \\ \mathcal{A}_1(3, :) \end{bmatrix} \mathbf{s}_1, \quad (3.24)$$

or

$$\begin{aligned} q(1) &= \mathcal{A}_1(1, :)\mathbf{s}_1 \\ q(2) &= \mathcal{A}_1(2, :)\mathbf{s}_1, \\ q(3) &= \mathcal{A}_1(3, :)\mathbf{s}_1 \end{aligned} \quad (3.25)$$

where  $\mathcal{A}_1(l, :)$  is the  $l$ -th line of the matrix  $\mathcal{A}_1$ . If account is taken of the stage in which the information from VL 1 is used to estimate the interference in the VL 2, the following linear system can be formulated

$$\begin{cases} \mathcal{A}_1(2, :)\mathbf{s}_1 = q(2) \\ \mathcal{A}_1(1, :)\mathbf{s}_1 = q(1) \end{cases}, \quad (3.26)$$

where  $\mathbf{s}$ ,  $q(1)$  and  $q(2)$  are the unknowns, and  $\mathcal{A}_1(1, :)$  and  $\mathcal{A}_1(2, :)$  are considered to be constant on the basis of the Assumption 7. However, in the case where one line is set to be a reference line (in our case, the vectored line 1), it is then possible to estimate  $q(1)$  in the QAM symbol decision of this reference line at the beginning of the mitigation process.

From (3.26),  $q(2)$  can be completely expressed as  $\mathcal{A}_1(2, :)\mathcal{A}_1^{-1}(1, :)q(1)$ , where  $\mathcal{A}_1^{-1}(1, :)$  refers to the *pseudo inverse* [66] of  $\mathcal{A}_1(1, :)$ . A similar result can be found for the estimation of  $q(3)$  based on  $q(1)$ , which shows that, in this scenario, the estimation of the interference in one VL can be carried out on the basis of the information from only one other line. However, if this analysis is extended to a scenario with 3 VLs and 2 ALs, we get the following equations

$$\begin{aligned} q(1) &= \mathcal{A}_1(1, :)\mathbf{s}_1 + \mathcal{A}_2(1, :)\mathbf{s}_2 \\ q(2) &= \mathcal{A}_1(2, :)\mathbf{s}_1 + \mathcal{A}_2(2, :)\mathbf{s}_2 \cdot \\ q(3) &= \mathcal{A}_1(3, :)\mathbf{s}_1 + \mathcal{A}_2(3, :)\mathbf{s}_2 \end{aligned} \quad (3.27)$$

With regard to the task of estimating  $q(2)$  based on  $q(1)$  we get the following equations for the linear system

$$\begin{cases} \mathcal{A}_1(2, :)\mathbf{s}_1 + \mathcal{A}_2(2, :)\mathbf{s}_2 = q(2) \\ \mathcal{A}_1(1, :)\mathbf{s}_1 + \mathcal{A}_2(1, :)\mathbf{s}_2 = q(1) \end{cases}, \quad (3.28)$$

in which  $\mathbf{s}_1$ ,  $\mathbf{s}_2$ ,  $q(1)$  and  $q(2)$  are the unknowns, but, again,  $q(1)$  is obtained in the decision of the reference line. As can be seen in (3.28), the task of estimating  $q(2)$  based on  $q(1)$  yields an undetermined system [67], which means that  $q(2)$  cannot be completely defined. In contrast, in the estimation of  $q(3)$  based on  $q(1)$  and  $q(2)$ , we get

$$\begin{cases} \mathcal{A}_1(3, :)\mathbf{s}_1 + \mathcal{A}_2(3, :)\mathbf{s}_2 = q(3) \\ \mathcal{A}_1(2, :)\mathbf{s}_1 + \mathcal{A}_2(2, :)\mathbf{s}_2 = q(2) \\ \mathcal{A}_1(1, :)\mathbf{s}_1 + \mathcal{A}_2(1, :)\mathbf{s}_2 = q(1) \end{cases}, \quad (3.29)$$

in which according to the linear system theory, there is enough information to find  $q(3)$  [67], because in this stage of the DFE process  $q(1)$  and  $q(2)$  were already estimated, and then we have 3 equations and 3 unknowns ( $\mathbf{s}_1$ ,  $\mathbf{s}_2$  and  $q(3)$ ). Thus, we can conclude from the perspective of the linear system that the performance of the interference prediction for each VL, is effective when the linear system formed by this target VL and the VLs that provide information for prediction is of the type determined [66], i.e., when the number of VLs providing information for the predictor is at least equal to the number of ALs generating the interference. In this case, the unknowns are the signals transmitted by the ALs and the interference observed in target VL. The condition above ensures an effective prediction regardless of the phase alignments revealed in Sec. 3.3.

In situations which yield undetermined systems, we can quantify the error when solving the linear system as follows. Let us take the situation in (3.28) as an example. Isolating  $\mathbf{s}_1$  in the second equation we get

$$\mathbf{s}_1 = \mathcal{A}_1^{-1}(1, :)[q(1) - \mathcal{A}_2(1, :)\mathbf{s}_2]. \quad (3.30)$$

Applying (3.30) in the first equation of (3.28) yields

$$\begin{aligned}
q(2) &= \mathcal{A}_1(2, :) \{ \mathcal{A}_1^{-1}(1, :) [q(1) - \mathcal{A}_2(1, :) \mathbf{s}_2] \} + \mathcal{A}_2(2, :) \mathbf{s}_2 \\
&= \mathcal{A}_1(2, :) \mathcal{A}_1^{-1}(1, :) q(1) - \mathcal{A}_1(2, :) \mathcal{A}_1^{-1}(1, :) \mathcal{A}_2(1, :) \mathbf{s}_2 + \mathcal{A}_2(2, :) \mathbf{s}_2 \\
&= \mathcal{A}_1(2, :) \mathcal{A}_1^{-1}(1, :) q(1) + [\mathcal{A}_2(2, :) - \mathcal{A}_1(2, :) \mathcal{A}_1^{-1}(1, :) \mathcal{A}_2(1, :)] \mathbf{s}_2. \tag{3.31}
\end{aligned}$$

On the basis of the Assumption 6 and the formulation in (3.21), we can write  $\mathcal{A}_1(2, :) = e^{j(\phi_{2,1} - \phi_{1,1})} \mathcal{A}_1(1, :)$ , because

$$\begin{aligned}
e^{j(\phi_{2,1} - \phi_{1,1})} \mathcal{A}_1(1, :) &= e^{j(\phi_{2,1} - \phi_{1,1})} [g_1 e^{j[\phi_{1,1}]}, g_1 e^{j[\phi_{1,1} - 2\pi k/2K]}, \dots, g_1 e^{j[\phi_{1,1} - 2\pi k(2K-1)/2K]}] \\
&= [g_1 e^{j[\phi_{2,1}]}, g_1 e^{j[\phi_{2,1} - 2\pi k/2K]}, \dots, g_1 e^{j[\phi_{2,1} - 2\pi k(2K-1)/2K]}] \\
&= \mathcal{A}_1(2, :). \tag{3.32}
\end{aligned}$$

Then, (3.31) can be simplified to

$$\begin{aligned}
q(2) &= \mathcal{A}_1(2, :) \mathcal{A}_1^{-1}(1, :) q(1) + [\mathcal{A}_2(2, :) - e^{j(\phi_{2,1} - \phi_{1,1})} \mathcal{A}_1(1, :) \mathcal{A}_1(1, :)^{-1} \mathcal{A}_2(1, :)] \mathbf{s}_2 \\
&= \mathcal{A}_1(2, :) \mathcal{A}_1^{-1}(1, :) q(1) + [\mathcal{A}_2(2, :) - e^{j(\phi_{2,1} - \phi_{1,1})} \mathcal{A}_2(1, :)] \mathbf{s}_2. \tag{3.33}
\end{aligned}$$

The part referring to the error in (3.33) is the one that contains the unknown  $\mathbf{s}_2$ . According to Sec. 3.3, the prediction will be made perfectly when  $\phi_{2,1} - \phi_{1,1} = \phi_{2,2} - \phi_{1,2}$ , or  $\phi_{2,2} = \phi_{2,1} - \phi_{1,1} + \phi_{1,2}$ . When this condition is applied in the brackets of (3.33), the part regarding the error leads to zero, because

$$\begin{aligned}
e^{j(\phi_{2,1} - \phi_{1,1})} \mathcal{A}_2(1, :) &= e^{j(\phi_{2,1} - \phi_{1,1})} [g_1 e^{j[\phi_{1,1}]}, g_1 e^{j[\phi_{1,1} - 2\pi k/2K]}, \dots, g_1 e^{j[\phi_{1,1} - 2\pi k(2K-1)/2K]}] \\
&= [g_2 e^{j[\phi_{2,1} - \phi_{1,1} + \phi_{1,2}]}, \dots, g_2 e^{j[\phi_{2,1} - \phi_{1,1} + \phi_{1,2} - 2\pi k(2K-1)/2K]}] \\
&= [g_2 e^{j[\phi_{2,2}]}, \dots, g_2 e^{j[\phi_{2,2} - 2\pi k(2K-1)/2K]}] \\
&= \mathcal{A}_2(2, :). \tag{3.34}
\end{aligned}$$

The above formulation does not include the factor thermal noise. When this is taken into account, the total amount of interference observed in the vectored group becomes:

$$\mathbf{z} = \begin{bmatrix} \mathcal{A}_1(1, :) & \dots & \mathcal{A}_M(1, :) \\ \vdots & \ddots & \vdots \\ \mathcal{A}_1(L, :) & \dots & \mathcal{A}_M(L, :) \end{bmatrix} \begin{bmatrix} \mathbf{s}_1 \\ \vdots \\ \mathbf{s}_M \end{bmatrix} + \begin{bmatrix} \Psi_1(1, :) & \dots & \Psi_\infty(1, :) \\ \vdots & \ddots & \vdots \\ \Psi_1(L, :) & \dots & \Psi_\infty(L, :) \end{bmatrix} \begin{bmatrix} \nu_1 \\ \vdots \\ \nu_\infty \end{bmatrix}, \tag{3.35}$$

---

where the second term in the right-hand side of (3.35) represents the thermal noise according to the formulation in Sec. 3.2.3,  $\mathbf{z}$  represents the total noise observed at the receivers of the vectored group,  $\Psi_\zeta(l)$  is the channel from some noise source  $\zeta$  to the VL  $l$ , and  $\nu_1 \cdots \nu_\infty$  are the realizations in the infinite-dimensional AWG noise vector. In this case, the number of dimensions in the interference space is always greater than the dimension in the space spanned by the signals produced within the vectored lines. As a result, the linear system will always be underdetermined, with an infinite number of unknowns as a result of the thermal noise, so that it is impossible to determine the  $z(l)$  elements with complete accuracy. However, in situation in which the power of the AXT much greater than the power of the AWGN, the magnitude of the terms regard to the AWGN in each equation will be small, and then a considerable parcel of the AXT can be predicted.



# Chapter 4

## Mitigation of Alien Crosstalk for Downstream DSL Transmissions Impaired by Multiple Interferers

In this chapter we present a method to mitigate AXT produced by multiple sources, based only in one reference line, named AMMIS. This algorithm is suitable for downstream transmission, because in this situation is hard to coordinate multiple lines due to the geographical separation between the transceiver of the side of the customers, and then the AXT mitigation methods found in the literature tend do not achieve their better performance.

### 4.1 System Model for AMMIS

For the AMMIS we consider a downstream DSL transmission in frequency domain using *Discrete Multitone Modulation*, in which data is conveyed by the *transmission channel* (TC). This transmission is impaired by some alien crosstalk sources, that leads to an interference term at the received signals. Additionally, the TC is served by a *reference channel* (RC) (as in Fig. 4.1), which can be either another twisted pair or an alternative transmission mode, such as the *common mode* [79]. For example, an extra line can be found in quad cables. The common mode can be accessed through a transceiver hardware modification to obtain the signal from the center tap of its transformers [86].

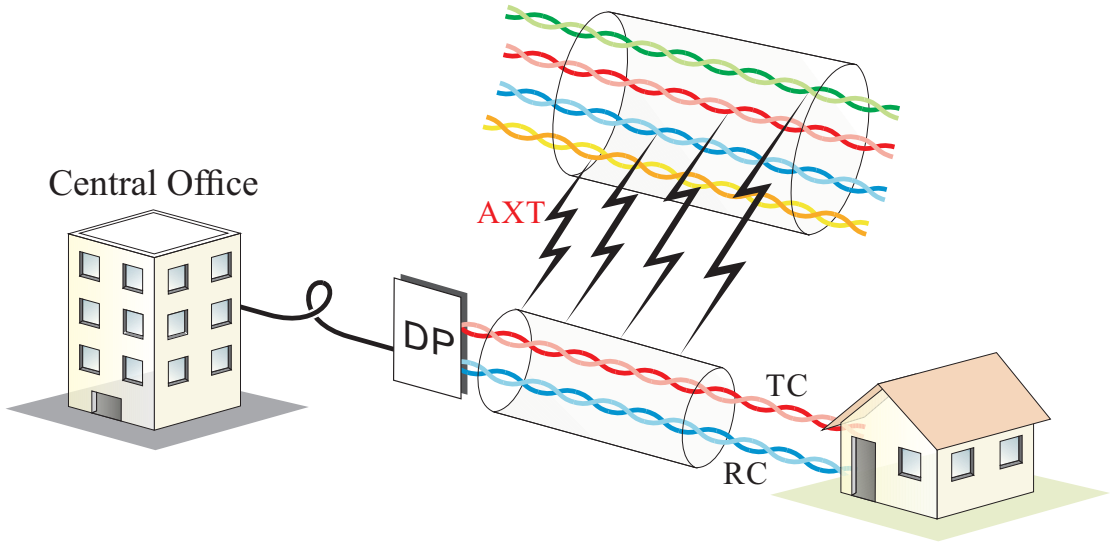


Figure 4.1: System model for a DSL transmission in TC with one RC and multiple interference sources.

In this study it is assumed that all the coordinated channels are synchronized, which is a plausible constraint according to [27]. For the sake of simplicity and to focus on the description of the novel method, we will assume a single TC/RC pair here, but the algorithm can be scaled to support several TCs, which will be shown in the Sec. 4.2.1. Then, for a synchronized transmission, we can represent the received signals in a given tone  $k$  by

$$\begin{aligned} \mathbf{y}_k &= \mathbf{H}_k \mathbf{x}_k + \mathbf{q}_k + \mathbf{n}_k \\ &= \mathbf{H}_k \mathbf{x}_k + \mathbf{z}_k, \end{aligned} \quad (4.1)$$

where  $\mathbf{y}_k = [y_{TC} \ y_{RC}]^T$  is a  $2 \times 1$  vector with the received symbols both in TC and RC,  $\mathbf{H}_k$  is a  $2 \times 2$  matrix with the direct channels of the TC and RC in its diagonal, and the crosstalk channels between TC and RC in its off diagonal,  $\mathbf{x}_k$  is a  $2 \times 1$  vector with the transmitted symbols  $[x_{TC} \ x_{RC}]^T$ ,  $\mathbf{q}_k$  is a  $2 \times 1$  vector with the AXT observed in the TC and the RC,  $\mathbf{n}_k$  is a  $2 \times 1$  vector that denotes background noise which can be modelled as additive white Gaussian noise, and  $\mathbf{z}_k = \mathbf{q}_k + \mathbf{n}_k$ , in a way that (4.1) can be rewritten as

$$\begin{bmatrix} y_{TC} \\ y_{RC} \end{bmatrix} = \mathbf{H}_k \begin{bmatrix} x_{TC} \\ x_{RC} \end{bmatrix} + \begin{bmatrix} z_{TC} \\ z_{RC} \end{bmatrix}. \quad (4.2)$$

The subscript  $k$  is omitted in the next paragraphs since a per-tone processing is assumed.

## 4.2 AXT Mitigation for Multiple Interference Sources (AMMIS)

This section outlines details of the method *AXT Mitigation for Multiple Interference Sources*, or AMMIS. This method needs to be executed both at the transmitter and receiver, where the combination of these stages makes it possible to mitigate the AXT and decode the transmitted symbols simultaneously. We begin by carrying out the pre-processing at the transmitter to make the equivalent channel decodable, and hence the resulting channel will be triangular. Let the square matrix  $\widehat{\mathbf{H}}$  represent the equivalent channel, i.e., the channel observed by the transmitted symbols after the pre and post-processing. Let  $\widehat{\mathbf{H}}'$  have the  $QR$  decomposition [51]

$$\widehat{\mathbf{H}}' = \mathbf{Q}\mathbf{R}, \quad (4.3)$$

where  $\mathbf{Q}$  is a unitary complex matrix and  $\mathbf{R}$  is an upper triangular matrix. Pre multiplying the transmitted symbols by  $\mathbf{Q}$ ,  $\tilde{\mathbf{x}} = \mathbf{Q}\mathbf{x}$ , we obtain

$$\begin{aligned} \tilde{\mathbf{y}} &= \widehat{\mathbf{H}}\tilde{\mathbf{x}} + \mathbf{v} \\ &= (\mathbf{Q}\mathbf{R})'\mathbf{Q}\mathbf{x} + \mathbf{v} \\ &= \mathbf{R}'\mathbf{Q}'\mathbf{Q}\mathbf{x} + \mathbf{v} \\ &= \mathbf{R}'\mathbf{x} + \mathbf{v}, \end{aligned} \quad (4.4)$$

where  $\mathbf{v}$  represents the resulting interference (after processing) at the receiver and the superscript  $'$  indicates the conjugate transpose (Hermitian). The equation in the last line of (4.4) indicates the resulting effect of the transmission, which also consider the processing at receiver that will be presented in the next paragraphs.

At the receiver the method begins with the *conditioning signal* stage, in which the received signals will be applied to successive matrix multiplications. In this stage, the proposed method requires an interference correlation matrix to be estimated during a training phase, which is given by [47]

$$\mathbf{C}_z = E[\mathbf{z}\mathbf{z}']. \quad (4.5)$$

From  $\mathbf{C}_z$  we obtain the whitening matrix  $\mathbf{W} = \mathbf{G}_z^{-1}$ , where  $\mathbf{G}_z$  is a lower triangular matrix, obtained from the Cholesky decomposition [67]  $\mathbf{C}_z = \mathbf{G}_z\mathbf{G}_z'$ . In *show-time* phase, the whitening matrix is used at the receiver in the expression

$$\begin{aligned} \hat{\mathbf{y}} &= \mathbf{W}\mathbf{y} \\ &= \mathbf{W}\widehat{\mathbf{H}}\tilde{\mathbf{x}} + \mathbf{W}\mathbf{z}. \end{aligned} \quad (4.6)$$

This stage makes the correlation matrix of the interference term,  $\mathbf{Wz}$ , a  $2 \times 2$  identity matrix  $\mathbf{I}$ , because

$$\begin{aligned} E[\mathbf{Wz z}'\mathbf{W}'] &= \mathbf{W}E[\mathbf{z z}']\mathbf{W}' \\ &= \mathbf{G}_z^{-1}\mathbf{C}_z\mathbf{G}_z^{-'} \\ &= \mathbf{I}. \end{aligned} \quad (4.7)$$

At this stage the correlation matrix of the reminiscent interference has a canonical form, in which a similar process can be used to the one used to make it diagonal, and impose on it a desired behavior. Then, to make the correlation matrix to have the form  $\mathbf{C}_u = \mathbf{G}_u\mathbf{G}_u'$ , we left multiply  $\hat{\mathbf{y}}$  by  $\mathbf{G}_u$ , to get

$$\begin{aligned} \tilde{\mathbf{y}} &= \mathbf{G}_u\hat{\mathbf{y}} \\ &= \mathbf{G}_u\mathbf{W}\mathbf{H}\tilde{\mathbf{x}} + \mathbf{G}_u\mathbf{Wz} \\ &= \mathbf{G}_u\mathbf{W}\mathbf{H}\tilde{\mathbf{x}} + \mathbf{v}, \end{aligned} \quad (4.8)$$

where  $\mathbf{v} = \mathbf{G}_u\mathbf{Wz}$  is a  $2 \times 1$  column vector that represents the reminiscent interference, which has the correlation matrix

$$\begin{aligned} E[\mathbf{v v}'] &= E[\mathbf{G}_u\mathbf{Wz z}'\mathbf{W}'\mathbf{G}_u'] \\ &= \mathbf{G}_uE[\mathbf{Wz z}'\mathbf{W}']\mathbf{G}_u' \\ &= \mathbf{G}_u\mathbf{I}\mathbf{G}_u' \\ &= \mathbf{C}_u. \end{aligned} \quad (4.9)$$

Now we define the equivalent channel  $\hat{\mathbf{H}} = \mathbf{G}_u\mathbf{W}\mathbf{H}$ , and according to (4.4) and (4.3), the channel observed by the transmitted symbols is given by the  $\mathbf{R}'$  matrix, which makes the end-to-end transmission to be

$$\begin{aligned} \tilde{\mathbf{y}} &= \mathbf{R}'\mathbf{x} + \mathbf{v} \\ \begin{bmatrix} \tilde{y}_{TC} \\ \tilde{y}_{RC} \end{bmatrix} &= \begin{bmatrix} R(1,1) & R(1,2) \\ 0 & R(2,2) \end{bmatrix}' \begin{bmatrix} x_{TC} \\ x_{RC} \end{bmatrix} + \begin{bmatrix} v_{TC} \\ v_{RC} \end{bmatrix} \\ \begin{bmatrix} \tilde{y}_{TC} \\ \tilde{y}_{RC} \end{bmatrix} &= \begin{bmatrix} R(1,1)^* & 0 \\ R(1,2)^* & R(2,2)^* \end{bmatrix} \begin{bmatrix} x_{TC} \\ x_{RC} \end{bmatrix} + \begin{bmatrix} v_{TC} \\ v_{RC} \end{bmatrix}, \end{aligned} \quad (4.10)$$

where the superscript  $*$  denotes complex conjugation,  $R(i, j)$  denotes the element in row  $i$  and column  $j$  of  $\mathbf{R}$  matrix, and  $v_{TC}$  and  $v_{RC}$  denote the reminiscent interference in the TC and RC, respectively.

The conditioning signal step, in which the behavior of the correlation matrix of the interference was induced (4.8), was carried out to ensure the interference in the TC could be suitably predicted based on the interference observed in the RC, that comprises the next stage called *AXT removal*. The taps of this predictor can be found through the Cholesky decomposition of the correlation matrix of the reminiscent interference [58]. However, to get a predictor through this strategy, the data referring to the first line of the correlation matrix are used to predict the data related to the second line [47]. This means, we must generate a correlation matrix of the reminiscent interference in which the position of  $v_{tc}$  and  $v_{rc}$  are changed

$$\mathbf{b} = \begin{bmatrix} v_{rc} \\ v_{tc} \end{bmatrix}, \quad (4.11)$$

Finally, we compute the correlation matrix  $\mathbf{C}_b = E[\mathbf{b}\mathbf{b}']$ , which can be decomposed into  $\mathbf{G}_b\mathbf{D}_b\mathbf{G}_b'$ , where  $\mathbf{G}_b$  is a monic matrix [47] and  $\mathbf{D}_b$  is a diagonal matrix. After this, the predictor for the reminiscent interference at the TC is given by

$$\dot{v}_{TC} = G_b(2, 1)v_{RC}, \quad (4.12)$$

where  $G_b(2, 1)$  is the element in the second line of the first column of the  $\mathbf{G}_b$ , and  $\dot{v}_{TC}$  is the prediction of  $v_{TC}$ .

In our method the RC is only used to support information for TC, and only pilot symbols are transmitted in this channel. Then, we begin the decoding by subtracting the known part of the received signal at the RC as

$$\begin{aligned} \check{y}_{RC} &= \tilde{y}_{RC} - R(2, 2)^*x_{RC} \\ &= R(1, 2)^*x_{TC} + R(2, 2)^*x_{RC} + v_{RC} - R(2, 2)^*x_{RC} \\ &= R(1, 2)^*x_{TC} + v_{RC}. \end{aligned} \quad (4.13)$$

From this we derive the prediction of the  $v_{TC}$  by multiplying  $\check{y}_{RC}$  by  $G_b(2, 1)$ , which yields

$$\begin{aligned} G_b(2, 1)\check{y}_{RC} &= G_b(2, 1)[R(1, 2)^*x_{TC} + v_{RC}] \\ &= G_b(2, 1)R(1, 2)^*x_{TC} + G_b(2, 1)v_{RC} \\ &= G_b(2, 1)R(1, 2)^*x_{TC} + \dot{v}_{TC}, \end{aligned} \quad (4.14)$$

and we subtract  $\dot{v}_{TC}$  from this sum, which yields

$$\begin{aligned} \check{y}_{TC} &= \tilde{y}_{TC} - G_b(2, 1)R(1, 2)^*x_{TC} - \dot{v}_{TC} \\ &= R(1, 1)^*x_{TC} + v_{TC} - G_b(2, 1)R(1, 2)^*x_{TC} - \dot{v}_{TC} \\ &= [R(1, 1)^* - G_b(2, 1)R(1, 2)^*]x_{TC} + e_{TC}, \end{aligned} \quad (4.15)$$

where  $e_{TC}$  represents the error in the prediction of the  $v_{TC}$ , i.e.,  $e_{TC} = v_{TC} - \hat{v}_{TC}$ . Now, the AXT is mitigated in the TC the equalization can be performed by adjusting the *frequency equalizer* (FEQ) from the standard  $1/R(1,1)^*$ , to

$$FEQ = \frac{1}{R(1,1)^* - G_b(2,1)R(1,2)^*}. \quad (4.16)$$

Following this, the signal can be submitted to the QAM symbol decision operation, in order to get the estimation of the  $x_{TC}$ ,  $\bar{x}_{TC}$ . From (4.15), it can be observed that the channel gain observed by the  $x_{TC}$  is

$$\tau = R(1,1)^* - G_b(2,1)R(1,2)^*, \quad (4.17)$$

which allows us to represent the *signal-to-interference-plus-noise ratio* (SINR) to the TC according to [20], per tone, as

$$SINR_{TC} = \frac{\mathcal{E}_{TC}|\tau|^2}{E[e_{TC}e'_{TC}]}, \quad (4.18)$$

where  $\mathcal{E}_{TC}$  is the transmission power of the  $x_{TC}$  per tone. The whole AMMIS processing is shown in Fig. 4.2, where *Dec* denotes the QAM symbol decision operation.

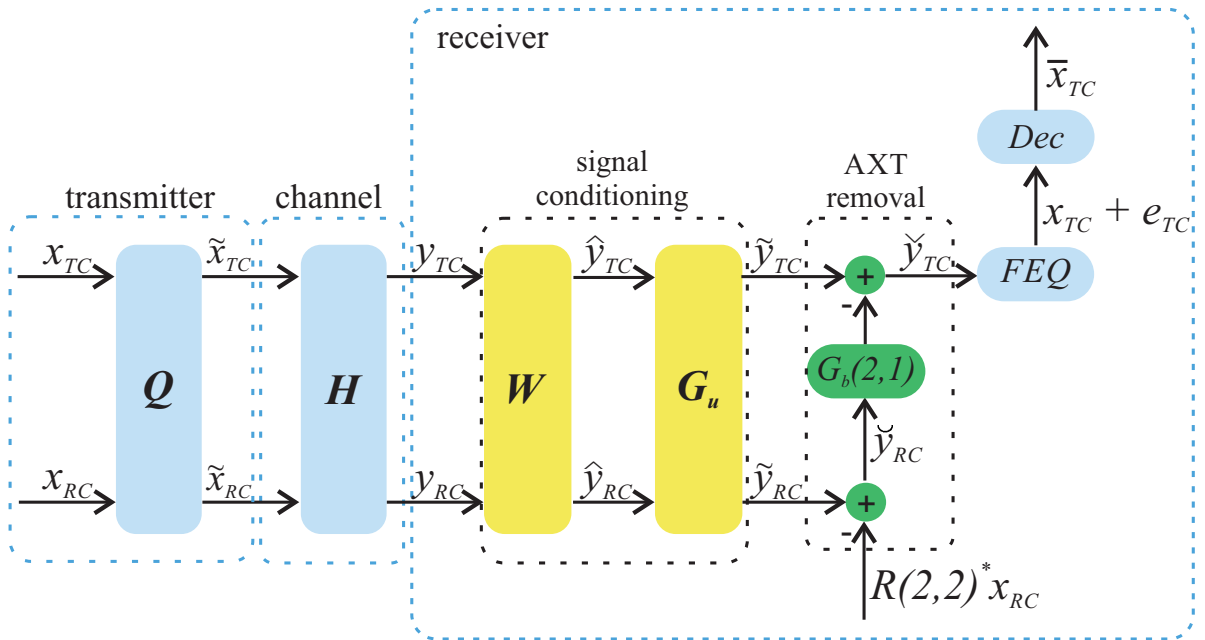


Figure 4.2: The schematic representation of the AMMIS method.

#### 4.2.1 The Effect of Vectoring on AMMIS

To achieve high data rates, the G.fast standard adopts *vectoring* [68]. This makes it logical to evaluate the performance of AMMIS when it is applied to a group of coordinated

lines, or vectored group (VG). From this perspective, our model can be expanded to  $L$  coordinated TC/RC pairs as

$$\begin{aligned} \ddot{\mathbf{y}} &= \ddot{\mathbf{H}}\mathbf{P}\ddot{\mathbf{x}} + \ddot{\mathbf{z}} \\ \begin{bmatrix} \mathbf{y}_l \\ \vdots \\ \mathbf{y}_L \end{bmatrix} &= \ddot{\mathbf{H}}\mathbf{P} \begin{bmatrix} \tilde{\mathbf{x}}_l \\ \vdots \\ \tilde{\mathbf{x}}_L \end{bmatrix} + \begin{bmatrix} \mathbf{z}_l \\ \vdots \\ \mathbf{z}_L \end{bmatrix}, \end{aligned} \quad (4.19)$$

where  $\ddot{\mathbf{x}} = [\tilde{\mathbf{x}}_1 \dots \tilde{\mathbf{x}}_L]^T$ , in which  $\tilde{\mathbf{x}}_l$  is a column vector that contains the transmitted symbols in TC and RC of the  $l$ th TC/RC pair,  $\ddot{\mathbf{H}}$  is a  $2L \times 2L$  matrix which contains all the direct channel of the TCs and RCs in its diagonal and the crosstalk channels among them in out-of-diagonal elements,  $\ddot{\mathbf{z}} = [\mathbf{z}_1 \dots \mathbf{z}_L]^T$  contains the total interference observed by all lines, and  $\mathbf{P} = (1/\beta)\ddot{\mathbf{H}}^{-1}\text{diag}(\ddot{\mathbf{H}})$  is the precoder applied to remove the crosstalk among the coordinated channels, in which  $\text{diag}(\cdot)$  represents the diagonal of a matrix, and  $\beta$  is a factor used to control the transmission power of the transmitted symbols [68]. In this situation, the received symbols become

$$\begin{aligned} \ddot{\mathbf{y}} &= \beta^{-1}\text{diag}(\ddot{\mathbf{H}})\ddot{\mathbf{x}} + \ddot{\mathbf{z}} \\ &= \beta^{-1} \begin{bmatrix} H_1(1,1) & 0 & \dots & 0 & 0 \\ 0 & H_1(2,2) & \dots & 0 & 0 \\ \vdots & \vdots & \ddots & \vdots & \vdots \\ 0 & 0 & \dots & H_L(1,1) & 0 \\ 0 & 0 & \dots & 0 & H_L(2,2) \end{bmatrix} \begin{bmatrix} \tilde{x}_{TC1} \\ \tilde{x}_{RC1} \\ \vdots \\ \tilde{x}_{TCL} \\ \tilde{x}_{RCL} \end{bmatrix} + \begin{bmatrix} \tilde{z}_{TC1} \\ \tilde{z}_{RC1} \\ \vdots \\ \tilde{z}_{TCL} \\ \tilde{z}_{RCL} \end{bmatrix}, \end{aligned}$$

where  $H_l(c, c)$  is the element at the position  $(c, c)$  of the channel matrix of the  $l$ -th TC/RC pair,  $\tilde{x}_{TCl}$  is the transmitted symbol in the TC of the  $l$ -th TC pair, and  $\tilde{z}_{TCl}$  is its correspondent interference. The result of the (4.20) indicates that the effect of a vectorized coordinate group on AMMIS is to diagonalize  $\mathbf{H}$  in (4.1), (4.6) and (4.8), but each  $\tilde{\mathbf{x}}_l$  keeps its precoding applied in the AMMIS (4.4) independently from the other users. Then, AMMIS can be normally employed for each TC/RC pair. Additionally, the SINR is scaled by  $(1/\beta)^2$

$$\text{SINR}_{TC} = \frac{\rho|\tau|^2}{\beta^2 E[e_{TC}e'_{TC}]}. \quad (4.20)$$

# Chapter 5

## Results

In this chapter, we present the simulation results of the formulations outlined in the previous chapter. Additionally, we present some cable measurements that we have made, which were used in some of the simulations.

### 5.1 Measurements

It is essential for system designers to know the behavior of the DSL links, because a knowledge of the transfer function and the electromagnetic ingress/egress can enable engineers to establish communication systems which operate effectively and at a suitable cost. This kind of information can be obtained in at least 2 ways: through channel modelling or from measurements. In this chapter we will focus on the measurements, which allow a piece of equipment to be used to analyse the electromagnetic properties of the cable.

#### 5.1.1 Network Analyzer - NA

The Network Analyzer is a device that is mainly used in laboratories to measure the electromagnetic properties of electronic components. The range of devices that can be measured with an NA covers from simple components like resistors and capacitors, up to complex electronic circuits, including cable arrangements. In general, the equipment measured by an NA is called *device under test* (DUT). Fig. 5.1 shows a network analyzer, or more specifically, the Agilent E5071C. This kind of equipment operates by transmitting a wave with a specific frequency to the DUT and evaluating the received signal, depending on the type of measurement employed.



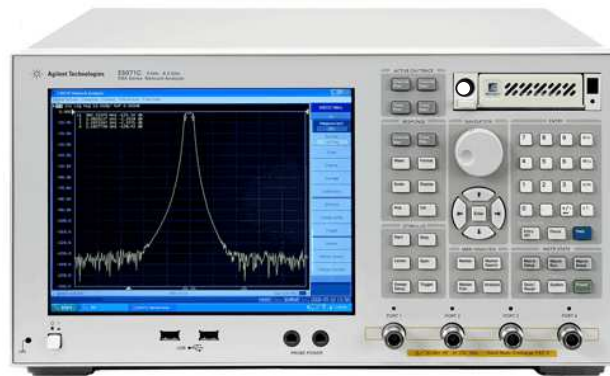


Figure 5.1: Network Analyzer Agilent E5071C.

### 5.1.2 Calibration

In general, the connectors of the equipment used in the measurements are not balanced, which do not allows to plug the twisted pairs directly on the NA. In view of this, it is necessary to put an interface between the NA and the cable. However, when this interface is added, it becomes a part of the measurement. Moreover, since we do not want this interface to affect the measurement, a procedure is adopted called *calibration*, that mitigates the effects of the interface on the measurements.

In the interface, generally a BALUN (balanced-unbalanced) is used, which is a transformer that has some of its wires grounded [69, 71]. However, as well as allowing this conversion to take place, the balun also changes the voltage, current and electrical impedance (as a standard transformer) of the signals which pass through its terminals. The impedance transformation is thus an important feature that has to be evaluated, because the balanced side must “match” the cable impedance, in order to avoid problems with reflections [70].

### 5.1.3 Cable Measurements

As a means of obtaining realistic channels for our simulations, we made measurements of the coupling between 50 m long twisted-pairs belonging to different CAT5 and CAT6 cables. CAT5 and CAT6 are high quality cables which are generally used in Ethernet, but its use for DSL transmission is also considered in the standardization [27]. These cables consists of 4 twisted pairs that are spirally arranged, as schematically shown in Fig. 5.2. The twist rate among the pairs is distinct to reduce the impedance matching and, consequently, the coupling among the pairs [72].

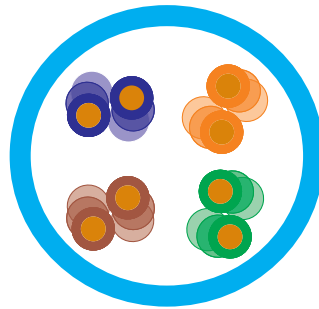


Figure 5.2: The cross section scheme of a CAT5 and a CAT6 cable.

Even though the main objective of the experiment was to measure the crosstalk channels, we also measured the direct channels for the sake of making a comparison. In this measurement campaign we have used 3 cables: 2 CAT5 cables, which we called CAT5 A and CAT5 B, and one CAT6 cable. The twisted-pairs in the CAT5 B cable were adopted as the vectored group, which means that the in-domain crosstalk was regarded as the crosstalk between the pairs of this cable. Meanwhile, AXT (or out-of-domain crosstalk) was considered to be the coupling between the twisted-pairs of the CAT5 A and CAT6 to the pairs of the CAT5 B, as illustrated in Fig. 5.3. In this figure is evident the connections for the measurement of crosstalk channels, in which the terminals of the VNA are plugged to the ends of different twisted pairs.

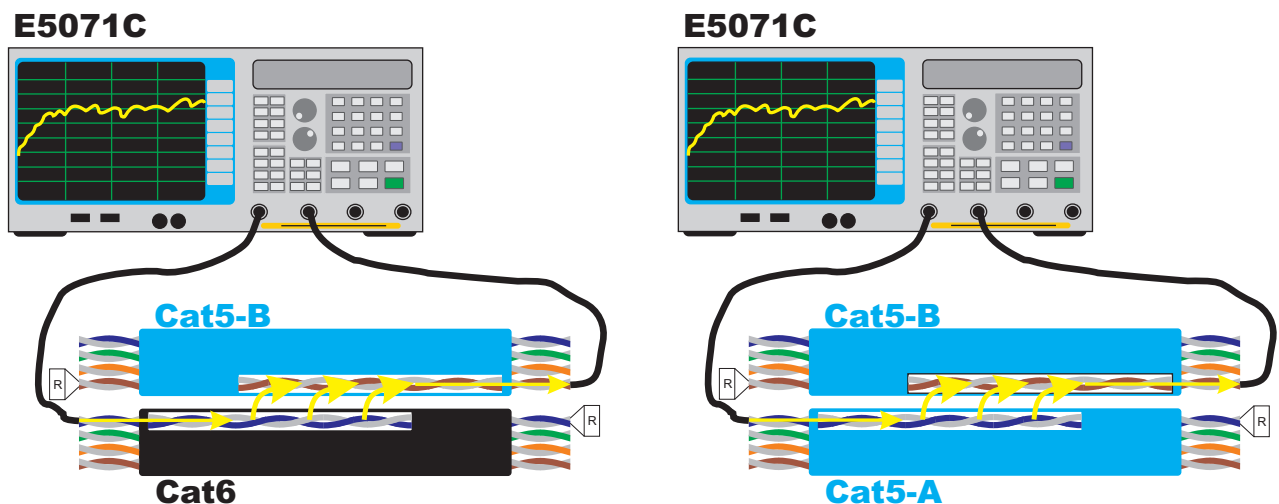


Figure 5.3: Measurement scheme for the coupling between different CAT5 and CAT6 cables.

Fig. 5.4 summarizes the terminology of the measurements performed, in which the direct channel is the transfer function obtained by a measurement in which the ends of the same twisted-pair are plugged to the VNA.

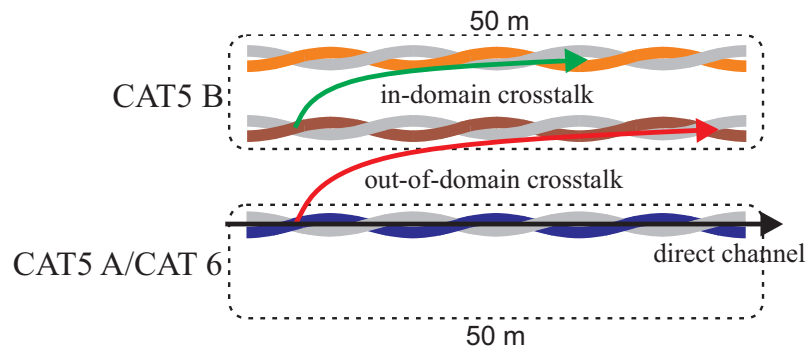


Figure 5.4: Measurement setup. In-domain crosstalk is regarded as the crosstalk between twisted-pairs of the same CAT5 cable, while out-of-domain crosstalk is the coupling between pairs of distinct cables. The direct channel is also illustrated.

The following devices were used in the measurements:

- Agilent E5071C network analyzer;
- North Hills BALUN 50 - 100  $\Omega$ , 100 KHz - 300 MHz;
- 50  $\Omega$  connectors used to match free ends of the pairs and to conduct the calibration;
- MULTILAN Cat-5e U/UTP 24AWGx4P cable, 50 m long.
- GIGALAN Cat-6 U/UTP 23AWGx4P cable, 50 m long.

The measurements were carried out in a frequency range of 100 kHz to 220 MHz. In total, 112 measurements were evaluated, 12 direct channels (4 for each cable), 12 crosstalk channels for the lines of the same cable (in a total of 36), and 64 AXT channels (32 from CAT5 A to CAT B and CAT6, and 32 from CAT6 to CAT5 B and CAT5 A). The aim of the experiments was to investigate the effects of AXT in situations involving the arrangement of cabling inside buildings.

Fig. 5.5 and Fig. 5.6 summarize all the measurements of coupling between the CAT5 cables and also between the CAT5 and CAT6 cables. Although, is difficult to identify the curves pertaining to crosstalk inside and between different cables, these curves allow us to verify the difference between the magnitude of the direct channel and the crosstalk channels.

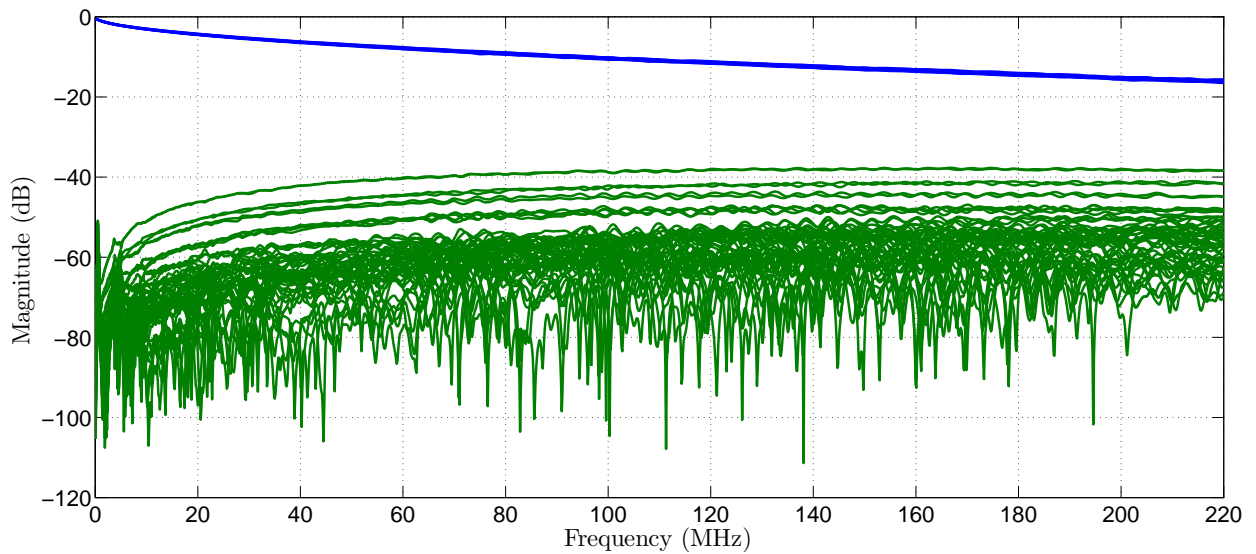


Figure 5.5: All the measurements in the scenario with 2 CAT5 cables. The blue lines represent the direct channels and the green lines are the coupling, both in-domain and out-of-domain.

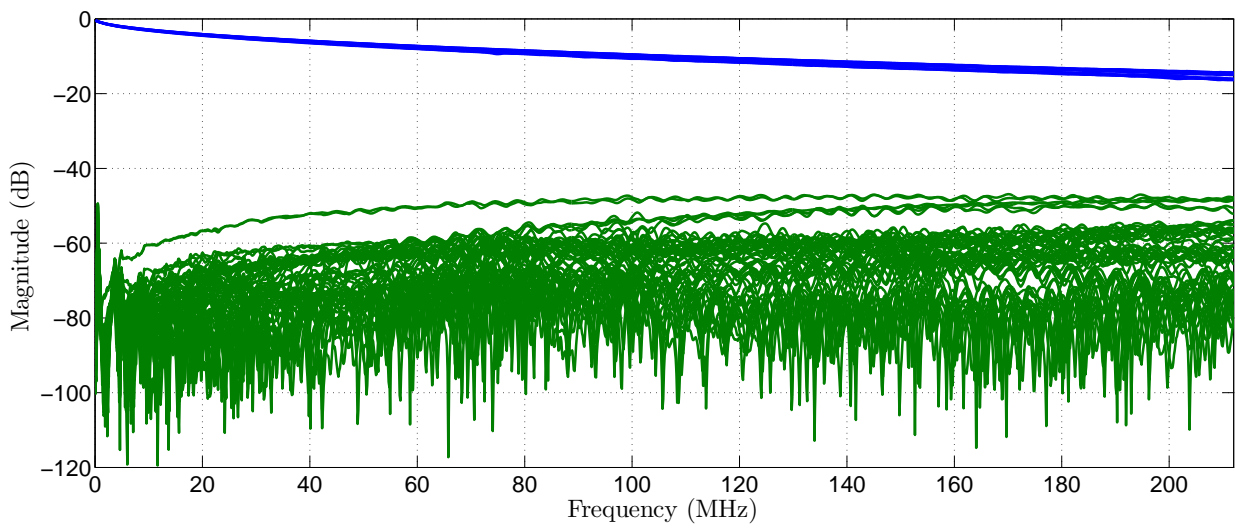


Figure 5.6: All measurements in the scenario with the CAT5-B cable and the CAT6 cable. The blue lines represent the direct channels and the green ones are the coupling, both in-domain and out-of-domain.

Fig. 5.7 and Fig. 5.8 only display the out-of-domain crosstalk in the situation of coupling between 2 CAT5 cables, and in the scenario involving both a CAT5-B cable and a CAT6, respectively. When these figures are compared, it is clear that in general the coupling caused

by the CAT6 cable over the CAT5 one is smaller than the coupling between the CAT5 cables. This can be concluded from the magnitude of the coupling in Fig. 5.8, which in the worst case is approximately  $-50$  dB, whereas, in Fig. 5.7 the coupling channels reaches more than  $-40$  dB. This is an expected pattern due to the high quality of the cat6 cables, which implies in the reduction of the coupling.

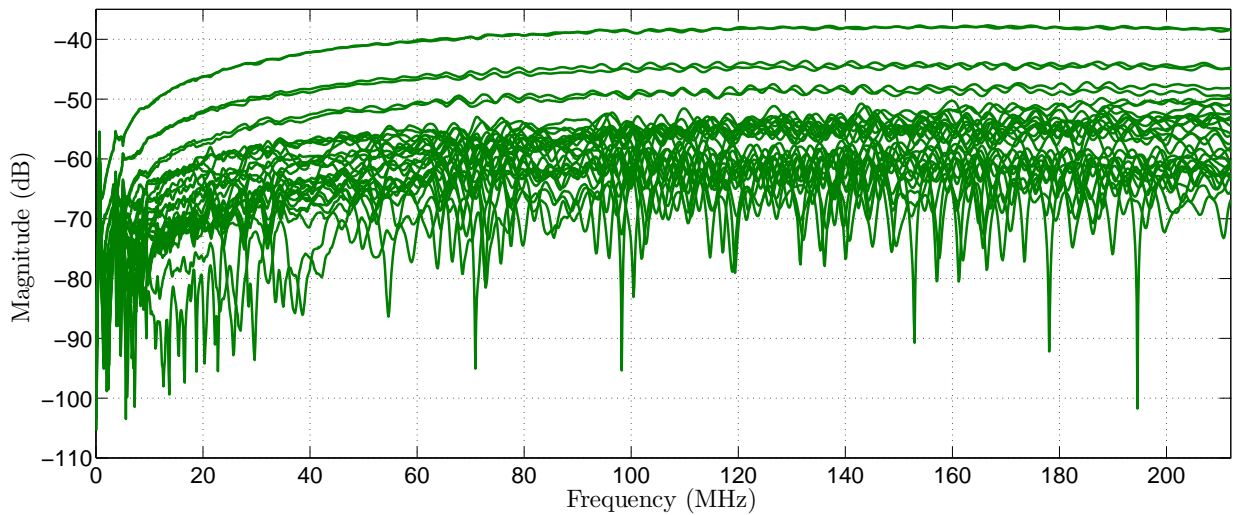


Figure 5.7: Out-of-domain coupling in the scenario with 2 CAT5 cables.

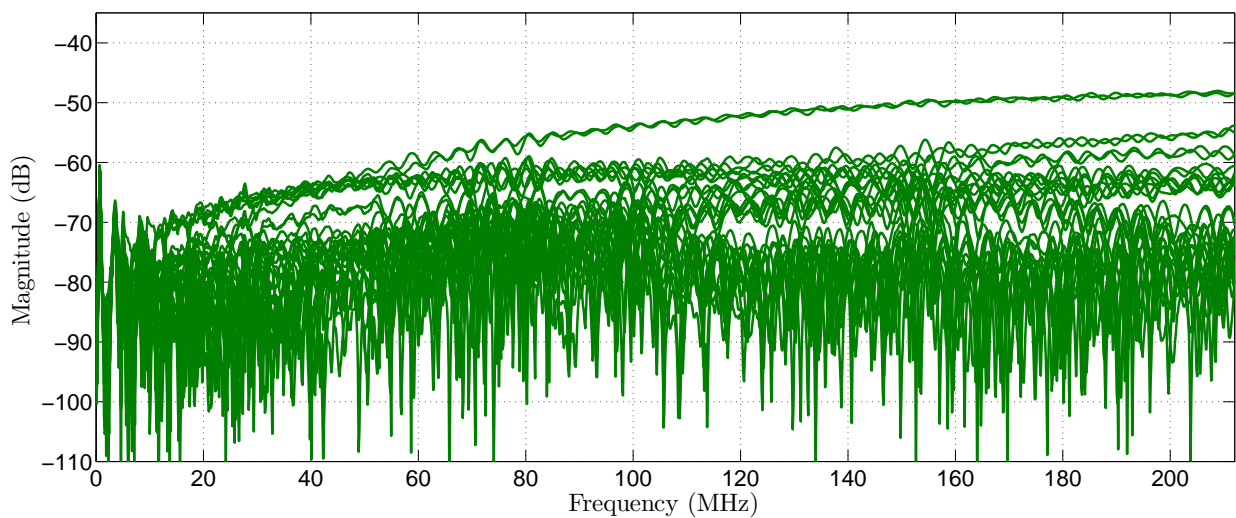


Figure 5.8: Out-of-domain coupling in the scenario with the CAT6 cable and the CAT5 B cable.

Due to the proximity between the pairs pertaining to the same cable, it is possible to

identify channel measurements where the incoming AXT channels are stronger than their own in-domain crosstalk channels, as shown in Fig. 5.9. However, other factors than the proximity between the twisted pairs affects the magnitude of the coupling. For example, in [72] is showed that the impedance matching between the twisted-pairs is an important parameter in the definition of the magnitude of crosstalk. Then, we can observe cases in which the gains of out-of-domain coupling are, on average, are weaker than those of in-domain coupling, as depicted in Fig. 5.10. Hence, it is possible to conclude that AXT channels can be as strong as self-crosstalk channels even when there are high quality cables such as CAT5. This suggests that AXT mitigation methods may be essential for improving the performance of the system in many scenarios of interest.

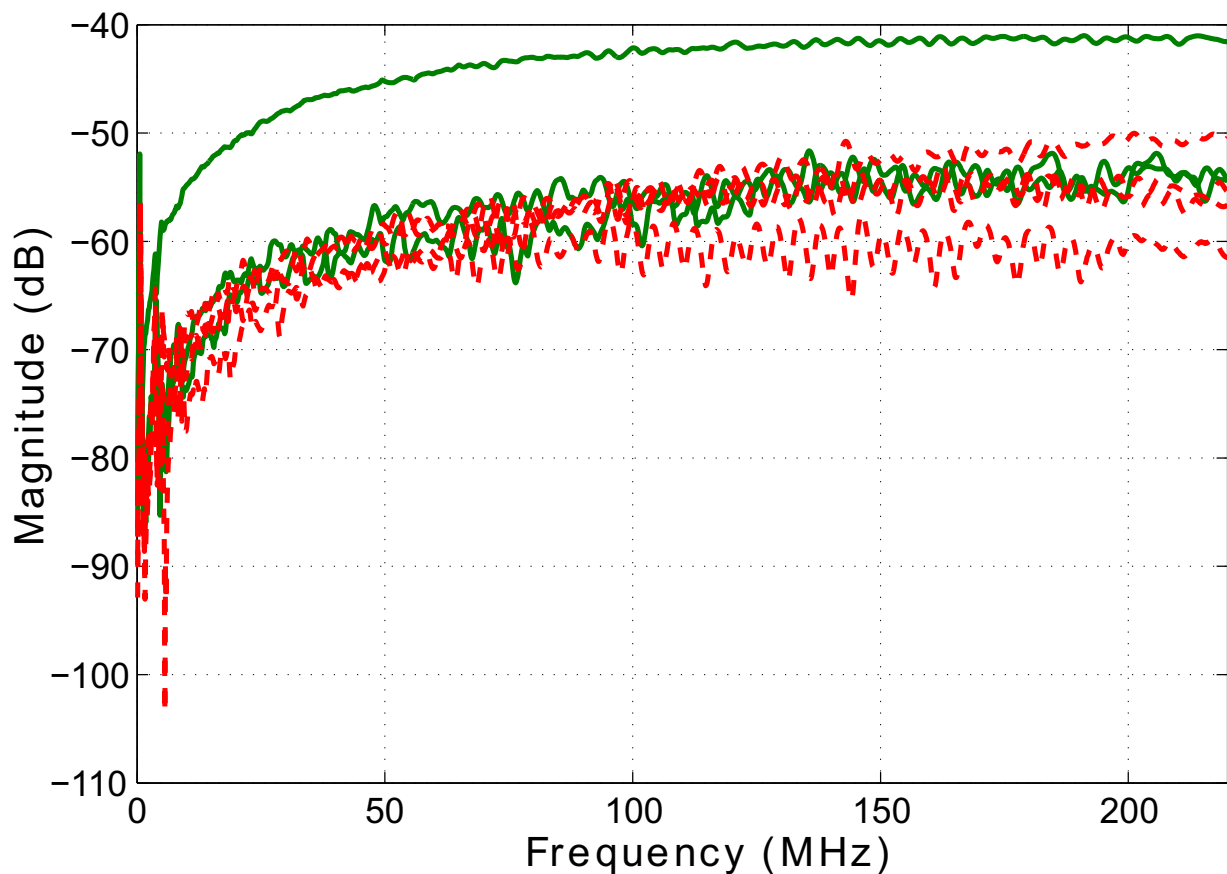


Figure 5.9: Case where the gains of out-of-domain coupling (red lines) are less than those of in-domain coupling (green lines) in the scenario with 2 CAT5 cables.

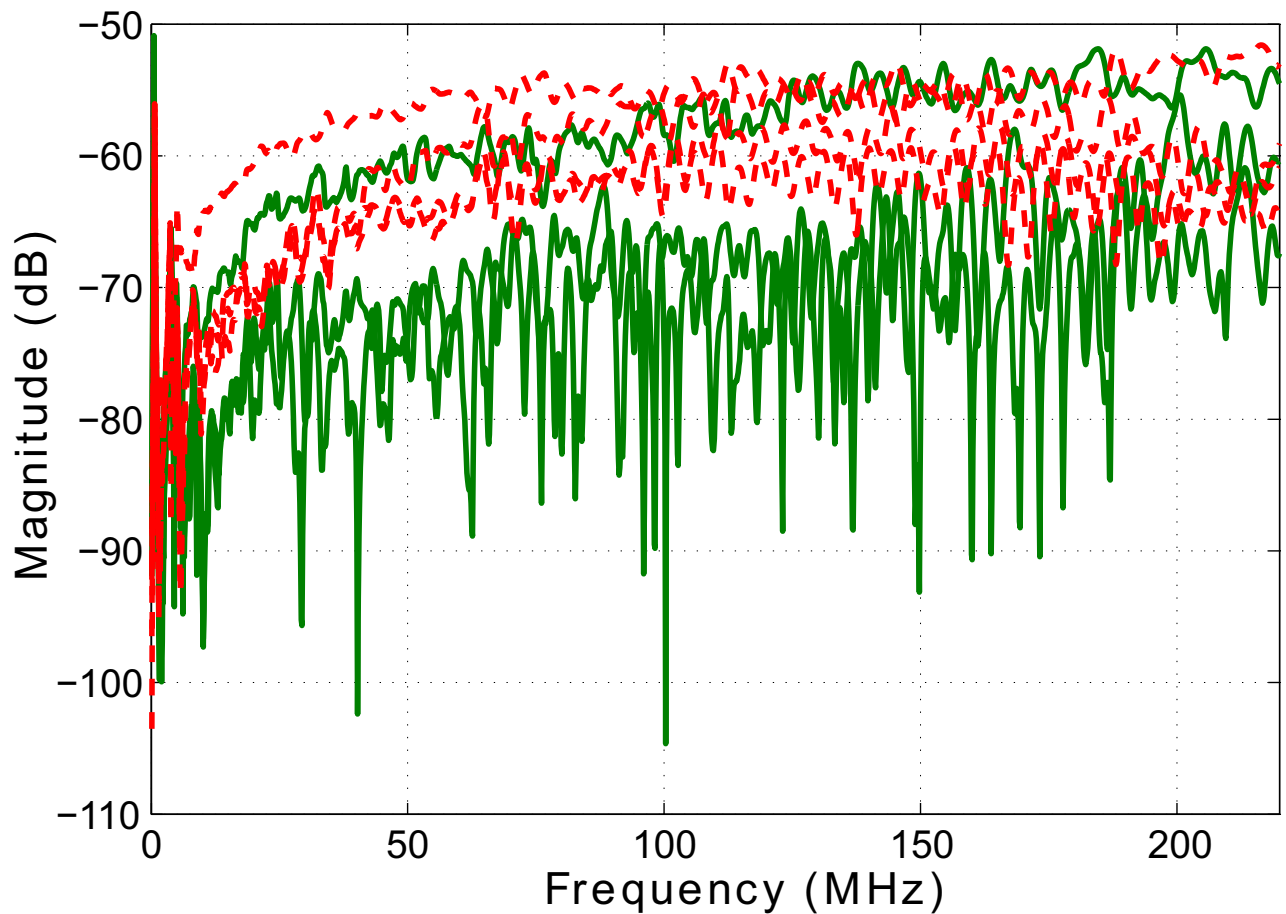


Figure 5.10: Case where the gains of out-of-domain coupling (red lines) are greater than in-domain coupling (green lines) in the scenario with 2 CAT5 cables.

## 5.2 Simulation Results

To validate the formulations presented in the Chapter 3 and Chapter 4, we carried out some simulations with the measurements of the previous section, measurements of other research groups, simulated channels and with some arbitrary data.

### 5.2.1 Results for the Correlation Analysis

In this section we will evaluate the validity of the formulation presented at the Sec. 3.1, through a comparison with a correlation obtained by a Monte Carlo simulation. In both situation the data regard to the channels were obtained from the coupling of the CAT5 A over CAT5 B, presented in the Sec. 5.1.3. Additionally, we have used the constraints listed in the

## Chapter 3

The correlation matrix was calculated by means of (5.1), repeated here by convenience

$$\mathbf{C}_q = \mathcal{E}_s \mathbf{C}_1 + \mathcal{E}_s \mathbf{C}_2 + \dots + \mathcal{E}_s \mathbf{C}_M, \quad (5.1)$$

where  $\mathbf{C}_1$  was derived from the AXT channels from the measurements. The Monte Carlo simulation were employed using the parameters in Table 5.1.

Table 5.1: Parameters used in the Monte Carlo simulation in the Sec. 5.2.1.

Parameter	Value
Input Signal	QAM symbols
Input Distribution	Uniform
Mean of the Distribution	0
Number of Tones	4096
Number of DMT symbols	1000

Fig. 5.11 shows the comparison of the real and imaginary parts of the element (3, 1) of the correlation matrix in a scenario with 4 AL and 4 VL. As can be seen in this plot, the correlation matrix produced by (3.4) fits well with result obtained from the Monte Carlo simulations. The difference between the approaches must be caused by the non ideal behavior of the random number routine and the number of realizations employed in Monte Carlo Simulations. In fact (3.4) represents the asymptotic behavior of the correlation matrix.



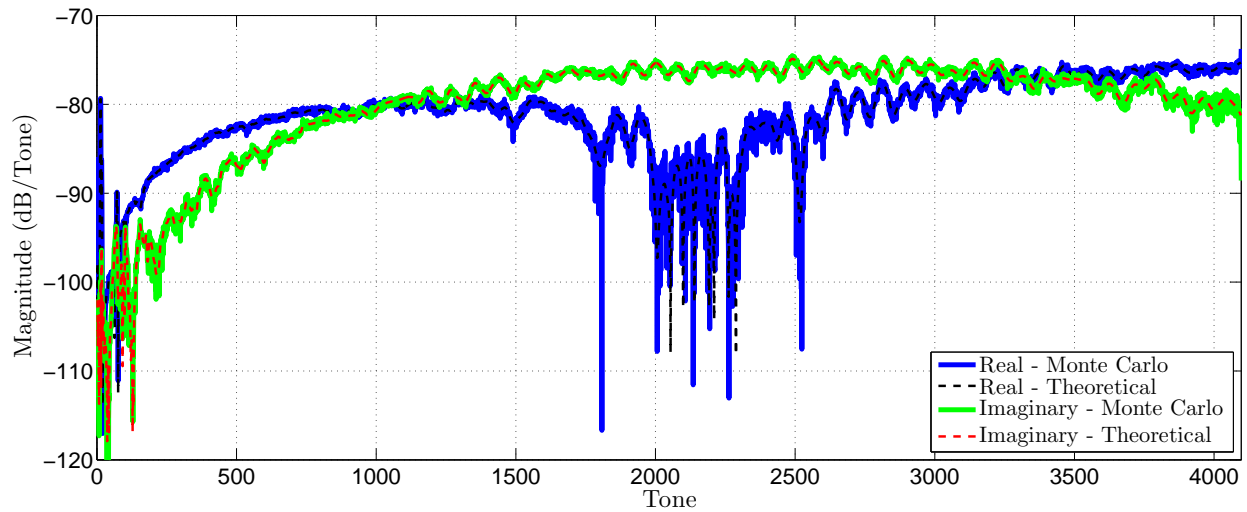


Figure 5.11: Comparison of the correlation matrix element produced by the Monte Carlo simulation and Theoretical derivation (both the real and imaginary part). Scenario with 4 AL and 4 VL. Element (3, 1) of the correlation matrix.

Fig. 5.12 shows a comparison between the correlation coefficient obtained from a Monte Carlo simulation and that obtained theoretically, by means of (3.18) in a scenario with thermal noise. The reduction of the correlation coefficient is clear in this diagram, which has presented a value less than one. In this plot we also can see that the correlation coefficient is very small in the low frequencies. This was expected because in this band the values of  $P_m$  are small, which increases the ratio in the denominator of (3.18), and hence sharply reduces the value of  $\rho'_{b,c}$ .

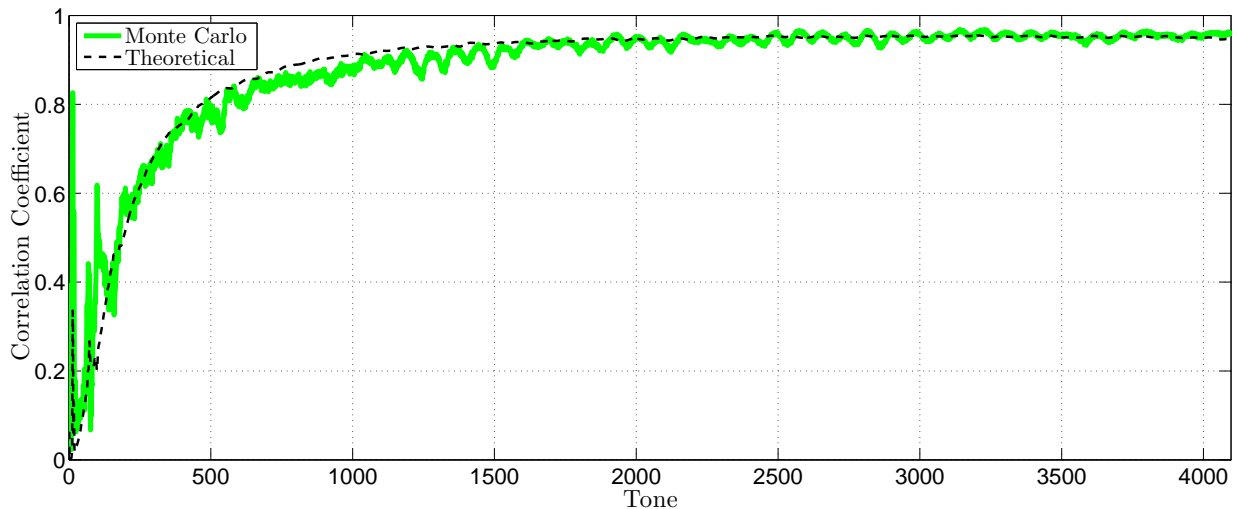


Figure 5.12: Comparison of correlation coefficient produced by the Monte Carlo simulation and Theoretical derivation in a situation with thermal noise. Scenario with 1 AL and 4 VL. Element (3, 1) of the correlation matrix.

The results in Fig. 5.11 and Fig. 5.12 indicate that (5.1) fits well in the data obtained by Monte Carlo simulation, and can be used to analyse the behaviour of the correlation of interference, as will be shown later.

## 5.2.2 Evaluation of the Effect of the AXT Channel Phase in the Correlation

To support the evaluation of the impact of the phase in the correlation, we have carried out simulations in which the AXT channel were arbitrarily defined, in which we had total control of the magnitude and phase. Table 5.2 and Table 5.3 summarize the results of these simulations, in which only one tone was used. These tables show the absolute correlation coefficient with regard to the magnitude of the AXT channel (in linear scale), and the difference of the channel phase of the AXT channels in the VLs. For example, the second line of Table 5.2 shows that the simulation is based on the assumption that the channel of an alien source has magnitude 1 whereas the other has magnitude of 10. The 2 phase values at the top of the part referent to *Channel Phase Differences*, indicates the channel phase difference for each alien source. For example,  $20^\circ - 60^\circ$  indicates that the first alien source has a channel phase difference of  $20^\circ$  between the 2 VLs, and the second has a channel phase difference of  $60^\circ$ .

Table 5.2: Absolute correlation coefficient according to the phase difference and magnitude of the AXT channels, in a scenario with 2 VL and 2 AL.

Channel Magnitude	Channel Phase Differences				
	$33^\circ - 33^\circ$	$151^\circ - 151^\circ$	$20^\circ - 60^\circ$	$45^\circ - 130^\circ$	$30 - 210^\circ$
1 – 1	1	1	0.93	0.7224	0.0068
1 – 10	1	1	0.9977	0.991	0.98
1 – 100	1	1	1	0.9999	0.9998

The first line of Table 5.2 confirms the analysis in Sec. 3.3, i.e., when the alien sources cause the same channel phase difference, the correlation is high, and the correlation decreases when the channel phase differences diverge. However, the numbers in the other lines of this table extend this evaluation to cases of channels with different magnitudes, in which the correlation remains relatively high, same with a high channel phase difference. The reason for this is that in these cases the difference of the magnitude allows one AL superimpose the other line, and this approximates to a scenario with only 1 AL. This result indicates that a system developed in some way that the lines transmit with different power, the correlation of the interference can be increased.

Table 5.3 extends this evaluation to the case with 3 AL. Again, when the phase differences are aligned (as in the  $33^\circ - 33^\circ - 33^\circ$  column), the correlation is maximum. In the first line, there is a case in which the magnitude of the coupling of the three ALs is the same, 1. In this situation the effect of the misalignment in the phase differences is evident, when in the extreme case ( $0^\circ - 120^\circ - 240^\circ$ ) the correlation tends to zero. In the second line, the coupling of one AL is much bigger than the other two, which implies all the scenarios in this line approximate to the one with only 1 AL, and then the correlation approximates to 1. In the third and fourth lines, there are situations where one AL has a much smaller coupling than the other two. In this case, the evaluation can be simplified for 2 ALs, and then the correlation tends to be higher in the fourth line of the column  $10^\circ - 190^\circ - 190^\circ$  (due to the alignment of the phase difference of the ALs with a magnitude of 100), and close to zero in the third line of this same column.

Table 5.3: The absolute correlation coefficient according to phase difference and magnitude of the AXT channels, in a scenario with 2 VL and 3 AL.

Channel Magnitude	Channel Phase Differences			
	$33^\circ - 33^\circ - 33^\circ$	$10^\circ - 100^\circ - 100^\circ$	$10^\circ - 190^\circ - 190^\circ$	$0^\circ - 120^\circ - 240^\circ$
1 - 1 - 1	1	0.7418	0.3537	0.0118
1 - 1 - 10	1	0.9901	0.98	0.968
100 - 100 - 1	1	0.705	0.007	0.56
1 - 100 - 100	1	0.9999	0.9999	0.5

To accomplish the results above, we have performed simulations in a scenario with unsynchronized systems, but with the same modulation. 3 VL were used, which we named  $a$ ,  $b$  and  $c$  users, and 2 AL. Fig. 5.13 shows the correlation between the interferences observed in the users  $a$  and  $b$ , and between that observed in  $a$  and  $c$ . We can see in this diagram that the correlation between the users  $a$  and  $c$ , is greater than that between the users  $a$  and  $b$ .

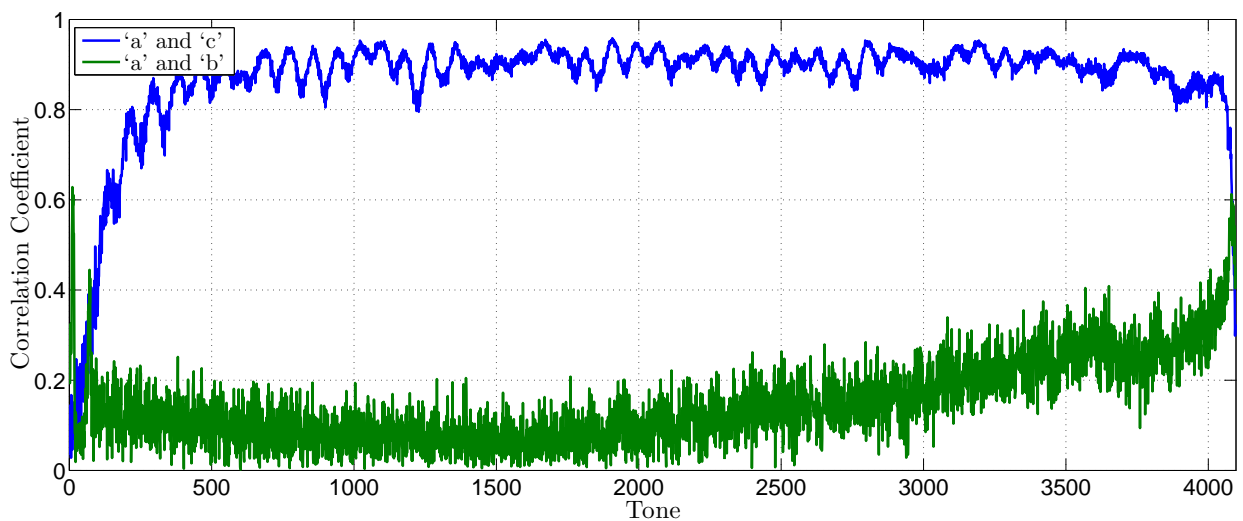


Figure 5.13: Absolute correlation coefficient between the users  $a$  and  $b$ , and  $a$  and  $c$ .

The reason for this is that the phase difference caused by the first AL on users  $a$  and  $b$ , and the phase difference caused by the second AL on users  $a$  and  $b$ , tends to differ by values of around  $180^\circ$ ,  $\pi$ , as shown in Fig. 5.14, which implies a reduction in correlation (as observed in Table 5.2 and 5.3). On the other hand, the phase difference caused by the first AL over users  $a$  and  $c$ , and the phase difference caused by the second AL over users  $a$  and  $c$  are similar in many tones (as depicted in Fig. 5.15), which shows a great concentration around  $0^\circ$  and  $360^\circ$ .

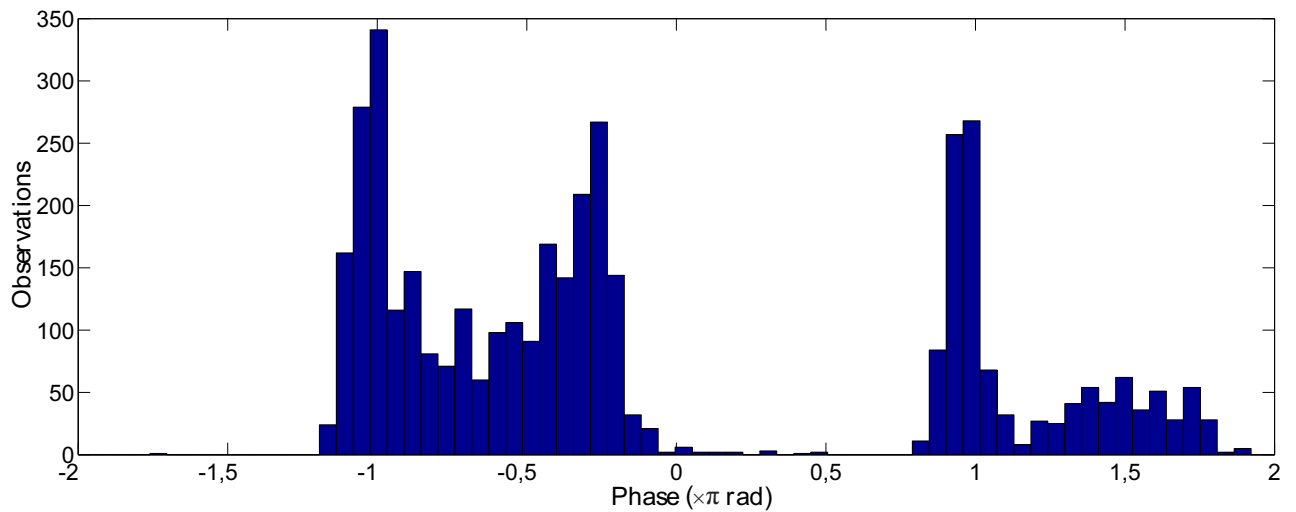


Figure 5.14: Histogram of the similarity between the phase difference caused by the first AL over users  $a$  and  $b$ , and the phase difference caused by the second AL over users  $a$  and  $b$ .

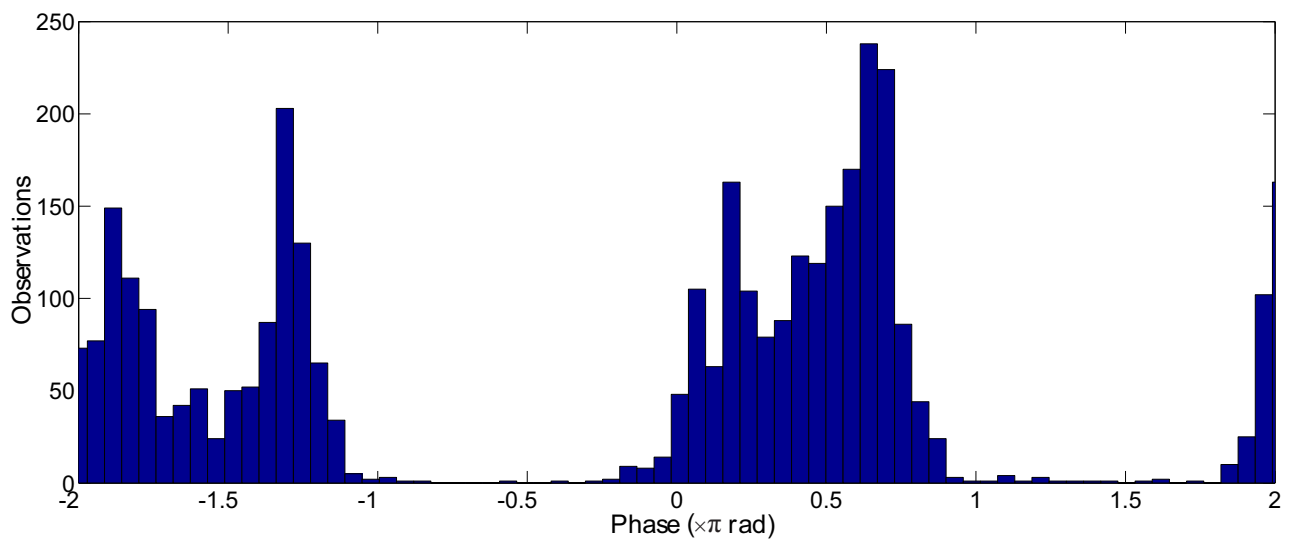


Figure 5.15: Histogram of the similarity between the phase difference caused by the first AL over users  $a$  and  $c$ , and the phase difference caused by the second AL over users  $a$  and  $c$ .

### 5.2.3 Results for Evaluation of the Ratio AL/VL in the Performance of the AXT Mitigation Methods

In this section we present the evaluation of performance of the methods RxPred and DFC according to the relation between the number of VLs providing information for the AXT

prediction and the number of alien sources causing the interference. Although DFC does not (explicitly) include prediction in its algorithm, the results show that the conclusions given in Sec. 3.4 can also be used to evaluate of the performance of DFC. These evaluations will be carried out through simulations, where the channel measurements described in Sec. 5.1 were used to make the simulations more representative of a real scenario.

The scenario adopted for the simulation was a MIMO transmission for RxPred, and receiver-side coordination for DFC. In both situations we considered DMT transmission on 4 VLs coexisting with a varying number of interferers, from 1 up to 4 ALs. For both vectored and alien aggregations, we have considered G.fast systems, in which the VLs were synchronized, but no synchronization was implemented between the vectored group and the alien group. Matlab<sup>®</sup> scripts developed by our group were used for the simulations. The simulations were designed to represent a time-domain transmission of signals generated in accordance with the system requirements, over the channels obtained from measurements. Table 5.5 summarizes the simulation parameters.

Table 5.4: Simulation Parameters.

Parameter	Value
Bandwidth	212 MHz
Number of Tones	4096
Tx PSD	-76 dBm/Hz
Background Noise PSD	-150 dBm/Hz
SINR Gap	9.75 dB
Noise Margin	6 dB

Fig. 5.16(a), Fig. 5.16(b), Fig. 5.17(a) and Fig. 5.17(b) show the aggregate rates achieved both before and after the AXT mitigation. Fig. 5.16(a) and Fig. 5.16(b) refer to the evaluation of the RxPred, and Fig. 5.17(a) and Fig. 5.17(b) show the performance of the DFC. In both cases the methods were evaluated when AXT was generated by CAT5 and CAT6 cables. To simplify the terminology, we will use the term *CAT5/CAT5* to denote the case when the interferer is a CAT5 cable, and *CAT6/CAT5* for the case in which the AXT is generated by the CAT6. In addition, these diagrams present an *upper bound*, which can be defined as the data-rate achieved in the absence of AXT, and on top of each group bar plot a figure of merit defined as the *recovered rate*, which measures how much of the upper bound is recovered in the presence of AXT when mitigation is employed. The latter is calculated as the ratio of the data-rate increase provided by the AXT mitigation method (i.e., difference between the

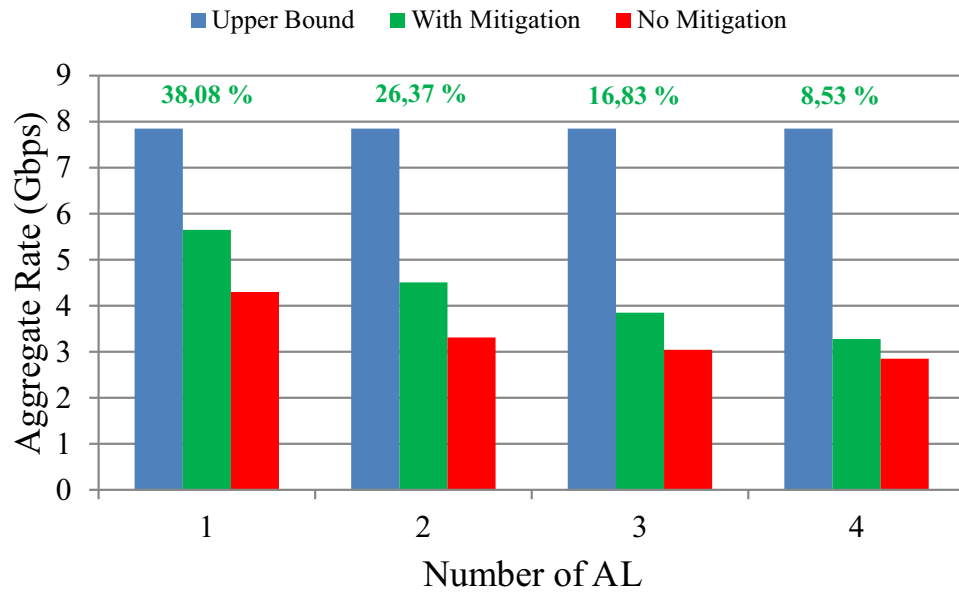
green and red bars), and the difference between the upper bound and the data-rates achieved when mitigation is not employed, although alien transmissions are present (i.e., the difference between the blue and red bars).

In general, Fig. 5.16(a), Fig. 5.16(b), Fig. 5.17(a) and Fig. 5.17(b), make it possible to detect a decrease in the recovery rate when the number of alien sources increases. For example, in the CAT5/CAT5 scenario (with 1 AL and using RxPred), approximately 38% of the data-rate was recovered, while in the scenario with 4 ALs only 8% was recovered. This suggests that the capacity to recover the data-rate tends to decrease when the number of ALs increases, as is also observed in general in the simulations with DFC. Another observation is the difference in the transmission rate reduction caused by interference in the CAT5/CAT5 and CAT6/CAT5 scenarios, in which in the CAT5/CAT6 scenarios the reduction of the transmission rate is less than in those of the CAT5/CAT5. This result is expected, owing to fact that the magnitude of the channels in CAT6/CAT5, in general is lower than in CAT5/CAT5 scenarios, as shows in Sec. 5.1.3. These figures also underline the importance of the AXT mitigation (because, as observed in the situations with more than 1 AL in the CAT5/CAT5 scenario), the aggregate rate with no mitigation is less than 4 Gbps, which suggests that in the average none user will achieve 1 Gbps, which was the target of the G.fast.

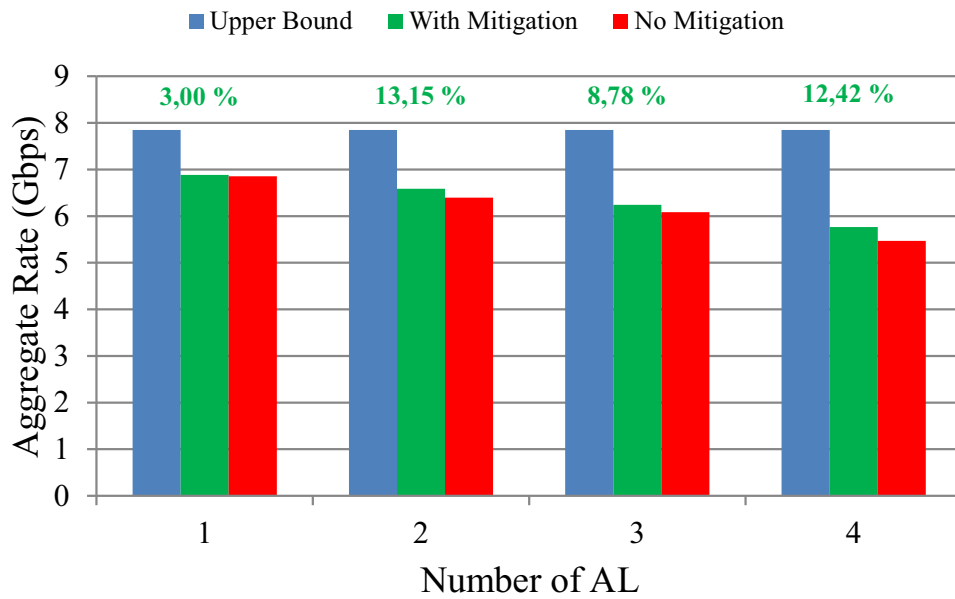
It is worth noting that the DFC yielded better results than RxPred, as observed in the aggregate rate achieved. This can be explained by the fact that DFC does not use vectoring, while RxPred does. The type of vectoring used here is the linear vectoring [28], where in accordance to the diagonal dominance of the channel matrix a penalty is applied to keep the transmission power in a suitable level [80]. Another factor is that the multiplication of the whitening matrix by the channel matrix, to obtain the QR decomposition, must have have an influence on the performance of the DFC, but we will leave this issue for a future study.

One alternative way of measuring the impact of the AXT mitigation in the data-rate (provided by RxPred), is the evaluation of the *prediction gains* of each VL. The prediction gains effectively measure the increase of SNR obtained from canceling the correlated portion of the noise that corrupts the received symbols. This can be defined as the ratio between the interference power before mitigation and the power of the reminiscent interference (ideally white) after mitigation.

Fig. 5.18, Fig. 5.19 and Fig. 5.20 show the prediction gains experienced by the VLs 2, 3 and 4 in the CAT5/CAT5 scenario, using RxPred, in situations with a distinct number of ALs. It should be noted that the performance experienced by line 2 was satisfactory up to the case where 1 AL is active in the binder. However, from this point onwards the standard of the performance sharply declines. A similar kind of behavior can be observed for the VLs



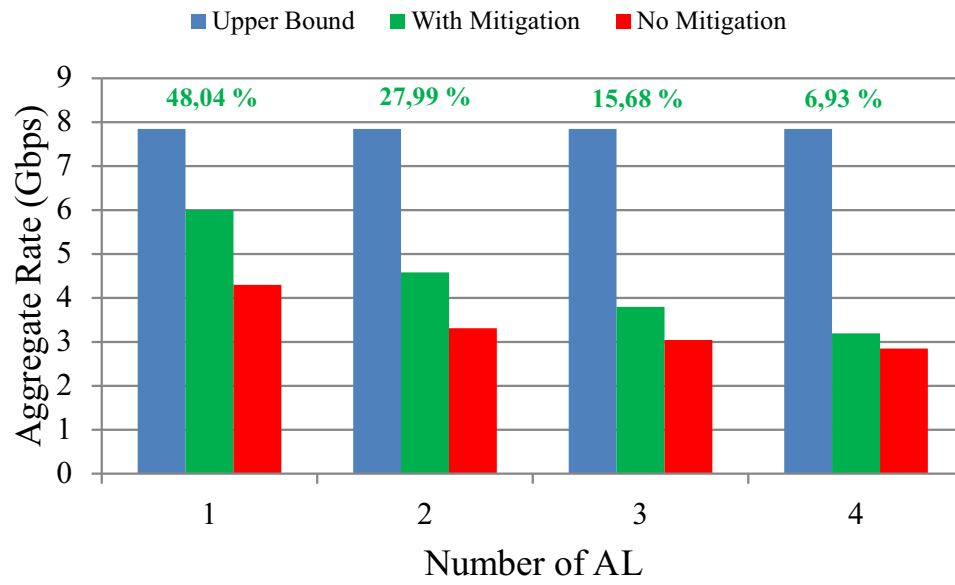
(a)



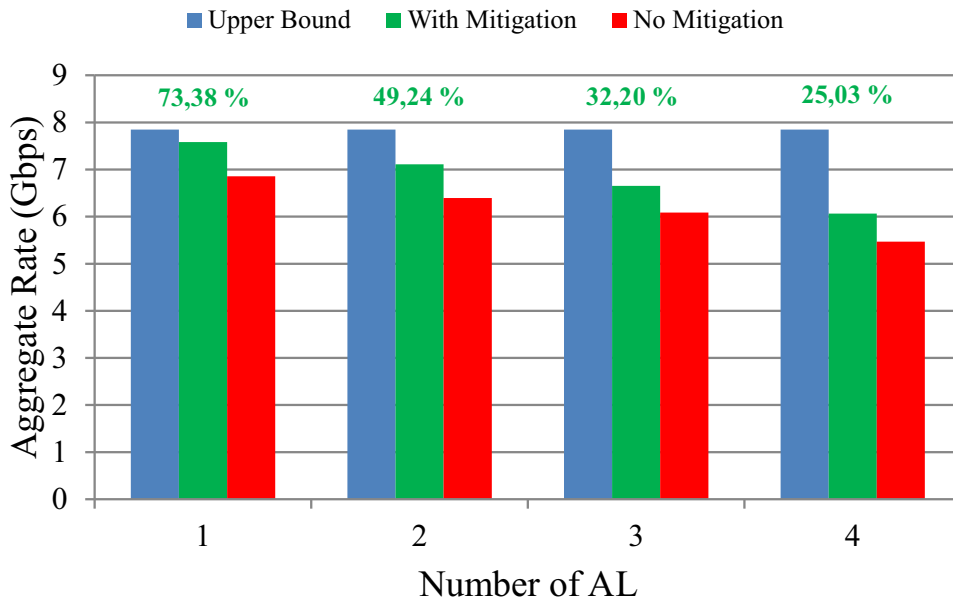
(b)

Figure 5.16: Aggregate rates before and after interference mitigation according to the number of ALs using the RxPred algorithm. The (a) refers to the CAT5/CAT5 scenarios, and (b) refers to the scenario CAT6/CAT5. The upper bound represents the aggregate rates achieved in the absence of alien transmissions and the percentage label indicates the *recovered rate*. The percentage in the top of each group bars indicates the amount of recovered rate in each scenario.





(a)



(b)

Figure 5.17: Aggregate rates before and after interference mitigation according to the number of ALs using the DFC algorithm. The (a) refers to the CAT5/CAT5 scenarios, and (b) refers to the scenario CAT6/CAT5. The upper bound represents the aggregate rates achieved in the absence of alien transmissions and the percentage label indicates the *recovered rate*. The percentage in the top of each group bars indicates the amount of recovered rate in each scenario.

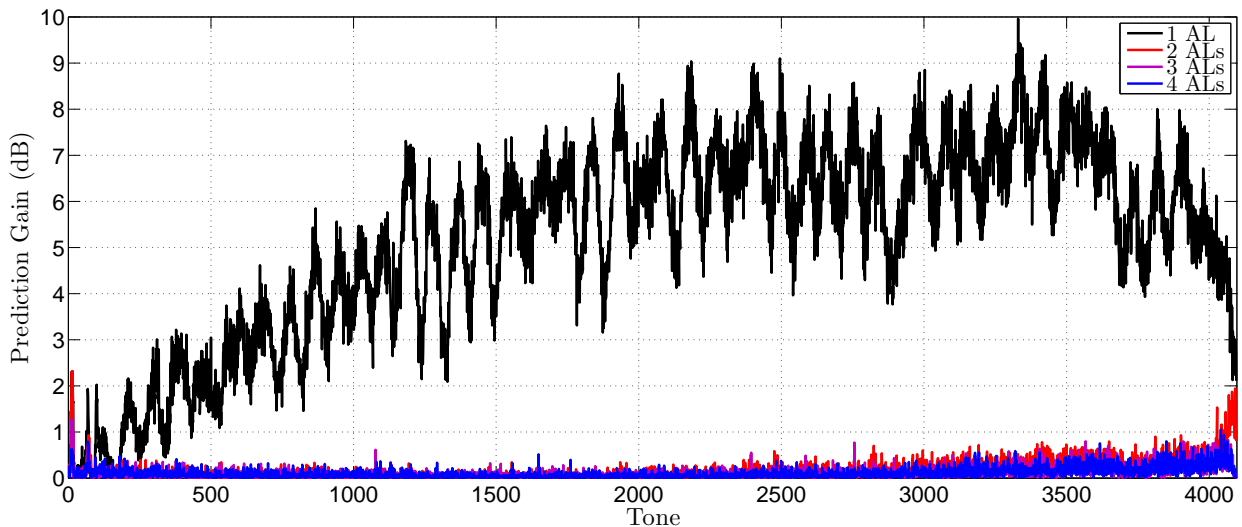


Figure 5.18: Prediction gain experienced by the VL 2 in scenario CAT5/CAT5, using RxPred.  $AL$  denotes number of ALs.

3 and 4, but now the limit of active ALs during which the improvement in the performance remains significant, is 2 and 3, respectively.

On basis of these observations, it is evident that the number of ALs comprising the overall interference influences the performance of each VL depending on its position in the decoding process<sup>1</sup>. For example, line 2 has 1 tap in its predictor (information that comes from the VL 1 using RxPred), and its limit of interferers to reasonable performance is 1 AL. This means that, whenever the number of predictor taps for a given VL is less than the number of ALs comprising the interference, the overall performance of the mitigation process provided by the RxPred method tends to decline, as observed in Sec. 3.4. When the CAT5/CAT5 scenario shown in Fig. 5.16 is re-evaluated for a scenario with 1 AL, for example, the VLs 2, 3 and 4 presented good performance improvements. In contrast, in a worst-case scenario with 4 active ALs, all the VLs experienced a poor prediction gain.

In Fig. 5.16(a), it is evident that the decrease of the recovered rate corresponds to the increase of the AL. However, in the scenario CAT6/CAT5, Fig. 5.16(b), we do not observe this asymptotic reduction. The reason for this is that the magnitude of the interference originating from the CAT6 lines is so weak that its power spectral density is close to the noise floor, as shown in Fig. 5.21, which shows the PSD of the AXT around  $-150$  dBm/Hz. Then, the background noise portion forming the input data at the predictor, becomes relatively high and the correlation matrix is predominantly white, i.e., occurs the reduction in of the

<sup>1</sup>As noted in [47], the decoding order does not change the sum rate.

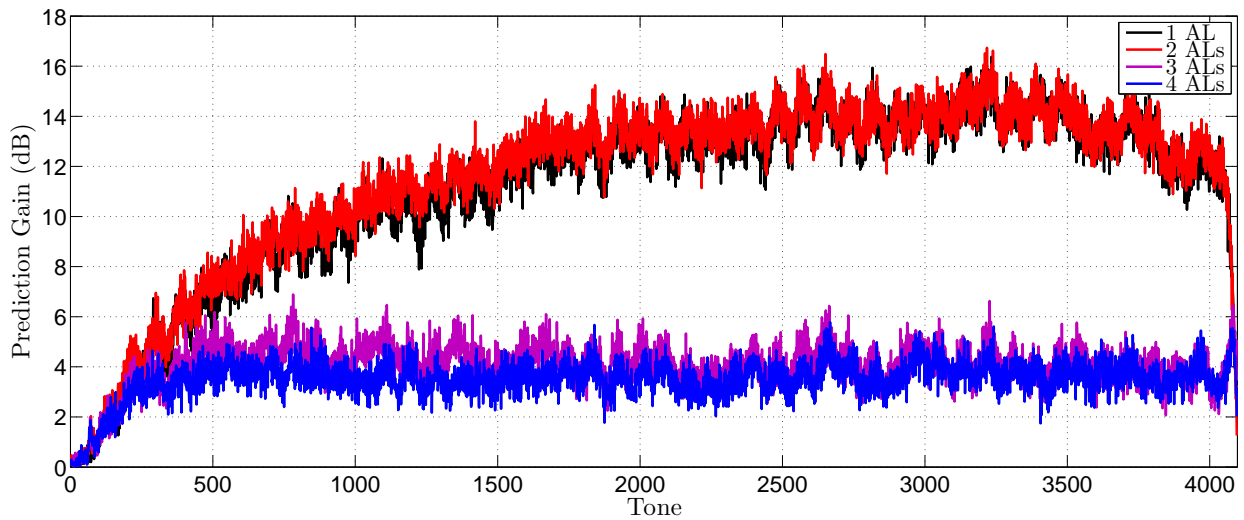


Figure 5.19: Prediction gain experienced by the VL 3 in scenario CAT5/CAT5, using RxPred. *AL* denotes number of ALs.

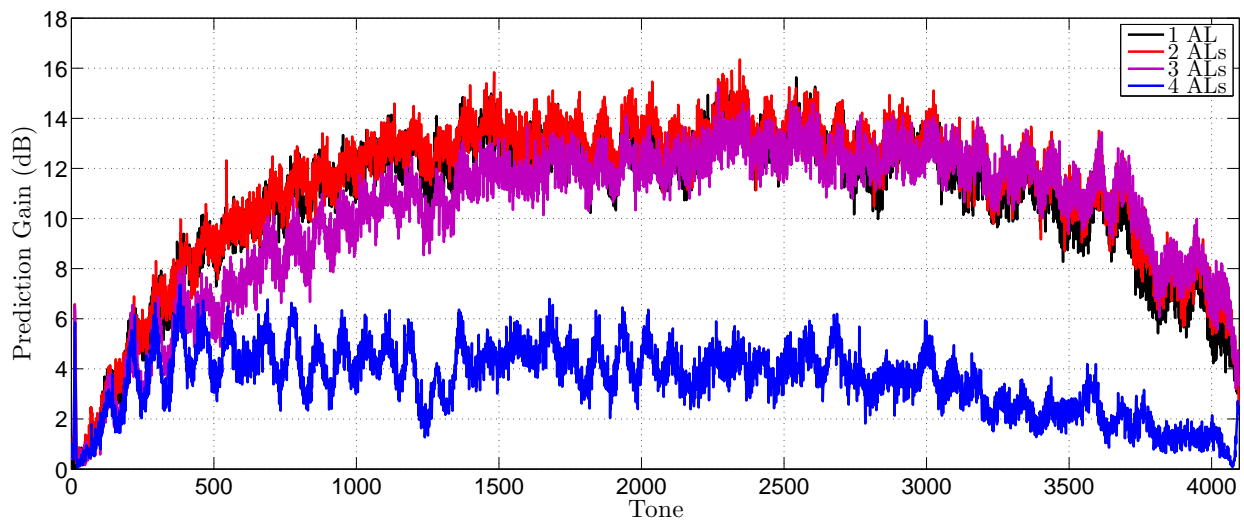


Figure 5.20: Prediction gain experienced by the VL 4 in scenario CAT5/CAT5, using RxPred. *AL* denotes number of ALs.

projection of the interferences among themselves [63], which implies the linear predictor is not able to provide expressive prediction gains, as also showed in [24].

Another interesting result was that the DFC in the CAT6/CAT5 scenario, achieved a better performance than RxPred. Moreover, The DFC has achieved a recovered rate of approximately 73%, compared with the 3% achieved by RxPred. These results deserves

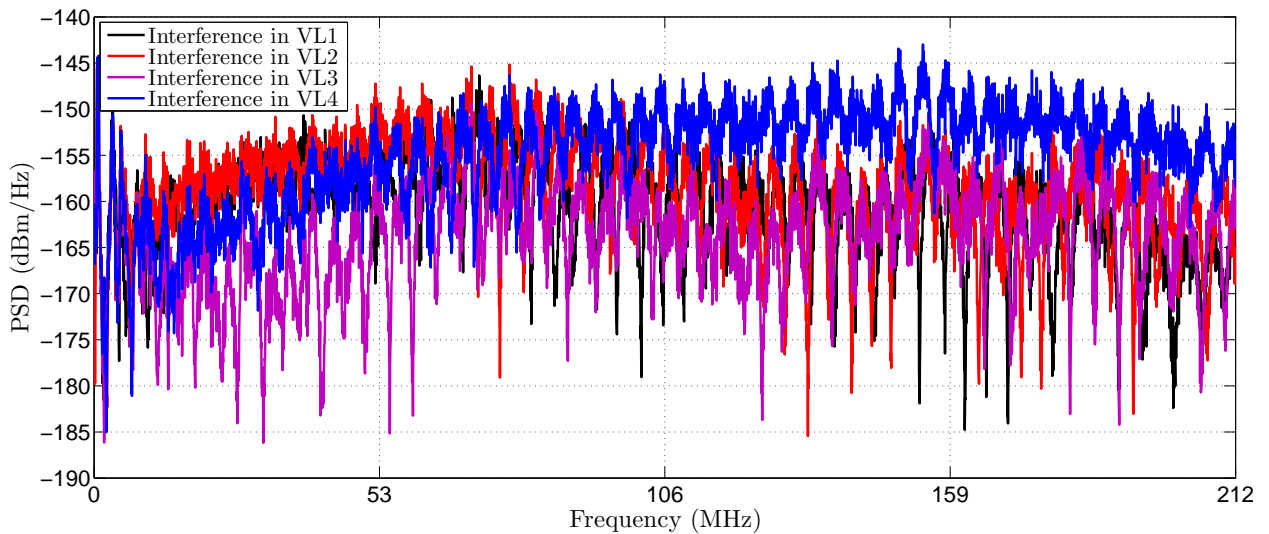


Figure 5.21: The PSD of the interference in each VL, in the scenario CAT6/CAT5, with 1 AL, using RxPred.

investigation, to confirm if the DFC really is superior to the RxPred in this scenario, or if there is a problem of matrix conditioning, for example. Nevertheless, the recovered rate of DFC in the CAT6/CAT5 scenario declined asymptotically.

Finally, as further confirmation and support evidence of the theory, we conducted an experiment with a physical apparatus, which involved an Agilent 81180B arbitrary waveform generator, an Agilent Infiniium MSO9104A oscilloscope, Northhills 0319NA baluns and 2 adjacent 10 m long quad cables, that we called QUADA and QUADB. QUADA was considered to be the interferer, and the pairs of QUADB comprised the vectored group. In the first situation, to simulate a scenario with 1 AL and 2 VL, the waveform generator was used to incorporate a random signal (4 dBm of output power) only in one pair of QUADA, and the signals observed in the two twisted pairs of QUADB were picked up using two ports of the oscilloscope, in which both equipments (the arbitrary waveform generator and the oscilloscope) were configured to work in the same sampling rate. In a second situation, we incorporated signals in the two pairs of the QUADA, and then was created a scenario with 2 ALs and 2 VLs. In both experiments all the free ends of the twisted pairs were matched with  $100\ \Omega$  loads, and the baluns were shielded to reduce the effect of the interferences from outside of the experiment. The data were obtained from both experiments and the prediction gains were computed offline by means of a MatLab script. Fig. 5.22 shows the results, which corroborate those the simulations discussed earlier, i.e., the prediction gains experienced by the second line of the QUADB in the scenario with 2 AL was considerable small than in the scenario

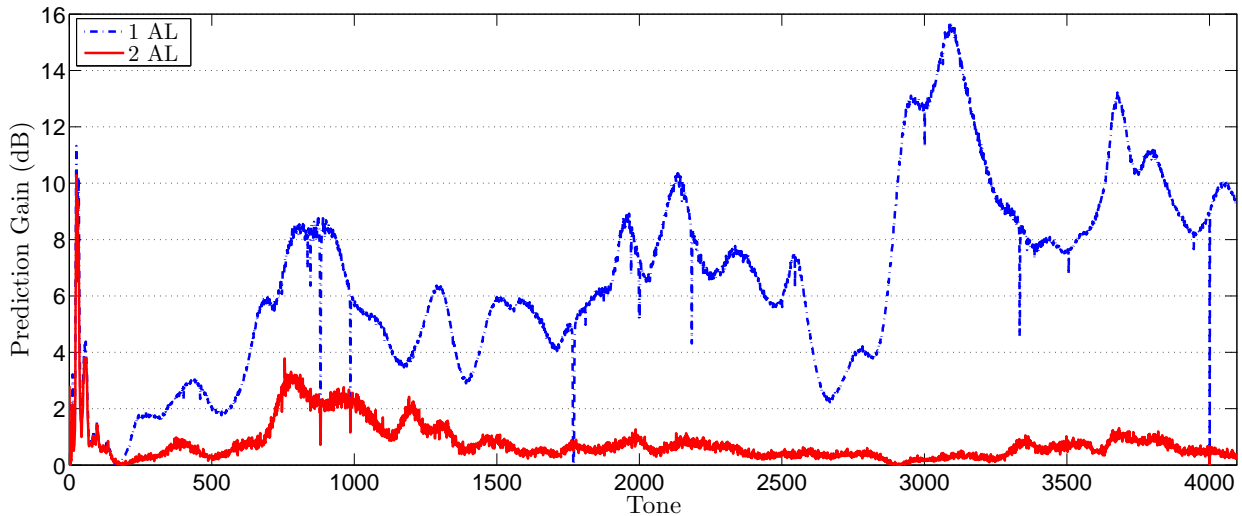


Figure 5.22: Results of the experiment with two longitudinally adjacent quad cables. The lines represent the prediction gain of the second line of a vectored group with two lines, in scenarios with 1 and 2 ALs.

with a single interferer.

These results agree with the formulation set out in Sec. 3.4, and strengthen the need to search for algorithms which can act in a suitable way in scenarios with many interferers.

### 5.3 Evaluation of the AMMIS

In this section there is a performance evaluation of AMMIS, which is compared with two other AXT mitigation methods: the one discussed in [51] (denoted *DFC*) and the third method in [47] (called here *RxPred*, chosen because it had an equivalent performance to the ones obtained with the first and second methods in [47]). Two scenarios were examined for this evaluation and the methods were compared with respect to their simulated bit rates, which were evaluated in the Matlab platform. Although *DFC* was not originally thought to be suitable for downstream [51] (due to the absence of coordination at receiver), the presence of the RC makes its implementation possible.

The channels of the first scenario (SCEN1) were measured with an Agilent E5071C network analyzer, using a setup composed by a 100 m long quad cable encapsulated in a bundle with three other quad cables. In this scenario, the extra twisted pair of the target quad cable was used as the RC and all the pairs of the three other quad cables caused

Table 5.5: Simulation parameters for evaluation of the AMMIS performance.

Parameter	Value
Bandwidth	100 MHz (SCEN1)/212 MHz (SCEN2)
Transmission PSD	-76 dBm/Hz
Interference PSD	-76 dBm/Hz
Background Noise PSD	-150 dBm/Hz
SINR Gap	9.75 dB
Noise Margin	10 dB

interference, in a total of 6 alien crosstalk sources. The *Computer Simulation Technology* (CST) software was used to simulate scenarios with varying difficulty to the algorithms. From these simulations, the second scenario (SCEN2) was chosen to be discussed here because it is particularly problematic for AMMIS (and other methods), due its weak coupling channels, which yield AXT level close to background noise. SCEN2 represents DSL transmission over a 50 m long *Category 6* (Cat6) twisted pair. The CST simulator provided information about the common mode, that is used as the RC. In SCEN2, the transmission was impaired by the AXT generated by 4 *Category 5* twisted pairs.

G.fast downstream transmissions were assumed in both scenarios and the parameters of the simulations are shown in the Table 5.5, where PSD denotes *power spectrum density*.

Fig. 5.23 and Fig. 5.24 show the simulation results for SCEN1 and SCEN2, respectively. In both scenarios, we evaluated the downstream aggregated transmission rates achieved by RxPred and DFC (i. e., the sum of the rates available in the TC and the RC, because in these methods both channels convey useful data), but for AMMIS only the downstream transmission rate in the TC is used, given that its RC transmits only pilot symbols. In these figures “*No Mitigation*” indicates the data rate achieved in a transmission in the presence of AXT but without mitigation. The  $\mathbf{C}_u$  matrix used by AMMIS was obtained from the interference correlation matrix generated from a simulation of a scenario with 2 coordinated lines and only 1 AL. This will induce the interference to behave like one that is generated by only one source, which allows an effective AXT mitigation in (4.15) with prediction that is based in one reference channel [81].

Comparing Fig. 5.23 and Fig. 5.24, it can be noted that the transmission rates achieved by RxPred and DFC, in the situation with 1 AL, are larger than that achieved by AMMIS. This can be attributed to the fact that with 1 AL and 1 RC, the standard AXT mitigation methods have a good performance [81]. However, with the increase in the number of ALs,

Table 5.6: Computational cost of the RxPred, DFC and AMMIS by tone.

Method	Additions	Multiplications	Decoding
RxPred	4	6	<b>2</b>
DFC	3	5	<b>2</b>
AMMIS	6	9	<b>1</b>

the AMMIS outperforms the other methods in the SCEN1, whereas AMMIS only achieves a better performance in the worst situation of the SCEN2. This behavior in the SCEN2 is mainly owing to the weak AXT channels in the differential mode of the Cat6. This causes low power interference in this mode and compensates for a poorer performance in some situations with multiple AXT (up to 3 ALs), keeping the aggregated transmission rate of RxPred and DFC in a high level, same with the poor transmission rate in the common mode due to the low SINR in this mode. However, the strong interference in the medium quality lines of the SCEN1 quickly reveals the decline in performance of RxPred and DFC, in which the bitrate provided by AMMIS in the situation with 6 alien lines was 717 Mbps against 584 Mbps achieved by DFC. These results confirm that AMMIS can achieve better results than standard AXT mitigation, in situations in which only 1 RC is available and multiple AXT sources impair a G.fast downstream transmission. In some situations (with  $AL = 0$ , for example) the bit rates of the AMMIS were small even than *No Mitigation*, a penalty due its channel gain to be given by the difference  $R(1, 1)^* - G_b(2, 1)R(1, 2)^*$ . A detailed analysis to determinate the parameters that impact this value will be treated in a future work.

Another advantage of AMMIS is that unlike the other methods, it is able to reduce the transmission power without reducing its transmission rate, because in AMMIS the RC only transmits pilot symbols, and then less power can be assigned to this channel. Additionally, this fact can also reduce the level of the interference in other systems, which tends to increase with the use of the extra channel (RC). On the other hand, this reduction in power cannot be carried out in the DFC and RxPred without a bit rate decrease, because it can affect their aggregated bit rate, which also depends on the RC.

With regard to the computational cost in showtime, the AMMIS processing needs more multiplications and additions than other methods, as shown in Tab. 5.6. By the other hand, the AMMIS requires only one decoding against two of the other methods. If we consider that decoding has complexity  $O(M)$ , where  $M$  denotes de size of the constellation, the AMMIS requires less operations in situations with  $M \geq 16$  [82].

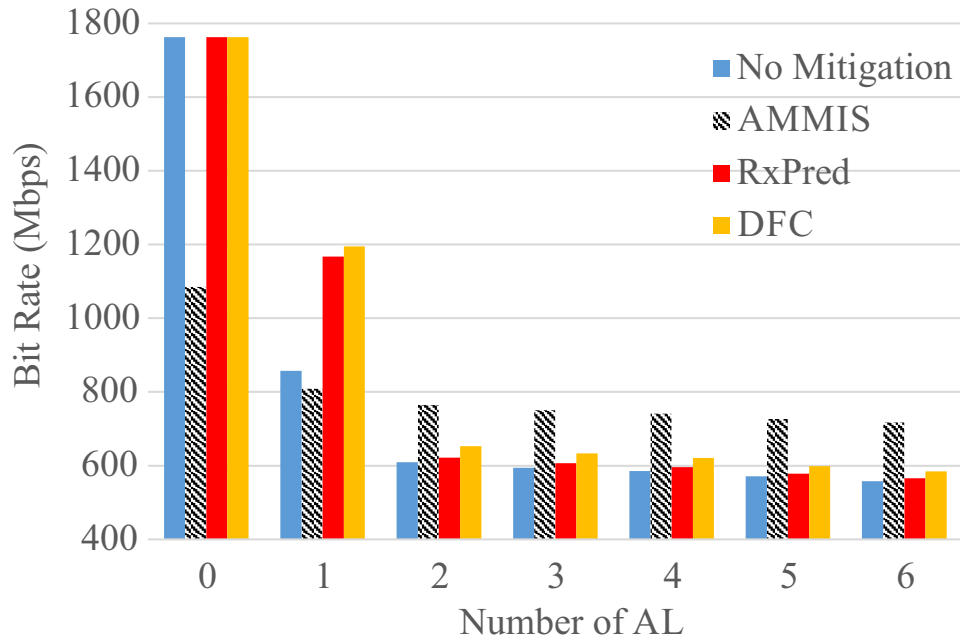


Figure 5.23: Transmission rates achieved by each mitigation method with a different number of ALs in SCEN1 - 212 MHz.

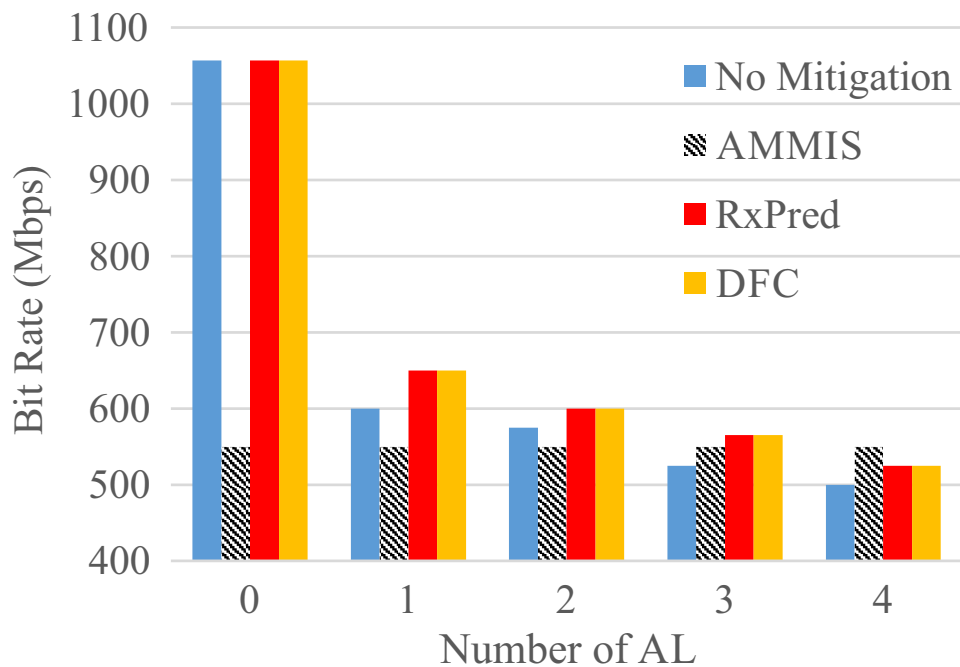


Figure 5.24: Transmission rates achieved by each mitigation method with a different number of ALs in SCEN2 - 100 MHz.



# Chapter 6

## Conclusions

This document has presented an investigation of the correlation characteristics of the AXT in the DSL systems; a formulation of mitigating algorithms for alien crosstalk performance, and consequently of a method to mitigate it in downstream G.fast transmissions impaired by multiple interference sources.

For this purpose, a set of alien crosstalk measurements containing coupling channels between pairs of both distinct and equal cables (CAT5 and CAT6) is presented. In these experiments a network analyzer was used to obtain the direct and coupling channels. The curves of the transfer functions show that out-of-domain crosstalk can be as strong as in-domain crosstalk in some cases, same in the high quality cables used. This fact represents a great problem for the current deployments of the DSL, because even with the use of vectoring, a significant portion of interference will affect the received signals. Then, the research of alien crosstalk mitigation algorithms on G.fast systems is a key requirement for its performance.

In the alien crosstalk model, we represented this external interference as the combined effect of a set of unsynchronized sources that use same modulation and rate as the coordinated lines. In this formulation we considered the coupling between each alien crosstalk source and a coordinated line, as the convolution of the time domain samples generated by the the interferer with the convolution matrix of the corresponding transfer function. The signal in in frequency domain are then obtained through a multiplication by the FFT matrix. Thus, we can model the total alien crosstalk in each tone of a vectored line and evaluate its characteristics.

In regard to the interference correlation, we presented a formulation which helps to understand the characteristics of the total interference caused by a set of alien lines. The formulation shows that the correlation between the interference observed in different pairs is maximum when the alien crosstalk is generate by only one source. However, when there is more than one line generating interference, this correlation tends to decrease due to the phase

---

misalignment of the crosstalk channels; additionally, we show the specific condition of the alignment phase, which yields high correlation therein.

Although the phase of the crosstalk channels has been set as the limiting factor, the last part of our modeling shows the condition for effective alien crosstalk prediction, according to the number of sources generating the interference and the number of taps used to predict the alien crosstalk in the target coordinated line. For this formulation, the alien crosstalk was modeled as a linear transformation, whereupon a linear system was organized in accordance to the number of alien crosstalk sources and the number of taps in the predictor; such a system is to be solved or not depending on a required condition for this to be solvable, that is, the number of alien sources must be less than or equal to the number of taps in the predictor of interference.

Moreover, the effect of the background noise on the correlation and prediction is investigated. In this aspect we modeled the background noise as a interference generated by an infinite number of spurious sources, which leads the correlation to be reduced and the effectiveness of the prediction to be impaired. However, the effects of the thermal noise are reduced when its power is small than the power of the alien crosstalk.

The alien crosstalk performance for the mitigating algorithms was evaluated with a varying number of alien lines. The simulations indicate that when the ratio between a certain number of alien lines and the number of vectored lines is high, the mitigation performance tends to be degraded, confirming our modelling. In particular, we have determined that when the number of alien lines is greater than the number of taps in the interference predictor of each vectored line, the exposed performance decreases sharply. Thus, the linear predictor performance is limited by the number of alien interferers. In regard to the effects of the background noise, we conclude that when the power of the alien crosstalk is similar to the thermal noise the bit rate improvements are reduced.

Furthermore, as support evidence of this theory, we carried out some practical experiments, involving around an arbitrary waveform generator, quad cables and a oscilloscope. The arbitrary waveform generator was used as the alien crosstalk sources, and the oscilloscope collected the signals which were evaluated off-line. These experiments yielded similar results to the simulations, wherein the situations with equal number of alien sources and taps in the predictor the SINR improvements were greater than with more alien lines than taps for prediction.

As solution to the disadvantageous situations for alien crosstalk mitigation exposed above, we proposed a method. called AMMIS. The our algorithm is suitable for DSL downstream transmissions in which the transmission channel (in which the useful data is

transmitted) has access to the signals in a reference channel (a support line which transmit only pilot symbols), and in which the transmission is impaired by multiple alien crosstalk sources, which is a typical challenge for the methods found in the literature. This is prediction based method which requires processing at transmitter and receiver, in which the transmission and the reference channel are treated in MIMO approach. The combination of the operations in both ends of the whole channel induces the interference to have features like one generated by only one interference source, which allows use of only one tap (or only a reference line) to effectively predict the alien crosstalk at the transmission channel.

This method was compared with two other alien crosstalk mitigation methods, in which the simulations considered both common mode or other twisted pair as reference line. The proposed method achieved better data rates than other mitigation methods in G.fast scenarios when the number of interference sources is relatively large.

For example, its performance was better in a scenario with a medium quality cable, in which the bitrate provided by AMMIS was 20% greater than one achieved by the other methods. However, the bitrate presented by AMMIS in situations with weak interference or few number of alien lines, was smaller than the bitrates of the other algorithms. Further, the AMMIS has potential to use less power because it uses the reference line only to transmit pilot signals. In regard to computational cost, the AMMIS requires more additions and multiplications, but less decoding operations.

Together, the results presented in this work allow the DSL system designers better to plan the infrastructure. Additionally, it gives new information to develop algorithms in order to get alien crosstalk mitigation that can effectively reduce the interference in scenarios with many interferers.

Future works include:

1. The optimization of the AMMIS in accordance with its resulting channel gain, because, as commented at the Sec. 5.3, this parameter is a key aspect in the performance of the AMMIS, and can to improve its performance in regard to the bit rate achieved.
2. A study of the applicability of the our correlation modelling on *model order selection*. This type of evaluation can be carried out through the analysis of the prediction gain obtained from the Cholesky decomposition of the correlation matrix of the received signals. Thus, the number of sources generating the signal can be determined by the magnitude of the expected error in the prediction, as explained in the section about the performance of the prediction according to the number of interferers.
3. An evaluation of the impact of the level of Gaussianity on the performance of the

---

prediction based alien crosstalk mitigation methods, because the signals are generated based on the uniform distributions but the prediction theory is suitable for Gaussian sequences.

## 6.1 List of Publications

1. Diego de Azevedo Gomes, Igor Freire, Aldebaro Klautau and Evaldo Pelaes, “Feasibility of alien crosstalk mitigation with receiver-side MIMO processing on G.fast systems,” presented at the *2015 International Workshop on Telecommunications (IWT)*, Santa Rita do Sapucaí, Brazil, Jun. 14 - 17, 2015.
2. Diego de Azevedo Gomes, Cláudio de Castro Coutinho Fiho and Evaldo Gonçalves Pelaes, “An Empirical Rate Balanced Alien Xtalk Mitigation Method for G.fast Systems,” presented at the *XXXIV Simpósio Brasileiro de Telecomunicações*, Santarém, Brazil, Aug. 30 - Sep. 02, 2016.
3. Diego de Azevedo Gomes, Claudomiro Sales, Daynara Dias Souza, Evaldo Pelaes and João Crisóstomo Weil Albuquerque da Costa, “Improving PLC to DSL Interference Mitigation Methods by Considering Mode Conversion Effects,” presented at the *XXXIV Simpósio Brasileiro de Telecomunicações*, Santarém, Brazil, Aug. 30 - Sep. 02, 2016.
4. Marx Freitas, Daynara Dias Souza, Brenda Sousa, Diego de Azevedo Gomes, Claudomiro Jr., Roberto Menezes Rodrigues and João Crisóstomo Weyl Costa, “Utilizando a segunda camada do modo fantasma para aprimoramento de aplicações G.fast”, presented at the *XXXV Simpósio Brasileiro de Telecomunicações e Processamento de Sinais*, São Pedro, Brazil, Sep. 03 - 06, 2017.
5. Diego de Azevedo Gomes, Eduardo Medeiros, Aldebaro Klautau and Evaldo Pelaes, “Mitigation of Alien Crosstalk for Downstream DSL Impaired by Multiple Interferers”, *IEEE Communications Letters*, vol. 21, issue 11, pp. 2380 - 2383, Aug. 2017.

# Appendix A

## Error Power Analysis of Linear Prediction Based on Cholesky Decomposition

As exposed across the text, the taps of prediction for method RxPred are given by elements of lower triangular matrix from Cholesky decomposition (in this case we have used the LDL decomposition), of cross correlation matrix, and that the estimative of prediction error power is taken from diagonal matrix of previous factorization. In this section we will explain how the elements of cross correlation matrix interacts in order to define the prediction error power.

Let us take as reference the cross correlation matrix below, derived from a scenario with 3 vectored users

$$\begin{aligned} \mathbf{C}_q &= E[\mathbf{q}\mathbf{q}'] \\ &= E \begin{bmatrix} E[q(1)q(1)^*] & E[q(1)q(2)^*] & E[q(1)q(3)^*] \\ E[q(2)q(1)^*] & E[q(2)q(2)^*] & E[q(2)q(3)^*] \\ E[q(3)q(1)^*] & E[q(3)q(2)^*] & E[q(3)q(3)^*] \end{bmatrix} \end{aligned} \quad (\text{A.1})$$

The LDL decomposition factors the  $\mathbf{C}_q$  in the way  $\mathbf{C}_q = \mathbf{G}\mathbf{D}\mathbf{G}'$ , which in this case will

yield

$$\begin{aligned}
\mathbf{C}_q &= \mathbf{G}\mathbf{D}\mathbf{G}' \\
&= \begin{bmatrix} 1 & 0 & 0 \\ G(2,1) & 1 & 0 \\ G(3,1) & G(3,2) & 1 \end{bmatrix} \begin{bmatrix} D(1,1) & 0 & 0 \\ 0 & D(2,2) & 0 \\ 0 & 0 & D(3,3) \end{bmatrix} \begin{bmatrix} 1 & G(2,1)^* & G(3,1)^* \\ 0 & 1 & G(3,2)^* \\ 0 & 0 & 1 \end{bmatrix}
\end{aligned} \tag{A.2}$$

Then, the elements of  $\mathbf{D}$  matrix, according to [67], are expressed by

$$D(j, j) = C_q(j, j) - \sum_{c=1}^{j-1} G(j, c)G(j, c)^*D(c, c) \tag{A.3}$$

and the elements of  $\mathbf{G}$  are given by

$$G(i, j) = \frac{1}{D(j, j)} \left( C_q(i, j) - \sum_{c=1}^{j-1} G(i, c)G(j, c)^*D(c, c) \right) \tag{A.4}$$

Solving  $D(j, j)$  and  $G(i, j)$  for each element of  $\mathbf{D}$  and  $\mathbf{G}$  matrices, we get

$$D(1, 1) = E[q(1)q(1)^*]$$

$$G(2, 1) = \frac{E[q(2)q(1)^*]}{E[q(1)q(1)^*]}$$

$$G(3, 1) = \frac{E[q(3)q(1)^*]}{E[q(1)q(1)^*]}$$

$$\begin{aligned} D(2, 2) &= E[q(2)q(2)^*] - G(2, 1)G(2, 1)^*E[q(1)q(1)^*] \\ &= E[q(2)q(2)^*] - E[q(2)q(1)^*] \left( \frac{E[q(2)q(1)^*]}{E[q(1)q(1)^*]} \right)^* \end{aligned}$$

$$\begin{aligned} G(3, 2) &= \frac{E[q(3)q(2)^*] - G(3, 1)G(2, 1)^*E[q(1)q(1)^*]}{D(2, 2)} \\ &= \frac{E[q(3)q(2)^*] - E[q(3)q(1)^*] \left( \frac{E[q(2)q(1)^*]}{E[q(1)q(1)^*]} \right)^*}{E[q(2)q(2)^*] - E[q(2)q(1)^*] \left( \frac{E[q(2)q(1)^*]}{E[q(1)q(1)^*]} \right)^*} \end{aligned}$$

$$\begin{aligned} D(3, 3) &= E[q(3)q(3)^*] - G(3, 1)G(3, 1)^*D(1, 1) - G(3, 2)G(3, 2)^*D(2, 2) \\ &= E[q(3)q(3)^*] - E[q(3)q(1)^*]G(3, 1)^* \\ &\quad - \left[ E[q(3)q(2)^*] - E[q(3)q(1)^*] \left( \frac{E[q(2)q(1)^*]}{E[q(1)q(1)^*]} \right)^* \right] G(3, 2)^* \end{aligned} \quad (\text{A.5})$$

Now let us to analyse each equation.  $D(1, 1)$  is the prediction error power of interference in user 1, which is equal to the power of the interference in that user,  $E[q(1)q(1)^*]$ , what is coherent with RxPred procedure, in which the user 1 is the reference one and do not gain any benefit of the mitigation process.

The coefficient  $G(2, 1)$  relates the correlation between  $q(1)$  and  $q(2)$ , and the variability of the  $q(1)$ . Similarly,  $G(3, 1)$  relates the correlation between  $q(1)$  and  $q(3)$ , and the variability of the  $q(1)$ .

The prediction error power of user 2,  $D(2, 2)$ , is defined as the difference between the variability of the interference in user 2, and the variability of the its prediction. If we take  $D(2, 2)$  as a measure of quality of the prediction of  $q(2)$ ,  $D(2, 2)$  indicates how much of the variability of  $q(2)$  can be explained by its predictor [64]. Opening this equation we can see that

the value of the  $D(2, 2)$  depends on degree of correlation between  $q(1)$  and  $q(2)$ ,  $E[q(1)q(2)^*]$ , scaled by the tap  $G(2, 1)$ .

The expansion of  $G(3, 2)$  shows that the coefficient of the prediction of  $q(3)$  based on innovation of the  $q(2)$  is equal to the correlation between  $q(3)$  and  $q(2)$ , minus the correlation between  $q(3)$  and  $q(1)$ , and  $q(2)$  and  $q(1)$ . This subtraction show us that the predictor generated by Cholesky decomposition consider the projections of the interferences among themselves to define the taps of the predictor. Remembering that the predictor for  $q(3)$  is composed by 2 taps,  $G(3, 1)$  and  $G(3, 2)$ , when  $G(3, 2)$  is calculated the algorithm subtracts the projection between  $q(3)$  and  $q(1)$  (which was already accounted in the tap  $G(3, 1)$ ), and the projection between  $q(2)$  and  $q(1)$  (which do not involve the interference to be predicted,  $q(3)$ ).

Finally,  $D(3, 3)$ , again indicates how much the variability of  $q(3)$  is explained by the prediction based on innovation of the  $q(1)$  and  $q(2)$ . Here,  $D(3, 3)$  depends on the correlation between  $q(3)$  and  $q(1)$ ,  $E[q(3)q(1)^*]$ , and on the correlation between  $q(3)$  and  $q(2)$ . The correlation previous computed and the correlation which do not related to the interference to be predicted, i.e., correlation which do not involve  $q(3)$ , are discounted. In general, the  $D$ 's indicates how much the variability of target interference can be explained by predictor applied to estimate it, and that the  $D$ 's depends on the level of correlation among interference in target user and the interference observed in the users that serve information for the predictor.



# Bibliography

- [1] Chris Dunford, “Prologue,” in *Local-Loop and DSL Reference Guide*, Ontario, Canada: EXFO, 2014, pp. 2-4.
- [2] Chris Dunford, “What is DSL?,” in *Local-Loop and DSL Reference Guide*, Ontario, Canada: EXFO, 2014, pp. 2-4.
- [3] Jochen Maes and Carl J. Nuzman, “The past, present, and the future of copper access,” *Bell Labs Technical Journal*, vol. 20, pp. 1-10, Mar. 2015.
- [4] M. Guenach, J. Maes, M. Timmers, O. Lamparter, J.-C. Bischoff, and M. Peeters, “Vectoring in DSL systems: Practices and Challenges,” presented at the *2011 IEEE Global Telecommunications Conference (GLOBECOM 2011)*, Kathmandu, Nepal, Dec. 5-9, 2011.
- [5] Philip Golden, Hervé Didieu, and Krista S. Jacobsen, “DSL Specific Integrated Circuits: A Silicon Perspective,” in *Implementation and Applications of DSL Technology*, Boca Raton, FL, USA: Taylor & Francis Group, 2008, pp. 67-94.
- [6] Philip Golden, Hervé Didieu, and Krista S. Jacobsen, “Introduction to DSL,” in *Fundamentals of DSL Technology*, Boca Raton, FL, USA: Taylor & Francis Group, 2008, pp. 126-149.
- [7] Philip Golden, Hervé Didieu, and Krista S. Jacobsen, “Fundamentals of Multi-Carrier Modulation,” in *Fundamentals of DSL Technology*, Boca Raton, FL, USA: Taylor & Francis Group, 2008, pp. 187-216.
- [8] Philip Golden, Hervé Didieu, and Krista S. Jacobsen, “Noise and Noise Modelling on the Twisted Pair Channel,” in *Fundamentals of DSL Technology*, Boca Raton, FL, USA: Taylor & Francis Group, 2008, pp. 79-104.
- [9] Thomas Starr, Massimo Sorbara, John M. Cioffi, Peter J. Silverman, “DSL Advances,” Upper Saddle River, NJ, USA: Prentice Hall, 2003.

- 
- [10] Thomas Starr, Massimo Sorbara, John M. Cioffi, Peter J. Silverman, “Review of Transmission Fundamentals for DSLs,” in *DSL Advances*, Upper Saddle River, NJ, USA: Prentice Hall, 2003.
- [11] Dong Wei, Amir Fazlollahi, Guozhu Long, and Eric Wang, “G.fast for FTTdp: Enabling Gigabit Copper Access,” presented at the *Globecom Workshops*, Austin, TX, USA, pp. 668-673, Dec. 8- 12, 2014.
- [12] Wouter Lanneer, Paschalis Tsiiaflakis, Jochen Maes and Marc Moonen, “Linear and Nonlinear Precoding Based Dynamic Spectrum Management for Downstream Vektored G.fast Transmission,” in *IEEE Transactions on Communications*, vol. 65, issue 03, pp. 1247-1259, Mar. 2017.
- [13] Vladimir Oksman, Rainer Strobel, Xiang Wang, Dong Wei, Rami Verbin, Richard Goodson, and Massimo Sorbara, “The ITU-T’s New G.fast Standard Brings DSL into the Gigabit Era,” *IEEE Communications Magazine*, vol. 64, issue 3, pp. 118-126, Mar. 2016.
- [14] Werner Coomans, Rodrigo Bastos Moraes, Koen Hooghe and Jochen Maes, “The 5th Generation Broadband Copper Access,” in *Proceedings of the 9th ITG Symposium*, Berlin, Germany, 2015, Apr. 20-21.
- [15] Werner Coomans, Rodrigo Bastos Moraes, Koen Hooghe, Alex Duque, Joe Galaro, Michael Timmers, Adriaan J. van Wijngaarden, Mamoun Guenach and Jochen Maes, “XG-fast: the 5th generation broadband,” in *IEEE Communications Magazine*, vol. 32, issue 12, pp. 83-88, Dec. 2015.
- [16] P. Ödling, T. Magesacher, S. Höst, P. O. Börjesson, M. Berg, and E. Areizaga, “The Fourth Generation Broadband Concept,” *IEEE Communications Magazine*, vol. 47, issue: 1, pp. 62-69, Feb. 2009.
- [17] J. M. Cioffi, “A Multicarrier Primer,” *ANSI Contribution*, Clearfield, FL, USA, T1E1.4/91-157, 1991.
- [18] Alan V. Oppenheim and Ronald W. Schaffer, “Sampling of Continuous-Time Signals,” in *Discrete-Time Signal Processing*, Upper Saddle River, NJ, USA: Pearson Higher Education, pp. 154-273, 2010.
- [19] Tong Bai, Hongming Zhang, Rong Zhang, Lie-Liang Yang, Anas F. Al Rawi, Jiankang Zhang and Lajos Hanzo, “Discrete Multi-Tone Digital Subscriber Loop Performance in the Face of Impulsive Noise,” in *IEEE Access*, vol. 5, pp. 10478-10495. Jun. 2017.

- 
- [20] E. Karipidis, N.D. Sidiropoulos, A. Leshem, and L. Youming, "Capacity Statistics for Short DSL Loops from Measured 30 MHz Channel Data," presented at the *2005 IEEE 6th Workshop on Signal Processing Advances in Wireless Communications*, New York, NY, USA, Jun. 5-8, 2005.
- [21] T. Magesacher, S. Haar, and F. Zukunft, "Analysis of the Noise Environment in Future Twisted-Pair Access Technologies," presented at the *2001 IEEE Emerging Technologies Symposium on BroadBand Communications for the Internet Era Symposium digest*, Richardson, TX, USA, Sep. 10-11, 2001.
- [22] Jochen Maes, Carl Nuzman, and Paschalis Tsiaflakis, "Sensitivity of nonlinear precoding to imperfect channel state information in G.fast," presented at the *2016 24th European Signal Processing Conference (EUSIPCO)*, Budapest, Hungary, 29 Aug.-2 Sept., 2016.
- [23] R. Locatelli, S. Brini, L. Fanucci, and C. Del-Toso, "An optimized digital RFI cancellation scheme for DMT-based VDSL systems," presented at the *The 8th International Conference on Communication Systems, 2002. ICCS 2002*, Singapore, Nov. 28, 2002.
- [24] Khaled M. Ali, Geoffrey G. Messier, and Stephen W. Lai, "DSL and PLC co-existence: An interference cancellation approach," *IEEE Transactions on Communications*, vol. 62, issue 9, pp. 3336-3350, Aug. 2014.
- [25] Amir R. Forouzan, Marc Moonen, Michael Timmers, Mamoun Guenach, and Jochen Maes, "On the Achievable Bit Rates of DSL Vectoring Techniques in the Presence of Alien Crosstalkers," presented at the *2012 IEEE Global Communications Conference (GLOBECOM)*, Anaheim, CA, USA, Dec. 3-7, 2012.
- [26] Redouane Zidane, Sean Huberman, Christopher Leung, and Tho Le-Ngoc, "Vectored DSL: Benefits and Challenges for Service Providers," *IEEE Communications Magazine*, vol. 51, issue 2, pp. 152-157, Feb. 2013.
- [27] "Fast Access to Subscriber Terminals (FAST): Physical Layer Specification," ITU-R G.9701, 2014.
- [28] R. Cendrillon, G. Ginis, E. V. den Bogaert, and M. Moonen, "A near-optimal linear crosstalk precoder for downstream VDSL," *IEEE Transactions on Communications*, vol. 55, no. 5, pp. 860-863, 2007.
- [29] "Self-FEXT cancellation (vectoring) for use with VDSL2 transceivers," ITU-T Rec. G.993.5, 2010.

- 
- [30] Aditya Awasthi, Naofal Al-Dhahir, Oren E. Eliezer, and Poras T. Balsara, "Alien Crosstalk Mitigation in Vectored DSL Systems for Backhaul Applications," presented at the *2012 IEEE International Conference on Communications (ICC)*, Ottawa, ON, Canada, pp. 3852 -385, Jun. 10-15, 2012.
- [31] Jonathan Gambini and Umberto Spagnolini, "Wireless over cable for femtocell systems," *IEEE Communications Magazine*, vol. 51, no. 5, pp. 178-185, May 2013.
- [32] T. H. Yeap, D. K. Fenton, and P. D. Lefebvre, "A Novel Common-Mode Noise Cancellation Technique for VDSL Applications," *IEEE Transactions on Instrumentation and Measurement*, vol. 52, issue 4, pp. 1325-1334, Aug. 2003.
- [33] T. Magesacher, P. Ödler, and P. O. Börjesson, "Adaptive Interference Cancellation Using Common-Mode Information in DSL," presented at the *2005 13th European Signal Processing Conference*, Antalya, Turkey, Sept. 4-8, 2005.
- [34] Thomas Magesacher, Per Ödler, Per Ola Börjesson, and Shlomo Shamai, "Information Rate Bounds in Common-Mode Aided Wireline Communications," *Transactions on Emerging Telecommunications Technologies*, vol. 17, issue 5, pp. 533-545, Sept. 2005.
- [35] T. Magesacher, P. Ödler, and P. O. Börjesson, "Analysis of Adaptive Interference Cancellation Using Common-Mode Information in Wireline Communications," *EURASIP Journal on Advances in Signal Processing*, vol. 2007, Jul. 2007.
- [36] A. Homayoun Kamkar-Parsi, Gilles Bessens, and Martin Bouchard and Tet H. Yeap, "Wideband Crosstalk Interference Cancelling on xDSL Using Adaptive Signal Processing and Common-Mode Signal," in *IEEE International Conference on Acoustics, Speech, and Signal Processing, 2004. Proceedings. (ICASSP 04)*., Montreal, Que., Canada, 2004, May 17-21.
- [37] A. H. Kamkar-Parsi, M. Bouchard, G. Bessens, and T. H. Yeap, "A wideband crosstalk canceller for xDSL using common-mode information," *IEEE Transactions on Communications*, vol. 53, issue 2, pp. 238-242, Mar. 2005.
- [38] M. Tsatsanis, C. S. Smith, and B. A. Itri, "Common mode noise cancellation," US Patent US20050053229 A1, March 10, 2005.
- [39] Michail Tsatsanis, Mark A. Erikson, and Sunil Shah, "Multiline Transmission in Communication Systems," US Patent 2006/0056522 A1, Mar. 16, 2006.
- [40] T. Magesacher, P. Ödler, P. O. Börjesson, B. Henkel, T. Nordström, R. Zukunft, and S. Haar, "On the Capacity of the Copper Cable Channel Using the Common Mode,"

- 
- presented at the *IEEE Global Telecommunications Conference, 2002. GLOBECOM 02*, Taipei, Taiwan, pp. 1269-1273, Nov. 17-21, 2002.
- [41] J. Huber and R. Fischer, "Dynamically coordinated reception of multiple signals in correlated noise," in *1994 IEEE International Symposium on Information Theory, 1994. Proceedings*, Trondheim, Norway, 1994, 27 June-1 July.
- [42] Carlos A. Belfiore and John H. Park, "Decision Feedback Equalization," *Proceedings of the IEEE*, vol. 67, issue 8, pp. 1143-1156, Aug. 1979.
- [43] John G. Proakis and Massoud Salehi, "Digital Communication Through Band-Limited Channels," in *Digital Communications*, New York, NY, USA: The McGraw-Hill Companies, Fifth Edition, 2008, pp. 597-688.
- [44] J. M. Cioffi and G. D. Forney Jr., "Generalized decision feedback equalization for packet transmission with ISI and Gaussian noise," in *Communications, Computation, Control and Signal Processing: A Tribute to Thomas Kailath*, New York, NY, USA: Springer Science+Business Media, 1997, pp. 79-128.
- [45] M. Tsatsanis, "Vectoring techniques for multi-line 10MDSL systems," T1E1.4 committee, contribution 2002-196, Aug. 2002.
- [46] Michail Tsatsanis, Mark A. Erickson, and Sunil Shah, "Multiline transmission in communication systems," US Patent US 7,349,780 B2, March 25, 2008.
- [47] George Ginis and Chia-Ning Peng, "Alien crosstalk cancellation for multipair digital subscriber line systems," *EURASIP Journal on Applied Signal Processing*, vol. 2006, no. 1, pp. 1-12, Dec. 2006.
- [48] G. G. Raleigh and J. M. Cioffi, "Spatio-Temporal Coding for Wireless Communication," *IEEE Transactions on Communications*, vol. 46, issue 3, pp. 357-366, Mar. 1998.
- [49] P. K. Pandey, M. Moonen, and L. Deneire, "MMSE-Based Partial Crosstalk Cancellation for Upstream VDSL," presented at the *2010 IEEE International Conference on Communications*, Cape Town, South Africa, May 23-27, 2010.
- [50] P. Biyani, A. Mahadevan, S. Prakriya, P. Duvaut, and S. Prasad, "Co-operative Alien Noise Cancellation in Upstream VDSL: A New Decision Directed Approach," *IEEE Transactions on Communications*, vol. 61, issue 8, pp. 3494-3504, Jun. 2013.
- [51] Ahmad Al Amayreh, Jérôme Le Masson, Maryline Héland and Meryem Ouzzif, "Alien crosstalk elimination in digital subscriber line systems," *IET Communications*, vol. 08, issue 10, pp. 1714-1723, Jul. 2014.

- 
- [52] F. Abdelkefi, P. Duhamel, and F. Alberge, "Impulsive Noise Cancellation in Multicarrier Transmission," *IEEE Transactions on Communications*, vol. 53, issue 1, pp. 94-106, Feb. 2005.
- [53] A. Gomaa, K. Z. Islam, and N. Al-Dhahir, "Two Novel Compressed-sensing Algorithms for NBI Detection in OFDM Systems," presented at the *IEEE International Conference on Acoustics Speech and Signal Processing*, Dallas, TX, USA, Mar. 14-19, 2010.
- [54] S. Jagannathan, C. Yu Chen, and J. M. Cioffi, "Interference Cancellation System," US Patent US 8,340,279 B2, December 25, 2012.
- [55] Gilbert Strang, "Symmetric Linear Systems," in *Introduction to Applied Mathematics*, Wellesley, MA, USA: Wellesley - Cambridge Press, 1986, pp. 1-86.
- [56] G. Ginis and J. M. Cioffi, "Vectored-DMT: a FEXT Canceling Modulation Scheme for Coordinating Users," presented at the *ICC 2001. IEEE International Conference on Communications*, Helsinki, Finland, Jun. 11-14, 2001.
- [57] Y. C. Eldar and A. V. Oppenheim, "MMSE Whitening and Subspace Whitening," *IEEE Transactions on Information Theory*, vol. 49, issue 7, pp. 1846-1851, Jul. 2003.
- [58] Simon Haykin, "Linear Prediction," in *Adaptive Filter Theory*, Prentice Hall, 3rd Edition, pp. 241-301, 1995.
- [59] Lloyd N. Trefethen and David Bau III, "Systems of Equations," in *Numerical Linear Algebra*, Philadelphia, PA, USA: SIAM: Society for Industrial and Applied Mathematics, 1st Edition, pp. 145-178, 1997.
- [60] L. Sandstrom, K. W. Schneider, L. L. Joiner, and A. Wilson, "Spatial Correlation of Alien Crosstalk in MIMO DSL Systems," *IEEE Transactions on Communications*, vol. 57, issue 8, pp. 2269-2271, Aug. 2009.
- [61] Alan V. Oppenheim and Ronald W. Schaffer, "The Discrete Fourier Transform," in *Discrete-Time Signal Processing*, Upper Saddle River, NJ, USA: Pearson Higher Education, pp. 623-715, 2010.
- [62] Alan V. Oppenheim and Ronald W. Schaffer, "Computation of the Discrete Fourier Transform," in *Discrete-Time Signal Processing*, Upper Saddle River, NJ, USA: Pearson Higher Education, pp. 716-791, 2010.
- [63] Peter Strobach, "The Linear Prediction Model," in *Linear Prediction Theory: A Mathematical Basis for Adaptive Filtering*, Berlin, Germany: Springer-Verlag Berlin, 1st edition, pp. 13-36, 1990.

- 
- [64] Samprit Chatterjee and Jeffrey S. Simonoff, "Multiple Linear Regression," in *Handbook of Regression Analysis*, Hoboken, NJ, USA: John Wiley & Sons, pp. 3-22, 2013.
- [65] Rudolf J. Freund, William J. Wilson, and Ping Sa, "Multiple Linear Regression," in *Regression Analysis: Statistical Modeling of a Response Variable*, Oxford, UK: Elsevier, 2nd Edition, pp. 73-115, 2006.
- [66] David C. Lay, "Symmetric Matrices and Quadratic Forms," in *Linear Algebra and Its Applications*, Boston, MA, USA: Pearson Education, Fourth Edition, pp. 393-433, 2012.
- [67] Gilbert Strang, "Introduction to Applied Mathematics," Wellesley, MA, USA: Wellesley - Cambridge Press, 2009, pp. 15-17.
- [68] Itsik Bergel, Amir Leshem, "The Performance of Zero Forcing DSL Systems," *IEEE Signal Processing Letters*, vol. 20, issue 5, pp. 527-530, May 2013.
- [69] "Application Note on Transformers," Mini Circuits, AN-20-002 Rev.: B, M150261, 2015.
- [70] J. William H. Hayt and J. A. Buck, "Transmission Lines," in *Engineering Electromagnetics*, New York, NY, USA: The McGraw-Hill Companies, 6th ed., 2001, pp. 435-483.
- [71] "Single-to-differential Conversion in High-frequency Applications," ATMEL, Rev 5359A-BDC-01/04, 2004.
- [72] A. Lago, C. Penalver, J. Marcos, J. Doval-Gandoy, A. Melendez, O. Lopez, F. Santiago, F. Freijedo, J. Vilas, and J. Lorenzo, "Geometric Analysis and Manufacturing Considerations for Optimizing the Characteristics of a Twisted Pair," *IEEE Transactions on Electronics Packaging Manufacturing*, vol. 32, issue 1, pp. 22-31, Jan. 2009.
- [73] Athanasios Papoulis and S. Unnikrishna Pillai, "Functions of One Random Variable," in *Probability, Random Variables, and Stochastic Processes*, New York, NY, USA: McGraw-Hill, Fourth Edition, pp. 123-168, 2002.
- [74] Steven M. Kay, "Expected Values for Discrete Random Variables," in *Intuitive Probability and Random Processes Using Matlab*, New York, NY, USA: Springer Science+Business Media, pp. 133-166, 2006.
- [75] Tolga M. Duman and Ali Ghrayeb, "Practical Issues in MIMO Communications," in *Coding for MIMO Communication Systems*, Chichester, West Sussex, ENG: John Wiley & Sons, 2007, pp. 267-286.

- 
- [76] Steven M. Kay, "Multiple Discrete Random Variables," in *Intuitive Probability and Random Processes Using Matlab*, New York, NY, USA: Springer Science+Business Media, pp. 167-214, 2006.
- [77] Alan V. Oppenheim and Ronald W. Schaffer, "Discrete-Time Signals and Systems," in *Discrete-Time Signal Processing*, Upper Saddle River, NJ, USA: Pearson Higher Education, pp. 9-98, 2010.
- [78] Richard Tolimieri, Myoung An and Chao Lu, "Linear and Cyclic Convolutions," in *Algorithms for Discrete Fourier Transform and Convolution*, New York, NY, USA: Springer-Verlag, 2nd Edition, 1997, pp. 101-196.
- [79] Thomas Magesacher, Per Ödling, Per Ola Börjesson, 'Information Rate Bounds in Common Mode Aided Wireline Communications', *Transactions on Emerging Telecommunications Technologies*, vol. 17, issue 5, pp. 505-605, Oct. 2006.
- [80] F. Müller, C. Lu, P.-E. Eriksson, S. Host, and A. Klautau, "Optimizing Power Normalization for G.fast Linear Precoder by Linear Programming," presented at the *2014 IEEE International Conference on Communications (ICC)*, Sydney, NSW, Australia, Jun. 10-14, 2014.
- [81] Diego de Azevedo Gomes, Igor Freire, Aldebaro Klautau and Evaldo Pelaes, "Feasibility of alien crosstalk mitigation with receiver-side MIMO processing on G.fast systems," presented at the *2015 International Workshop on Telecommunications (IWT)*, Santa Rita do Sapucaí, Brazil, Jun. 14-17, 2015.
- [82] O. O. Ogundile and D. J. J. Versfeld, "Improved reliability information for OFDM systems on time-varying frequency-selective fading channels," presented at the *2015 Wireless Telecommunications Symposium (WTS)*, New York, NY, USA, Apr. 15-17, 2015.
- [83] Keke Zu, Francisco C. B. F. Müller, Chenguang Lu, Per-Erik Eriksson and Aldebaro Klautau, "Rate Balancing Based Tomlinson-Harashima Precoding for G.Fast Systems," in *IEEE Communications Letters*, vol. 20, issue 08, pp. 1519-1522, Jun. 2016.
- [84] Tamar Makharashvili, Brian Booth, Kerry Martin, James Drewniak and Daryl G. Beetner, "Study of alien crosstalk to a BroadR-Reach<sup>®</sup> protocol based system," presented at the *2016 IEEE International Symposium on Electromagnetic Compatibility (EMC)*, Ottawa, ON, Canada, Jul. 25-29, 2016.
- [85] Tolga M. Duman and Ali Ghayeb, "Layered Space-Time Codes," in *Coding for MIMO Communication Systems*, Chichester, West Sussex, ENG: John Wiley & Sons, 2007, pp. 122-160.



- 
- [86] D. A. Gomes, G. Guedes, A. Klautau, E. Pelaes and Chenguang Lu, “DSL Phantom Mode Transmission: Cable Measurements and Performance Evaluation,” presented at the *4TH IEEE LATIN-AMERICAN CONFERENCE ON COMMUNICATIONS*, Cuenca, Ecuador, Nov. 7-9, 2012.
- [87] Gilbert Strang, “Linear Transformations,” in *Introduction to Applied Mathematics*, Wellesley, MA, USA: Wellesley - Cambridge Press, 2009, pp. 375-408.
- [88] Ramanjit Ahuja, Pravesh Biyani and Surendra Prasad, “Low complexity training methods for common mode aided cancellation of intermittent alien noise in downstream VDSL”, *IEEE Transactions on Communications*, vol. PP, issue 99, pp. 1 - 1, Jul. 2017.
- [89] Rainer Strobel Andreas Barthelme and Wolfgang Utschick, “Implementation aspects of nonlinear precoding for G.fast - coding and legacy receivers,” presented at the *5th European Signal Processing Conference (EUSIPCO)*, Kos, Greece, Aug. 28 - Sep. 02, 2017.
- [90] Andreas Barthelme, Rainer Strobel, Michael Joham and Wolfgang Utschick, “Weighted MMSE Tomlinson-Harashima Precoding for G.fast,” presented at the *2016 IEEE Global Communications Conference (GLOBECOM)*, Washington, DC, USA, Dec. 4 - 8, 2016.